DCPT-04-100
IPPP-04-50

January, 6th, Final Draft (without Executive summary)

The Case for Positron Polarisation at the Linear Collider*

G. MOORTGAT-PICK[1,10**], T. ABE[13], G. ALEXANDER[23], B. ANANTHANARAYAN[2], A.A. BABICH[3],D. BARBER[7], A. BARTL[4], S. CHEN[13], J. CLARKE[5], J.E. CLENDENIN[6], J. DAINTON[21], M. DIEHL[7], B. DOBOS[13], T. DORLAND[13], H. EBERL[8], K. FLOETTMANN[7**], H. FRAAS[9], J. GOODSON[13], J. GRAY[13], A. HAN[13], S. HEINEMEYER[10], S. HESSELBACH[4,9], T. HIROSE[25**], K. HOHENWARTER-SODEK[4], J. KALINOWSKI[24], T. KERNREITER[4], O. KITTEL[9], S. KRAML[10], W. MAJEROTTO[8], A. MARTINEZ[13], K. MOENIG[18], K. MOFFEIT[6], S. MORETTI[11], T. NAKANISHI**, O. NACHTMANN[12], F. NAGEL[12], U. NAUENBERG[13**], T. OMORI[15**], P. OSLAND[14], A.A. PANKOV[3], N. PAVER[16**], R. PITTHAN[6**], W. POROD[17], J. PROULX[13], P. RICHARDSON[1], S. RIEMANN[7**], S.D. RINDANI[18], T.G. RIZZO[6**], P. SCHÜLER[7**], C. SCHWANENBERGER[19], D. SCOTT[5], J. SHEPPARD[6**], A. STAHL[7,22**], H. STEINER**, G. WEIGLEIN[1], M. WOODS[6**], F. ZOMER[20] ETC. NOT YET FINAL

[1] *IPPP, University of Durham, U.K.*
[2] *Centre for Theoretical Studies, Indian Institute of Science,Bangalore, 560 012, India*
[3] *Pavel Sukhoi Technical University, Gomel, 246746 Belarus*
[4] *Institut für Theoretische Physik, Universität Wien, Austria*
[5] *Astec, Daresbury Lab, UK*
[6] *Stanford Linear Accelerator Center, Stanford, CA, 94309, USA*
[7] *DESY, Germany*
[8] *Inst. f. Hochenergiephysik, Österr. Akademie d. Wissenschaften, Austria*
[9] *Institut für Theoretische Physik, Universität Würzburg, Am Hubland, D-97074 Würzburg, Germany*
[10] Cern, Theory Division, Switzerland
[11] School of Physics and Astronomy, University of Southampton, Highfield, Southampton SO17 1BJ, UK.
[12] Institut für Theoretische Physik, Philosophenweg 16, 69120 Heidelberg, Germany
[13] University of Colorado, Boulder, USA
[14] Department of Physics, University of Bergen, Allégaten 55, N-5007 Bergen, Norway
[15] KEK, Japan
[16] Dipartimento di Fisica Teorica, Università di Trieste and
Istituto Nazionale di Fisica Nucleare, Sezione di Trieste, Trieste, Italy
[17] Institut für Theoretische Physik, Universität Zürich, Switzerland
[18] Theory Group, Physical Research Laboratory, Navrangpura, Ahmedabad 380 009, India

*For further informations, see `http://www.ippp.dur.ac.uk/~gudrid/power/write-up` .
**Member of Editorial Board

[19] Physikalisches Institut, Universität Bonn, 53112 Bonn, Germany
[20] LAL, Universite de Paris-Sud, Orsay Cedex, France
[21] University of Liverpool, UK
[22] RWTH Aachen, Germany
[23] Tel-Aviv, Israel
[24] Instytut Fizyki Teoretycznej, Uniwersytet Warszawski, Warsaw, Poland
[25]

Contents

List of Figures

List of Tables

Chapter 1

Executive Summary

Draft, O.version
It is expected that the results of the proton–proton Large Hadron Collider (LHC), which is just under construction at Cern and will start operation in the year 2007, together with the planned electron–positron International Linear Collider (ILC) will bring revolutionary new insights in understanding of the fundamental interactions of natures and of the structure of matter, space and time.

Striking features at the Linear Collider (LC) are its clear signatures, known and tunable beam energy, high luminosity and the availibility to provide polarised beams with a high polarisation degree which can be provided without loss in luminosity. Therefore the LC is well suited for detailed studies of directly accessible new particles as well as for indirect searches of new physics with high sensitivity in a to a large extent model-independent approach.

Since on the hunt for physics beyond the Standard Model maybe only small traces are visible, the LC provides optimal searches conditions to be prepared for 'the unexpected'. Beam polarisation plays an important part in that context. The polarisation of the electron beam is already forseen for the baseline design [172] with a high degree of at least 80% polarisation, expected are even 90%, the question arises, whether really polarised positrons in addition are needed and so far, this option is only discussed as possible upgrade option.

All possible processes in the experiment are either annihilation or scattering processes. In annihilation processes the helicities of the electron and positron depend on each other. Suitably polarised beams lead then to a quick enhancement of rates and also a suppression of possible background processes. In case of the expected new physics often only extremely small rates are expected and such a quick gain in luminosity gives an additional plus for possible discoveries.

In scattering processes, however, the helicities of the electron and positron are independent and are directly related to the produced (new) particle. Therefore with both beams simultaneously polarised, unique possibilities for probing directly the properties of the new particles occur. In order to reveal precisely the structure of the underlying physics in a model-independent approach it is very important to get direct access to properties of new particles like their quantum numbers spin, chirality, etc.

The existing baryon asymmetry in our universe cannot be explained by the small amount of CP violation in the Standard Model. New physics models like supersymmetry offer a large amount of possible new sources of CP violation. However, tight experimen-

tal bounds exist and running experiments will even strengthen these bounds. Therefore it will impose tremendous challenges to find unique traces of new possible sources of CP violation.

Applying both beams simultaneously polarised offers the unique possibility to exploit effects from transversely polarised beams which provide access to powerful CP sensitive observables like azimuthal asymmetries. Due to the vanishing electron mass, however, effects of transversely polarised beams only occur if both beams are polarised.

Therefore the availibility of both beams polarised may not only be important for the discovery of new particles but is crucial for revealing the right structure of the underlying physics in direct seaches.

Not only in direct searches the simultaneous polarisation of both beams offers crucial insight in the possible new physics candidates and offers model-independent analyses by proving a large amount of (new) observables but also for indirect searches the polarisation of both beams gives an additional joker.

Some scales of new physics as e.g. in the search for extra dimensions may be too large to be accessible in present as well as future experiments. Applying strategies for indirect searches may therefore be decisive in such cases. Due to the clean experimental environment and high statistics at a LC such indirect searches are also very promising. All such indirect searches suffer from a strong model dependence. However, in case that both beams polarised are available it is possible to reduce considerably the model dependence even in such indirect searches, with longitudinally as well as transversely polarised beams. In order to be prepared for 'the unexpected' the polarisation of both beams is a decisive tool.

Furthermore both beams polarised enable to apply tests of the Standard Model with unprecedented precision either at the Z-pole/WW threshold or at high energy. Such tests require to 'know' the polarisaton degree up to per mille level which is not possible wit polarimetry only. In order to apply a Blondel scheme both beams polarised beams are needed to reach the required precision.

In order to enable also the precision requirements both beams polarised at the LC are crucial. The physics case for the need of both beams polarised is therefore clearly worked out and in order to be prepare for 'the unexpected' the tool of both polarised beams is crucial.

We give in this report also an overview about possible designs for measuring the polarisation with up- and downstream polarimetry and for polarising the beams, in particular for the production of polarised positrons at the LC. Mainly three possible designs are discussed for polarising the positrons, which are all well advanced: the undulator-based scheme, the laser-based and the conventional scheme. It is technically visible to provide polarised beams without loss in luminosity and also comissioning problems could be prevented. The precise technical details for all designs will be given in forthcoming technical design reports. Therefore it is seasonable to foresee also polarised positrons for the baseline design in order to guarantee the miximal physics gain of the physics program at the Linear Collider.

Chapter 2

Introduction

2.1 General remarks

2.1.1 Polarised cross sections at an e^+e^- collider

In general the spin-averaged matrix element for any process at an $\mathrm{e^+e^-}$ collider is given by:

$$\begin{aligned} |\bar{\mathcal{M}}|^2 &= \frac{1}{4}\{(1-P_{e^-}P_{e^+})(|T_{\mathrm{RL}}|^2+|T_{\mathrm{LR}}|^2)+(P_{e^-}-P_{e^+})(|T_{\mathrm{RL}}|^2-|T_{\mathrm{LR}}|^2) \\ &\quad +(1+P_{e^-}P_{e^+})(|T_{\mathrm{RR}}|^2+|T_{\mathrm{LL}}|^2)+(P_{e^-}+P_{e^+})(|T_{\mathrm{RR}}|^2-|T_{\mathrm{LL}}|^2) \\ &+ (2P^T_{e^-}P^T_{e^+})[\cos 2\phi\, Re(T_{\mathrm{RL}}T^*_{\mathrm{LR}})-\sin 2\phi\, Im(T_{\mathrm{RL}}T^*_{\mathrm{LR}})+Re(T^*_{\mathrm{RR}}T_{\mathrm{LL}})]\}\,, \end{aligned} \quad (1)$$

where T_{ab} are the helicity amplitudes, a (b) denote the helicity of the e^- (e^+) and ϕ is the azimuthal angle, defined e.g. between the directions of the $e^\pm$ directions and the scattering plane.

In the limes $m_e \to 0$ ($\to T_{\mathrm{RR}} \times T_{\mathrm{LL}} = 0$) and if the transverse polarisation of the produced fermions is not measured the effect of transverse polarisations are absent in the ϕ averaged cross section in SM processes. Nevertheless effects of transverse polarisation could although be used in SM processes e.g. for the separation of light quark flavours [143]: the differential cross sections $d^2\sigma/d\cos\theta d\Phi$ depends on flavour dependent functions which can be separated when studying the azimuthal distribution. Further interesting effects of transverse polarisation for searches of physics beyond the SM, in particular for new sources of CP-violation, are given in sections 3.5.1, 3.6.1, 3.6.3, 3.6.5. A key issue for exploiting this option is to use specific diffential cross sections and define new (CP-odd) asymmetries. One should note, however, that contributions from transverse polarisation only appear in e^+e^- processes if both beams are polarised, cf. eq. 1.

In the following paragraphe we concentrate on longitudinally polarised beams and present some useful, well-known formulae. With respect to the remarks above any cross section at a e^+e^- collider can be subdivided (see Tab.2.1) in [135]:

$$\begin{aligned} \sigma_{P_{e^-}P_{e^+}} &= \frac{1}{4}\{(1+P_{e^-})(1+P_{e^+})\sigma_{\mathrm{RR}}+(1-P_{e^-})(1-P_{e^+})\sigma_{\mathrm{LL}} \\ &\quad +(1+P_{e^-})(1-P_{e^+})\sigma_{\mathrm{RL}}+(1-P_{e^-})(1+P_{e^+})\sigma_{\mathrm{LR}}\}, \end{aligned} \quad (2)$$

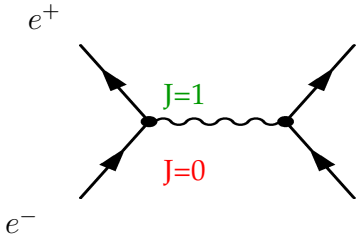

← only from RL,LR: γ, Z (e.g. in SM) or e.g. Z' (in NP)

← only from LL,RR: NP!

Figure 1: Possible configurations in annihilation diagrams: the helicities of the incoming e^+e^- beams are directly coupled. Within the Standard Model (SM) only the recombination into a vector particle with J=1 is possible, which is given by the LR and RL configurations. New physics (NP) models might allow J=0, which results LL or RR configurations.

where σ_{RL} stands for the cross section of the process when both the electron and the positron beam are 100% polarised in right-handed e^- and left-handed e^+; the cross sections σ_{LR}, σ_{RR} and σ_{LL} are defined analogously. We use the right-handed helicity basis, so that $P_{e^\pm} < 0$ means that the beam is left-handed polarised.

	e^-	e^+		
$\boldsymbol{\sigma_{\mathrm{RR}}}$	⟹	⟸	$\frac{1+P_{e^-}}{2} \cdot \frac{1+P_{e^+}}{2}$	$J_z = 0$
$\boldsymbol{\sigma_{\mathrm{LL}}}$	⟸	⟹	$\frac{1-P_{e^-}}{2} \cdot \frac{1-P_{e^+}}{2}$	
$\boldsymbol{\sigma_{\mathrm{RL}}}$	⟹	⟹	$\frac{1+P_{e^-}}{2} \cdot \frac{1-P_{e^+}}{2}$	$J_z = 1$
$\boldsymbol{\sigma_{\mathrm{LR}}}$	⟸	⟸	$\frac{1-P_{e^-}}{2} \cdot \frac{1+P_{e^+}}{2}$	

Table 2.1: Graphical representation of the various spin configurations in e^+e^- collisions. The thick arrow represents the direction of motion of the particle and the double-arrow its spin direction. The first column indicates the corresponding cross section, the third column the fraction of this configuration and the last column the total spin assuming a zero orbital angular momentum.

One has to distinguish two cases:
a) in annihilation diagrams the helicities of the incoming beams are coupled to each other, whereas
b) in exchanged diagrams the helicities of the incoming beams are directly coupled to the helicities of the final particles, see Fig. 2.

In case a) within the SM only the recombination into a vector particle with the total angular momentum $J = 1$ is possible, i.e. both beams have to carry opposite sign of helicities, $T_{\mathrm{LL}} = 0 = T_{\mathrm{RR}}$. New physics (NP) models might allow to produce also scalar particles, so that also $J = 0$ would be allowed, which results in same sign helicities of the incoming beams, see Fig. 1.

In case b) the exchanged diagrams could result in a vector, fermionic or scalar particle; the helicity of the incoming particle is directly coupled to the vertex and is independent of

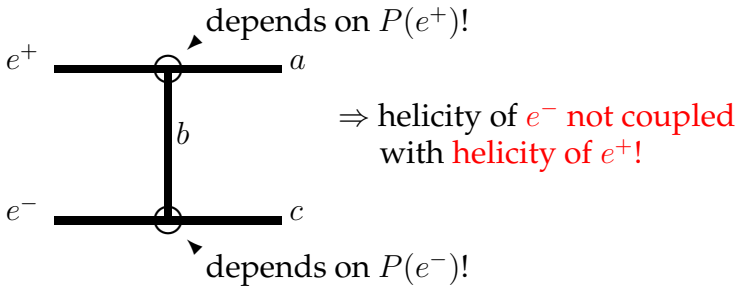

Figure 2: Possible configurations in exchanged diagrams: the helicity of the incoming e beam is directly coupled to the helicity of the final particle and is completely independent of the helicity of the second incoming particle. All possible helicity configurations are therefore possible in principle.

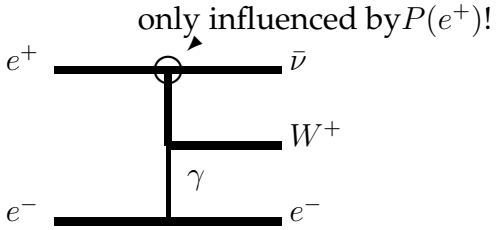

Figure 3: Single W^+ production: vertex $e^+W^+\bar{\nu}$ depends on $P(e^+)$.

the helicity of the second incoming particle. Therefore all possible helicity configurations are possible in principle, see Fig. 2. Prominent candidates for case b) are single W production, see Fig. 3, where the $e^+W^+\bar{\nu}$ is only influenced by $P(e^+)$, and Bhabha scattering, where the γ, Z exchange in the crossed channel leads to higher cross sections for the LL configuration than the LR configurations, see Table 2.2.

2.1.2 Effective polarisation and further definitions

In the case of e^+e^- annihilation into a vector particle (in the SM this would be $e^+e^- \to \gamma/Z^0$) only the two J=1 configurations σ_{RL} and σ_{LR} contribute, as already mentionened in sect.2.1.1, and the cross section for arbitrary beam polarisations is given by

$$\begin{aligned}
\sigma_{P_{e^-}P_{e^+}} &= \frac{1+P_{e^-}}{2}\,\frac{1-P_{e^+}}{2}\,\sigma_{RL} + \frac{1-P_{e^-}}{2}\,\frac{1+P_{e^+}}{2}\,\sigma_{LR} \\
&= (1-P_{e^-}P_{e^+})\,\frac{\sigma_{RL}+\sigma_{LR}}{4}\left[1 - \frac{P_{e^-}-P_{e^+}}{1-P_{e^+}P_{e^-}}\,\frac{\sigma_{LR}-\sigma_{RL}}{\sigma_{LR}+\sigma_{RL}}\right] \\
&= (1-P_{e^+}P_{e^-})\;\sigma_0\;[1 - P_{\text{eff}}\,A_{LR}] \qquad (3)
\end{aligned}$$

unpolarised	$P_{e^-} = -80\%$	$P_{e^-} = -80\%$, $P_{e^+} = -60\%$	$P_{e^-} = -80\%$, $P_{e^+} = +60\%$
4.50 pb	4.63 pb	4.69 pb	4.58 pb

Table 2.2: Bhabha scattering at $\sqrt{s} = 500$ GeV: due to the γ, Z exchange in the crossed channel all possible helicity configurations are allowed, e.g. the configuration LL leads to higher cross sections than LR.

		$\sigma_{\rm RL}/\sigma_0$	$\sigma_{\rm LR}/\sigma_0$	$\sigma_{\rm RR}/\sigma_0$	$\sigma_{\rm LL}/\sigma_0$	P_{eff}	$\mathcal{L}_{eff}/\mathcal{L}$
$P_{e^-}=0,$	$P_{e^+}=0$	0.25	0.25	0.25	0.25	0.	0.50
$P_{e^-}=-1,$	$P_{e^+}=0$	0	0.50	0	0.50	-1.00	0.50
$P_{e^-}=-0.8,$	$P_{e^+}=0$	0.05	0.45	0.05	0.45	-0.80	0.50
$P_{e^-}=-0.8,$	$P_{e^+}=+0.6$	0.02	0.72	0.08	0.18	-0.95	0.74

Table 2.3: Effective polarisation and the fraction of colliding particles for some values of beam polarisation

$$\text{with the unpolarised cross section} \qquad \sigma_0 = \frac{\sigma_{\rm RL}+\sigma_{\rm LR}}{4} \tag{4}$$

$$\text{the left-right asymmetry} \qquad \mathrm{A_{LR}} = \frac{\sigma_{\rm LR}-\sigma_{\rm RL}}{\sigma_{\rm LR}+\sigma_{\rm RL}} \tag{5}$$

$$\text{and the effective polarization} \qquad \mathrm{P_{eff}} = \frac{\mathrm{P}_{e^-}-\mathrm{P}_{e^+}}{1-\mathrm{P}_{e^+}\mathrm{P}_{e^-}} \tag{6}$$

One can already see from eq. 3 that one gets two effects enhancing the cross sections when using both beams polarised compared to the case with only polarised electrons (keeping in mind the P_{e^-} and P_{e^+} have different sign): $(1-P_{e^-}P_{e^+})>1$ as well as $|P_{eff}|>|P_{e^-}|$. Introducing the effective luminosity

$$\mathcal{L}_{eff}/\mathcal{L} = \frac{1}{2}(1-P_{e^-}P_{e^+}), \tag{7}$$

which gives the fraction of colliding particles, eq. (3) can be written as:

$$\sigma_{P_{e^-}P_{e^+}} = 2\,\sigma_0\,\mathcal{L}_{eff}\;[1\;-\;\mathrm{P_{eff}}\,\mathrm{A_{LR}}]\,. \tag{8}$$

Some values for the effective polarisation as well as for the effective luminosity are given in Table 2.3, which shows that the fraction of colliding particles can only be enhanced if both beams are polarised. The values of the effective polarization can be read from fig. 4. Notice that the effective polarization is closer to $100\ \%$ than any of the two beam polarizations. Further excellent reference see also [32].

In the experiment one would like to extract e.g. the two quantities σ_0 and $\mathrm{A_{LR}}$, regarding only SM annihilation processes into a vector particle. This can be done by running the experiment with two different polarization configurations. One would choose one setup with the electron beam predominantly left-handed and the positron beam right-handed and in the second setup one would reverse both spin directions. The cross sections measured with the two setups are denoted as σ_{-+} and σ_{+-} and are given by:

$$\sigma_{-+} = \frac{1}{4}\left\{(1+|P_{e^-}||P_{e^+}|)(\sigma_{\rm LR}+\sigma_{\rm RL})+(|P_{e^-}|+|P_{e^+}|)(\sigma_{\rm LR}-\sigma_{\rm RL})\right\} \tag{9}$$

$$\sigma_{+-} = \frac{1}{4}\left\{(1+|P_{e^-}||P_{e^+}|)(\sigma_{\rm LR}+\sigma_{\rm RL})-(|P_{e^-}|+|P_{e^+}|)(\sigma_{\rm LR}-\sigma_{\rm RL})\right\}. \tag{10}$$

It is then

$$\begin{aligned}\sigma_0 &= \frac{\sigma_{-+}+\sigma_{+-}}{2\,(1+|\mathrm{P}_{e^+}||\mathrm{P}_{e^-}|)}\\ \mathrm{A_{LR}} &= \frac{1}{|\mathrm{P_{eff}}|}\;A_{\rm obs} \;=\; \frac{1}{|\mathrm{P_{eff}}|}\;\frac{\sigma_{-+}-\sigma_{+-}}{\sigma_{-+}+\sigma_{+-}},\end{aligned} \tag{11}$$

where $A_{\rm obs}$ is the measured left-right asymmetry of processes with partially polarised beams.

Both quantities A_{LR} and σ_0 depend on the beam polarisations. The contribution of the uncertainty of the polarisation measurement to the error is – under the assumption that the errors are completely independent:

$$\frac{\Delta \mathrm{A_{LR}}}{\mathrm{A_{LR}}} = -\frac{\Delta \mathrm{P_{eff}}}{|\mathrm{P_{eff}}|} \tag{12}$$

$$\frac{\Delta \mathrm{P_{eff}}}{|\mathrm{P_{eff}}|} = \frac{x}{(|\mathrm{P}_{e^+}| + |\mathrm{P}_{e^-}|)\ (1 + |\mathrm{P}_{e^+}||\mathrm{P}_{e^-}|)} \sqrt{(1 - |\mathrm{P}_{e^-}|^2)^2\, P_{e^+}^2 + (1 - |\mathrm{P}_{e^+}|^2)^2\, P_{e^-}^2} \tag{13}$$

$$\frac{\Delta \sigma_0}{\sigma_0} = \frac{\sqrt{2}\, x}{1 + |\mathrm{P}_{e^+}||\mathrm{P}_{e^-}|} (|\mathrm{P}_{e^+}| + |\mathrm{P}_{e^-}|) \tag{14}$$

Equal relative precision $x := \Delta P_{e^-}/P_{e^-} \sim \Delta P_{e^+}/P_{e^+}$ for the measurement of the two beam polarizations is assumed.

In case that the relative errors of e^- and e^+ are fully correlated, like depolarisation effects from Bremsstrahlung, the errors are given by the linear sum:

$$\frac{\Delta \mathrm{P_{eff}}}{\mathrm{P_{eff}}} = \frac{1 + P_{e^+} P_{e^-}}{1 - P_{e^+} P_{e^-}}\, x \tag{15}$$

$$\frac{\Delta \sigma_0}{\sigma_0} = \frac{2\, x}{1 + |\mathrm{P}_{e^+}||\mathrm{P}_{e^-}|} (|\mathrm{P}_{e^+}| + |\mathrm{P}_{e^-}|) \tag{16}$$

It is immediately obvious from eqn. (13) and (15 that in both cases $\Delta P_{eff}/|P_{eff}| < \Delta P_{e^-}/|P_{e^-}|$ and one reduces the uncertainties when using both beams polarised!

The resulting uncertainties are shown in fig. 5. The error contribution from the polarimeter to the unpolarized cross section is rather small. For a polarimeter precision of $0.5\ \%$, it only becomes relevant for data samples with more than $4 \cdot 10^6$ signal events. For an electron beam polarization of $80\ \%$ there is a small improvement in the extraction of the unpolarized cross section due to positron beam polarization. The error introduced in $\mathrm{A_{LR}}$ by the polarization measurement is larger. Without positron beam polarization one is limited by the polarimeter ($\leq 0.5\ \%$ precision) for samples with more than 10^6 events.

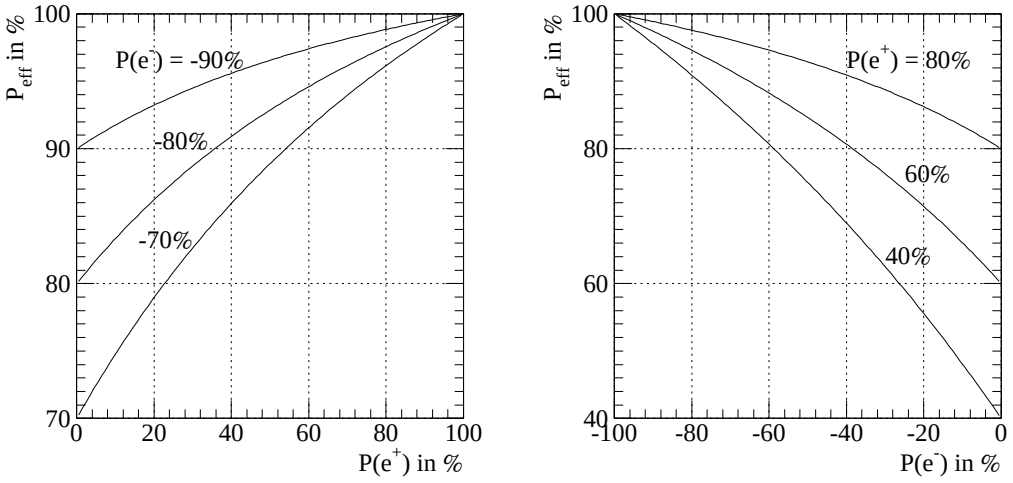

Figure 4: Effective polarization as a function of the beam polarization.

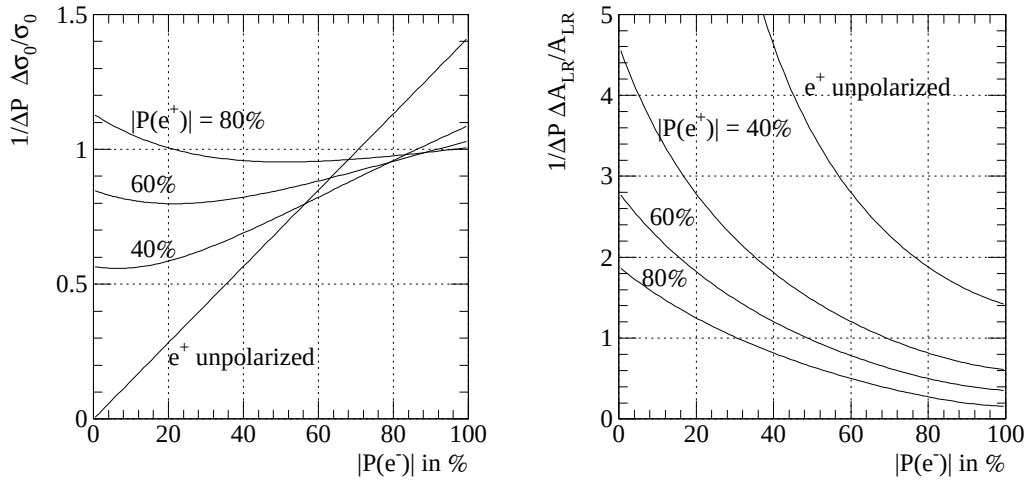

Figure 5: Left: Contribution of the uncertainty on beam polarization on the measurement of the unpolarized cross section. Right: Same for the left-right asymmetry. Both plots are normalized to the polarimeter resolution ΔP which is assumed to be identical for both beams.

The improvement due to positron beam polarization is substantial. For a positron polarization of $60\ \%$ the error on $\mathrm{A_{LR}}$ is reduced by a factor of 3.8.

2.2 Example: top couplings – influence of effective polarisation

Summary: Top quark production occurs only via γ, Z exchange and the influence of polarised beams can be described by the effective polarisation P_{eff}. Using both beams polarised leads to an improvement in the A_{LR} measurement and the determination of couplings, respectively, by about a factor 3.8 compared to the case with only polarised electrons. The limits for top FCN couplings in single top produuction are improved by about a factor 1.8 and the sensitivity or CP violating top couplings is improved by about a factor 1.4 when using both beams longitudinally polarised compared to the case with only polarised electrons.

The top quark is by far the heaviest fermion observed, yet all the experimental results tell us that it behaves exactly as would be expected for a third generation quark. Its large mass, which is close to the scale of electroweak symmetry breaking, renders the top quark a unique object for studying the fundamental interactions in the attometer regime. It is likely to play a key role in pinning down the origin of electroweak symmetry breaking [1]. High precision measurements of the properties and the interaction of top quarks will therefore be an essential part of the LC research program.

a) determination of top couplings at threshold

The production process occurs via γ, Z exchange and the scaling factors are given by the factors $(1 - P_{e^-})(1 + P_{e^+})$ and $(1 + P_{e^-})(1 - P_{e^+})$ and can be parametrized with the effective polarisation P_{eff}. In [2] polarization effects were studied at the top threshold. To

determine the top vector couplings, v_t one has to measure the left–right asymmetry A_{LR} with high accuracy. With an integrated luminosity of $\mathcal{L} = 300$ fb^{-1} precisions in A_{LR} and v_t of about 0.4% and 1% respectively can be achieved at the LC. The gain in using simultaneously polarized e^- and e^+ beams $(80, 60)$ is given by the higher effective polarization of $P_{eff} = 0.946$ compared to the case for only polarized electrons. This leads to an error reduction in A_{LR} by about a factor 3.8, see Eqn. (12), (13).

b) Limits for top FCN couplings

Limits on top FCN decay branching ratios can be obtained from top pair production, $e^+e^- \to t\bar{t}$ with subsequent $\bar{t}$ decays and from single top production in the process $e^+e^- \to t\bar{q} \to W^+b\bar{q}$, t off-shell [3]. Concerning limites coming from single top production, beam polarisation is a very efficient tool since it considerably reduces the dominant Wqq' background. The dominant background for the $t\bar{q}$ signal is given by $W^+q\bar{q}'$ production followed by W^+ decays into lepton pairs. With $(80, 0)$ background decreases by a factor of $5\,(\approx 1/[1 - P_{e^-}])$ while keeping 90% of the signal. With $(80, 45)$ the background is reduced by about a factor of $9\,(\approx 1/[1 - P_{e^-}][1 + P_{e^+}])$ and the signal is increased by 20% compared to the values for unpolarized beams [3], i.e. one improves S/B ($S/\sqrt{B}$) by about a factor 2.1 (1.7).

With e^- and e^+ polarization (80, 45), one improves the 3 σ discovery limits on γ^μ at $\sqrt{s} = 500$ GeV by a factor of 3 (a factor of 1.7 compared to only electron polarisation) and the limits on $\sigma^{\mu\nu}$ coupling at $\sqrt{s} = 800$ GeV by about a factor 2.6 (a factor 1.8 compared to electron polarisation only), Table 2.4. Beam polarisation only slightly improves the limits from top pair production, since in this case also the signal decreases slightly when suppressing the background [3].

A more recent study was made for $P_{e^-} = 80\%$, $P_{e^+} = 60\%$ at $\sqrt{s} = 500$ GeV with $\mathcal{L} = 345$ fb^{-1} and $\sqrt{s} = 800$ GeV with $\mathcal{L} = 534$ fb^{-1} including initial state radiation and beamstrahlung and using different kinematical cuts [4]. Comparison with the limits for FNC couplings from LHC show that the LC measurements are complementary in searches for FCN couplings. Whereas the LHC is superior in the discovery potential for γ^μ couplings, the LC at $\sqrt{s} = 800$ GeV with $P_{e^-} = 80\%$, $P_{e^+} = 60\%$ gains an order of magnitude for the discovery of $\sigma_{\mu\nu}$ couplings to the Z and the photon, see Table 2.5. One has to note, however, that true simulations for the ATLAS [5] and the CMS detector [8] lead to somewhat different results concerning the LHC discovery potential than given in Table 2.5.

The listed results show that although an enhancement of the effective polarisation has not the highest reputation in arguments for having both beams polarised, however, it improves the results concerning measurements of the top properties and enhances considerably the discovery potential for deviations from SM predictions.

c) Limits for CP violating top dipole couplings

In order to measure top dipole moments one applies asymmetries of the charged lepton produced in semi-leptonic decay of one of t and $\bar{t}$, while the other decays hadronically [6]. In this study the measured asymmetries are given in the laboratory frame, depending on final momenta instead on top polarisation and gives a direct handle on anomalous couplings in top production. Anomalous effects are included in production and decay as well $\mathcal{O}(\alpha_s)$ QCD correction which mainly influences the sensitivity through the $1/\sqrt{N}$ factor. All these asymmetries are a measure of CP violation in the unpolarised case as

	unpolarized beams	$\lvert P_{e^-}\rvert = 80\%$	$\lvert P_{e^-}\rvert = 80\%$, $\lvert P_{e^+}\rvert = 45\%$
	$\sqrt{s} = 500$ GeV		
$BR(t \to Zq)(\gamma_\mu)$	6.1×10^{-4}	3.9×10^{-4}	2.2×10^{-4}
$BR(t \to Zq)(\sigma_{\mu\nu})$	4.8×10^{-5}	3.1×10^{-5}	1.7×10^{-5}
$BR(t \to \gamma q)$	3.0×10^{-5}	1.7×10^{-5}	9.3×10^{-6}
	$\sqrt{s} = 800$ GeV		
$BR(t \to Zq)(\gamma_\mu)$	5.9×10^{-4}	4.3×10^{-4}	2.3×10^{-4}
$BR(t \to Zq)(\sigma_{\mu\nu})$	1.7×10^{-5}	1.3×10^{-5}	7.0×10^{-6}
$BR(t \to \gamma q)$	1.0×10^{-5}	6.7×10^{-6}	3.6×10^{-6}

Table 2.4: Single top production: 3 σ discovery limits on top flavour changing neutral couplings from top branching fractions at $\sqrt{s} = 500$ GeV with $\mathcal{L} = 300$ fb^{-1} and at $\sqrt{s} = 800$ GeV with $\mathcal{L} = 500$ fb^{-1} [3].

	LHC	ILC, $\sqrt{s} = 500$ GeV	ILC, $\sqrt{s} = 800$ GeV
$BR(t \to Zc)\ (\gamma_\mu)$	3.6×10^{-5}	1.9×10^{-4}	1.9×10^{-4}
$BR(t \to Zc)\ (\sigma_{\mu\nu})$	3.6×10^{-5}	1.8×10^{-5}	7.2×10^{-6}
$BR(t \to \gamma c)$	1.2×10^{-5}	1.0×10^{-5}	3.8×10^{-6}

Table 2.5: 3 σ discovery limit on top FCN couplings that can be obtained at LHC and ILC, $\sqrt{s} = 500$ GeV and $\sqrt{s} = 800$ GeV with $P_{e^-} = 80\%$, $P_{e^+} = 60\%$ for one year of operation [4].

well as in the polarised case if $P_{e^-} = -P_{e^+}$. However, if $P_{e^-} \neq -P_{e^+}$ the initial state is not invariant under CP. However, at leading order in α CP-invariant additional interactions can be neglected concerning contributions to these asymmetries. Limits are given for the CP violating dipole couplings, assuming one of them nonzero, the other taken to be vanishing. The limits at 90% c.l. are of the order of 0.1-0.2 at $\sqrt{s} = 500$ GeV. Using in addition asymmetries which depend on the azimuthal range improves the limit by about a factor 4-6. Using both beams polarised with $P_{e^-} = \pm 80\%$ and $P_{e^+} = \mp 60\%$improves the sensitivity by about a factor of 20-30% compared to the with only polarised electrons of $P_{e^-} = \pm 80\%$. In [7] an optimal observable analysis for $\gamma t\bar{t}$, $Zt\bar{t}$ and Wtb has been made. The beam polarisations P_{e^-} and P_{e^+} were adjusted to minimise the statistical error for the determination of each form factor. The measured asymmetry should be possible to detect at 5.5σ (4.3σ) level for bottom quarks (leptons) with unpolarised beams. Having both beams polarised with 80% the signal for bottoms (leptons) could reach even 16σ (6.6σ).

2.3 Experimental results: longitudinally polarised electrons at the SLC

Before concentrating on the physics reasons for having both beams polarised in the next chapter, it is interesting which results have already been achieved at the SLD experiment with the longitudinally polarised e^- beam at the SLC at SLAC. During its last year of running the SLC had an average longitudinal electron beam polarization $P_{e^-} = 77\%$, and polarimetry was developed that allowed the polarization to be determined to better than 0.5% [18].

At SLD a high precision measurement of the left-right asymmetry of Z-boson production was done. With the data obtained from 1996-98, where about three quarters of the total sample were taken, i.e. about 383 500 Z decays were collected, the pole value of the asymmetry was measured with high precision, $A^0_{LR} = 0.15056 \pm 0.00239$, [19]. The measurement required a precise knowledge of the absolute beam polarisation, but did not require knowledge of the absolute luminosity, detector acceptance and efficiency, provided the efficiency for detecting a fermion at some polar angle is equal to the efficiency for detecting an antifermion at the same polar angle.

The beam polarisation was measured by a Compton-scattering polarimeter. The accepted energy of the Compton electrons was in the range between 17 and 30 GeV. The kinematical minimum was at 17.36 GeV and was monitored by frequent scans of the detectors horizontal position during polarimeter operation. The analyzing powers of the detector channels incorporated resolution and spectrometer effects which differed typically about 1% from the theoretical Compton polarisation asymmetry function [20]. Polarimeter data were aquired continually during the operation of the SLC.

Two additional detectors were operated to assist in the calibration of the primary spectrometer based polarimeter. Although they were not used during collision, both provided a useful cross-check for the calibration procedure.

Altogether the systematic uncertainties affecting the polarisation measurements were a) laser polarisation, b) detector linearity, c) analysing power calibration and d) electric noise which lead to an uncertainty of about $\delta Pe/P_e \sim 0.5\%$, see Table2.6.

Some further effects had to be taken into account. The measured polarisation differs from the luminosity-weighted beam polarisation, which is the actual polarisation at the IP, the correction between the two polarisations is parametrised by the parameter chromaticity. The chromaticity is influenced by beam energy spread, polarisation transport, luminosity energy dependence and also by a small precession of the electron spin in the final focusing elements between the SLC IP and the polarimeter. The depolarisation due to the e^+e^- interaction turned out to be negligible. Summarising these three effects one ends up with an uncertainty due to chromaticity of about 0.15%, see Table 2.6.

Another source of uncertainties are systematical errors of the asymmetry. The measured left-right asymmetry A_m does not coincide with the theoretical asymmetry A_{LR} but is only related to it. The relation depends also on the mean luminosity-weighted polarisation as well as on any longitudinal positron polarisation with constant helicity (which was checked to be negligible), on electron current asymmetries from the polarised source, luminosity asymmetry, polarisation asymmetry, beam energy asymmetry (due to a beam loading of the accelerator) and an efficiency asymmetry (determined by the detector acceptance of the polar angle). The final uncertainties for A_{LR} turned out to be 0.52% relative

Uncertainty	$\delta P_e/P_e$	$\delta A_{LR}/A_{LR}$	$\delta A^0_{LR}/A^0_{LR}$
Laser polarisation	0.10%		
Detector linearity	0.20%		
Analysing power calibration	0.40%		
Electronic noise	0.20%		
Total polarimetry uncertainty	0.50%	0.50%	
Chromaticity and IP corrections		0.15%	
Corrections between measured and theoretical A_{LR}		0.07%	
A_{LR} systematic uncertainty		0.52%	0.52%
Electroweak interference corrections			0.39%
A^0_{LR} systematic uncertainty			0.64%

Table 2.6: Systematic uncertainties that affect the A_{LR} measurement. The uncertainty on the electroweak interference correction is caused by the uncertainty on the SLC energy scale, see [19].

error, see Table 2.6.

To end up with the pole asymmetry A^0_{LR} the derived asymmetry A_{LR} had to be corrected for residual effects arising from pure photon exchange and $Z\gamma$ interference, where these electroweak interference corrections depends sensitively on uncertainties from the cms energy. The systematical relative uncertainty for A^0_{LR} was finally around 0.64%, see Table 2.6, and lead to an determination of $\sin^2\theta^{eff}_W = 0.23107 \pm 0.00030$ with at that time unprecented accuracy.

The high-precision measurement of the left-right Z-boson cross section asymmetry shows what for a powerful tool polarised beams provide but also which effects have to be taken into account in order to get really the wanted high precision. The SLD experiment has perfectly demonstrated and exemplified how well all these effects are under control and has opened the way for exploiting beam polarisation at the ILC in a most appropriate way.

2.4 Tools for simulation studies: MC Event Generators

The use of numerical programs based on Monte Carlo (MC) techniques has become essential in performing any detailed experimental analysis in collider physics. In this section the so-called event generators are described and their inclusion of beam polarisation. These programs must be interfaced to both detector simulations and beam energy spectra to give a complete picture of the actual physics process.

Most MC event generators fall into one of two classes:

- **a) general-purpose (or multi-purpose) event generators**
  which aim to perform the full simulation of the event starting with the initial-state collider beams, proceeding through the hard scattering process and finishing with the final-state hadrons;

- **b) parton-level event generators**
  typically perform the hard scattering part of the simulation only, perhaps including decays, and rely on one of the general-purpose generators for the rest of the simulation.

During the LEP-era the experiments relied on the general-purpose event generators for the description of hadronic final states together with more accurate parton-level programs interfaced to the former ones for specific processes, *e.g.* two- and four-fermion production. At a future linear collider (LC), as one wishes to study final states with higher multiplicities, for example six or even eight particles, this mixed approach will become more important as these final states cannot be described by the general-purpose event generators.

General-purpose event generators

General-purpose event generators are e.g. HERWIG [144], ISAJET [145] and PYTHIA [146]. They use different phenomenological models and approximations. The major differences between the programs are in the approximations used in the parton shower evolution and the hadronisation stage.

There are also major differences between the generators in the treatment of spin correlation and polarisation effects. Both ISAJET and HERWIG include longitudinal polarisation effects in both SM and Supersymmetric (SUSY) production processes, while PYTHIA includes both longitudinal and transverse polarisations in many processes.

Another important difference is in the treatment of the subsequent decay of any heavy particle produced in the hard process. While HERWIG includes the full correlations in any subsequent decays using the method described in [147] both ISAJET and PYTHIA only include these effects in some processes, *e.g.* W pair production. To include transverse polarisation also in the HERWIG production stage is certainly possible.

The only program currently available in C++ which is capable of generating physics results is SHERPA (based on the APACIC++ [148] PS). Work is however underway to rewrite both PYTHIA [149] and HERWIG [150] in C++. Given the new design and structure of these programs the treatment of both spin correlation and polarisation effects should be much better than in the current FORTRAN programs, e.g. HERWIG++, should include full polarisation and correlation effects using the method of [147].

Parton-level event generators

There are a large number of programs available which calculate some set of hard processes, and are interfaced to one of the general-purpose generators, most often PYTHIA. Many of the two- [151] and four-fermion [152] generators were used by the LEP collaborations (see report of the LEP-II MC workshop for their detailed discussion). Some programs are written for six fermion processes, *e.g.*, LUSIFER [153], SIXFAP [154], EETT6F [155] and SIXPHACT [156]. Many of these codes use helicity amplitude techniques to calculate the matrix elementss and therefore either already include polarisation effects or could easily be modified to do so.

There are a number of codes available, which are capable of calculating and integrating the matrix elements for large numbers of final-state particles automatically:
– AMEGIC++ [157] makes use of helicity amplitude and is part of SHERPA.
– COMPHEP [158] uses the traditional trace techniques to evaluate the matrix elements; therefore it is at present not suitable to investigate polarisation/spin effects. However, the conversion to the use of helicity amplitudes techniques is currently planned.
– GRACE [159] (with the packages BASES and SPRING) uses the calculation of matrix elements via helicity amplitude techniques.
– HELAC/PHEGAS calculates cross sections [160, 161].
– MADGRAPH/MADEVENT [162] uses helicity amplitude techniques for the matrix elements to calculate cross sections (based on the HELAS [163] subroutines).
– WHIZARD [164] is an integration package which can use either COMPHEP, MADGRAPH or O'MEGA* [166] to calculate the matrix elements. Transverse beam polarisation is included.

The implementation of polarisation and correlation effects differs between these programs. In general, apart from COMPHEP (as noted), these programs are all based on helicity amplitude techniques at some point in the calculation and therefore the inclusion of both transverse and longitudinal beam polarisation is possible even where it is not currently implemented.

SUSY

Polarisation and spin correlation effects are particularly important in studying SUSY scenarios, in order to measure the fundamental parameters of the underlying model (hereafter, we assume the particle content of the MSSM).

HERWIG, PYTHIA and ISAJET all include longitudinal polarisation effects in SUSY production processes. There is also a parton-level program SUSYGEN [168], interfaced to PYTHIA, which includes these effects.

All these programs also differ in the inclusion of the correlations in the subsequent decays of the particles. While SUSYGEN includes these correlations using helicity amplitude techniques and HERWIG uses the method of [147], these effects are generally not included in either PYTHIA or ISAJET.

Among the parton-level programs, at present only COMPHEP and GRACE include SUSY processes, although both MADGRAPH and AMEGIC++ can be extended to add the additional interactions which are needed.

*O'MEGA uses the approach of [165] to evaluate the matrix elements but does not include yet any QCD processes.

Chapter 3

Searches for new physics with polarised e^- and e^+ beams

3.1 Determination of chiral quantum numbers of new physics particles

Summary: In order to test whether the Susy partners of the electrons/positrons carry the same chiral quantum numbers as their SM partners one has to separate the scattering process from the annihilation process. With both beams polarised the production vertices can be analysed independently. It is shown that polarised positrons are absolutely needed for such model tests since even a completely polarised electron beam is not sufficient.

We demonstrate the importance of having both beams polarised at one example of physics beyond the SM: Supersymmetry is one of the most motivated possibilities for NP. However, even its minimal version, the MSSM, leads to about 105 new free parameters. At future experiments, the LHC and the LC, one has - after detecting signals expected by Susy – to determine the Susy parameters as model independent as possible, as well as to prove the underlying Susy assumptions, e.g. that the Susy particles have to carry the same quantum numbers (with the exception of the spin) as their SM partners.

E.g. Susy transformations associate chiral (anti)fermions to scalars $e^-_{L,R} \leftrightarrow \tilde{e}^-_{L,R}$ but $e^+_{L,R} \leftrightarrow \tilde{e}^+_{R,L}$. In order to prove this association the use of both beam polarised is necessary [10]. The process $e^+e^- \to \tilde{e}^+\tilde{e}^-$ occurs via γ and Z exchange in the s–channel and via neutralino $\tilde{\chi}^0_i$ exchange in the t–channel. The association can be directly tested only in the t–channel and the use of polarised beams serves to separate this channel. We demonstrate this by isolation of the pair $\tilde{e}^+_L\tilde{e}^-_R$ by the RR configuration of the initial beams in an example where the selectron masses are close together, $m_{\tilde{e}_L} = 200$ GeV, $m_{\tilde{e}_R} = 195$ GeV so that $\tilde{e}_L$, $\tilde{e}_R$ decay via the same decay channels, directly into $\tilde{e}_{L,R} \to \tilde{\chi}^0_1 e$. At a LC it is possible to measure the selectron masses with an accuracy of about 1 GeV [52], e.g. via invariant mass spectra of the decay products. In addition all SM background events, e.g. from W^+W^- are strongly suppressed with this RR configuration. The other Susy parameters are taken as $M_1 = 100$ GeV, $M_2 = 210$ GeV, $\mu = 400$ GeV, $\tan\beta = 20$.

We demonstrate the importance of having both beans polarised in our example, Fig. 1, by isolation of the pair $\tilde{e}^+_L\tilde{e}^-_R$ applying right-handed polarisation of both beams (RR con-

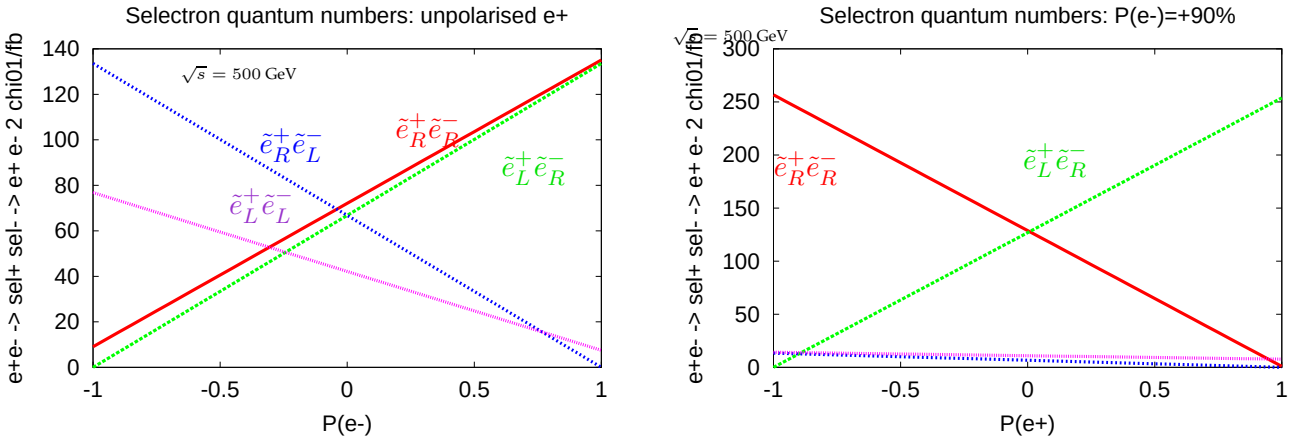

Figure 1: Separation of the selectron pair $\tilde{e}_L^-\tilde{e}_R^+$ in $e^+e^- \to \tilde{e}_{L,R}^+\tilde{e}_{L,R}^- \to e^+e^-2\tilde{\chi}_1^0$ is not possible with electron polarisation only (left); if, however, both beams are polarised the RR configuration separates the pairs and hence the association of the selectrons to the chiral quantum numbers can be exerimentally tested.

figuration, i.e. $P_{e^-} > 0$ and $P_{e^+} > 0$). The selectron masses are close together, $m_{\tilde{e}_L} = 200$ GeV, $m_{\tilde{e}_R} = 195$ GeV, so that both $\tilde{e}_L$, $\tilde{e}_R$ show the same decay, $\tilde{e}_{L,R} \to \tilde{\chi}_1^0 e$. Even extremely high electron polarisation, $P_{e^-} \geq +90\%$, is not sufficient to disentangle the pairs $\tilde{e}_L^+\tilde{e}_R^-$ and $\tilde{e}_R^+\tilde{e}_R^-$ and to test their association to the chiral quantum numbers, since both cross sections are very close to each other, Fig. 1 (left). Only with right-handed polarisation of both beams the pair $\tilde{e}_L^+\tilde{e}_R^-$ is clearly separated, see Fig. 1 (right). In addition, all SM background events, e.g. from W^+W^-, are strongly suppressed with this RR configuration.

3.2 Suppression of SM Background in new physics searches

3.2.1 Supersymmetry: Smuon mass measurement in the continuum

Summary: Smuon production occurs only via (V-A) interaction. In order to provide a possibility to measure the masses already in the continuum the suppression of the SM WW process is absolutely needed. Compared to the case with only a polarised electron beam the signal gains about a factor 1.8 and the background is suppressed by about a factor of 4 with $P_{e^+} = 80\%$. Providing both beams polarised may be decisive to observe all edges and measure $m_{\tilde{\mu}_{L,R}}$ already in the continuum.

It is well known that beam polarisation is suitable to suppress SM background processe in new physics searches. E.g. W^+W^- presents one of the worst backgrounds, however, it can easily be suppressed with right-handed electron/left-handed positron beams. The scaling factors are listed in Table 3.1, [13].

The background suppression may be decisive for the detection of new particles and the precise determination of their properties, e.g. the accurate measurement of $m_{\tilde{\mu}}$ in the continuum. In the case of $\tilde{\mu}^+\tilde{\mu}^-$ production we have only annihilation via γ and Z^0 exchange, therefore the initial beam configurations LR and RL are favoured. The predominant background for the signal is W^+W^- production. An example has been made [75] for the Susy reference point SPS3 [9], where the masses are

$$\tilde{\mu}_R = 178.3\,\text{GeV}, \quad \tilde{\mu}_L = 287.1\,\text{GeV}. \tag{1}$$

The cross sections are shown in Table 3.2 and one notes the considerable reduction in the WW production cross section for right-handed electrons and left-handed positrons. In Fig. 2 the expected muon energy distribution for an integrated luminosity of 500 fb^{-1} at $\sqrt{s} = 750$ GeV and the polarisation configuration $P_{e^-} = -80\%$, $P_{e^+} = +80\%$ (left) and $P_{e^-} = +80\%$, $P_{e^+} = -80\%$ (right) is shown. The background from W^+W^- decaying into the $\mu\nu$ final state is included. Only with polarised e^- and e^+ beams both edges, at around 65 GeV and at around 220 GeV, can be clearly reconstructed. The slepton masses can be determined in the continuum up to a few GeV. This shows the importance of positron polarisation for a clear observation of the low energy edge of the $\tilde{\mu}_L$, which cannot be clearly seen when the positron is unpolarised [75].

The mass reconstruction is involved in the case of selectrons. The e^+e^- energy spectra subtraction technique has been successfully applied to remove SM background [75]. Polarisation of both beams is needed to guarantee sufficient statistics. The mass measurements in the continuum are very important to outline strategies for further threshold scans for specific particles, cf. [52].

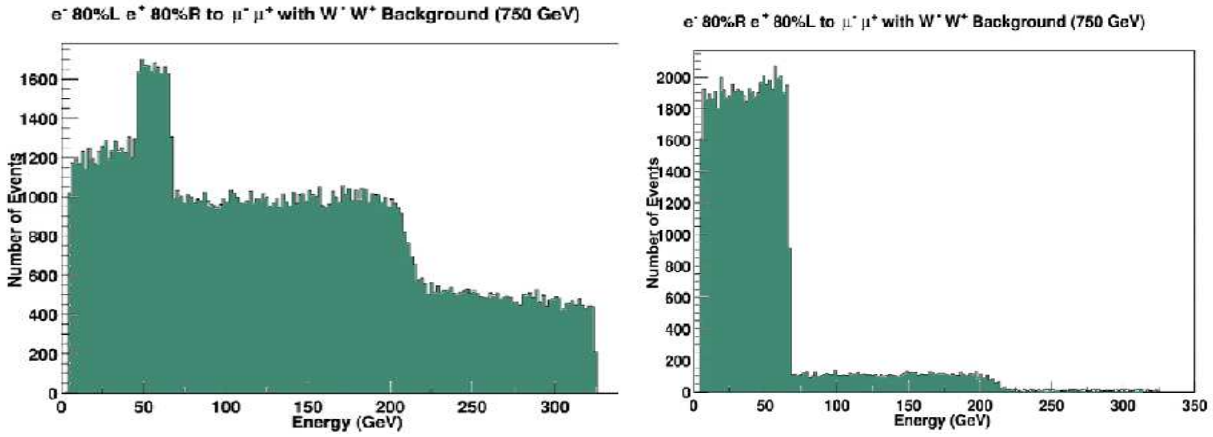

Figure 2: Energy spectrum of muons from $\tilde{\mu}_{L,R}$ decays into $\mu\nu$ final states including the W^+W^- background for the beam polarisations $P_{e^-} = -80\%$, $P_{e^+} = +80\%$ (left) and $P_{e^-} = +80\%$, $P_{e^+} = -80\%$ (right) for $\sqrt{s} = 750$ GeV[10].

Beam polarisation	$e^+e^- \to W^+W^-$	$e^+e^- \to ZZ$
$P_{e^-} = +80\%$, unpol. e^+	0.20	0.76
$P_{e^-} = -80\%$, unpol. e^+	1.80	1.25
$P_{e^-} = +80\%$, $P_{e^+} = -60\%$	0.10	1.05
$P_{e^-} = -80\%$, $P_{e^+} = +60\%$	2.85	1.91

Table 3.1: Scaling factors, i.e. ratios of polarised and unpolarised cross section $\sigma^{pol}/\sigma^{unpol}$, for WW and ZZ production.

Polarisation	$\sigma(\tilde{\mu}^+_R\tilde{\mu}^-_R)$/fb	$\sigma(\tilde{\mu}^+_L\tilde{\mu}^-_L)$/fb	$\sigma(W^+W^-)$/fb
$P_{e^-} = -80\%$, $P_{e^+} = -80\%$	11.44	5.06	1448.
$P_{e^-} = -80\%$, $P_{e^+} = +80\%$	21.23	37.74	12995.
$P_{e^-} = +80\%$, $P_{e^+} = -80\%$	82.99	8.37	198
$P_{e^-} = +80\%$, $P_{e^+} = +80\%$	11.44	5.06	1448
$P_{e^-} = -80\%$, e^+ unpol.	16.34	21.40	7241
$P_{e^-} = +80\%$, e^+ unpol.	47.21	6.72	824

Table 3.2: The cross sections for $e^+e^- \to \tilde{\mu}^+\tilde{\mu}^-$ in fb [75]. One observes a large reduction of the W^+W^- cross section when the electron is right handed and the positron is left handed. It helps significantly in observing $\tilde{\mu}_L$.

δ	M_D ($P_{e^-,e^+}=0$)	M_D ($P_{e^-}=80\%$)	M_D ($P_{e^-}=80\%$, $P_{e^+}=-60\%$	M_D@LHC
2	$\leq$4.48	$\leq$6.27	$\leq$7.86	4-7.5
3	$\leq$3.54	$\leq$4.63	$\leq$5.55	4.5-5.9
4	$\leq$2.91	$\leq$3.64	$\leq$4.23	5.0-5.3

Table 3.3: Discovery (5σ) reach in mass scale M_D in TeV for direct graviton production in the process $e^+e^- \to \gamma G$ at the LC for various numbers of extra dimensions δ and with a normalisation uncertainty of 0.3% [76]; the major background is $e^+e^- \to \nu\bar{\nu}\gamma$ which can be efficiently suppressed with beam polarisation. In the right column the discovery reach for M_D at the LHC is given for the process $pp \to$jet+G with 100 fb^{-1} [77].

3.2.2 Signatures of gravitation and extra dimensions

Summary: The signature for direct graviton production is a relatively soft photon and missing energy. The major background process $\gamma\nu\bar{\nu}$ production. It is possible to determine the mass scale as well as the number of extra dimensions independently. Background suppression with right-handed electrons and left-handed positrons is crucial. Compared to the case with only polarised electrons the background process is suppressed by about a factor of two with 60% positron polarisation whereas the signal is enhanced by about a factor of 1.5. Furthermore the discovery reach is enhanced by 25% (10%) depending on the number of extra dimensions $\delta = 2$ ($\delta = 7$).

The signature for direct graviton production in $e^+e^- \to \gamma G$ is a relatively soft photon and missing energy. The major background is $e^+e^- \to \gamma\nu\bar{\nu}$ and is largely irreducible. The study [76] is done for an integrated luminosity of 1000 fb^{-1} and 800 GeV with polarised beams. The background process shows nearly maximal asymmetry, therefore polarised beams are extremely effective in suppressing the background since ν couples only left-handed.

If extra dimensions are the cause of anomalous single photon rate, the $\sqrt{s}$ dependence of the cross section should follow $\sigma \sim s^{\delta/2}$. Measuring excess cross sections with polarised beams at two different energies, e.g. $\sqrt{s} = 500$ GeV and 800 GeV allows to determine the number of extra dimensions with rather high accuracy [76]. This can be seen from Fig. 3, where the cross section for $e^+e^- \to \gamma G$ as a function of the scale M_D for different numbers δ of extra dimensions is shown. Obviously the reduction of the background process via the use of polarised beams, in particular both beams polarised, may be crucial for the determination of the numbers of extra dimensions.

After applying effective cuts and background simulations the reach for the mass scale M_D of extra dimensions is given Table. 3.3. It is obvious that polarising both beams to a high degree maximises the LC potential for exploring this physics. For regions which can be compared at the LC and the LHC, the upper discovery reach in M_D is similar for both machines. However, for lower values of M_D and for higher valueas of δ the effective approach breaks down at the LHC, whereas at the LC if $\sqrt{s} \ll M_D$ the effective theory should still be valid [76]. The LC offers therefore a more model-independent test of the theory with determining M_D and δ independently.

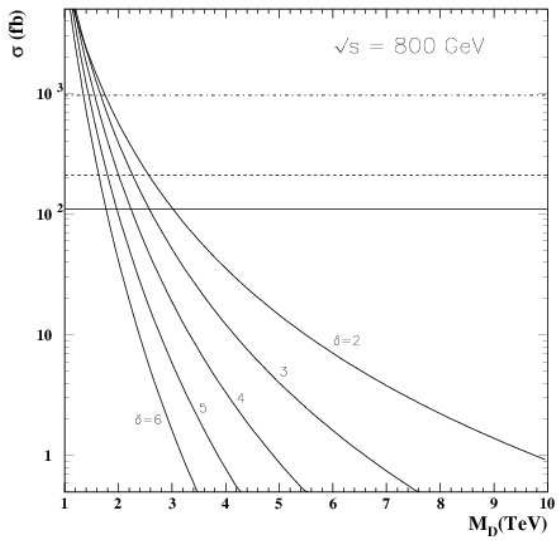

Figure 3: Total cross sections for $e^+e^- \to \gamma G$ at $\sqrt{s} = 800$ GeV as a function of the scale M_D for different numbers δ of extra dimensions. The cross section takes into account 80% electron and 60% positron polarisation. The three horizontal lines indicate the background cross sections from $e^+e^- \to \nu\bar{\nu}\gamma$ for both beams polarised (solid), only electron beam polarisation (dashed) and no polarisation (dot-dashed). The signal cross sections are reduced by a factor of 1.48 for the latter two scenarios [76].

3.3 Standard Model Higgs searches

Summary: One of the major physics goals at a Linear Collider is the precise analysis of all properties of the Higgs particle. For a light Higgs the two major Higgs production processes, Higgsstrahlung, $e^+e^- \to HZ$, and WW fusion, $e^+e^- \to H\nu\bar{\nu}$, will have similar rates; beam polarisation leads to a better separation by a factor of about four with $P_{e^-} = +80\%$, $P_{e^+} = -60\%$ compared to the case with only right-handed polarised electrons. Furthermore one gains a factor of 2 concerning WW background suppression. When determining the general higgs couplings the error is reduced by about 30% compared to the case with only polarised electrons.

If a Higgs particle exists in Nature and has been discovered at the Tevatron or the LHC, the accurate study of its production and decay properties can be performed in the clean environment of e^+e^- linear colliders in order to establish experimentally the Higgs mechanism as the mechanism of electroweak symmetry breaking [11]. The study of Higgs particles will therefore represent a central theme of the ILC physics programme. Beam polarisation does not play the key role for determining the Higgs properties, however, it is very helpful for separating the production processes, suppressing the dominant background processes and improving the accuracy in determining the general couplings. Having both beams polarised gets in this context only statistical importance. Since, however, the study of the Higgs properties plays one of the major goals in the ILC programme we list also the effect of simultaneous polarised beams in the Higgs sector.

3.3.1 Separation of production processes

Higgs production at a LC occurs mainly via WW fusion, $e^+e^- \to H\nu\bar{\nu}$, and Higgsstrahlung $e^+e^- \to HZ$. Polarizing both beams enhances the signal and suppresses background. In Table 3.4 the scaling factors, i.e. ratios of polarized and unpolarized cross section, are compared for two cases (1) $P_{e^-} = \pm 80\%$, which will be henceforth denoted by $(80, 0)$, and (2) $P_{e^-} = \pm 80\%$, $P_{e^+} = \mp 60\%$ denoted throughout the paper as $(80, 60)$ [12].

If a light Higgs with $m_H \leq 130$ GeV is assumed, which is the prefered range both by fits of precision observables in the SM [14] and also by predictions of SUSY theories (see e.g. [15]), Higgsstrahlung dominates for $\sqrt{s} \lesssim 500$ GeV and WW fusion for $\sqrt{s} \gtrsim 500$ GeV. At a LC with $\sqrt{s} = 500$ GeV and unpolarized beams the two processes have comparable cross sections. Beam polarization can be used to enhance the WW–Fusion signal with respect to the HZ contribution by a factor 1.6 (1.7) if electron (electron and positron) beam polarization is available (see Table 3.4). Further, variation of the relative amounts of Higgs-strahlung and WW fusion makes it possible to keep the systematics arising from the contributions to the fitted spectrum for these two processes smaller than the statistical accuracy.

3.3.2 Suppression of background

Beam polarization is very effective for background suppression. With right-handed electron polarization WW and single Z background can be strongly suppressed. The latter is only important at high s. With simultaneous polarization of e^- and e^+ one gains

Configuration	Higgs Production	
$(sgn(P_{e^-})sgn(P_{e^+}))$	$e^+e^- \to H\nu\bar{\nu}$	$e^+e^- \to HZ$
$(+0)$	0.20	0.87
(-0)	1.80	1.13
$(+-)$	0.08	1.26
$(-+)$	2.88	1.70

Table 3.4: Higgs production in Standard Model: Scaling factors, i.e. ratios of polarized and unpolarized cross section $\sigma^{pol}/\sigma^{unpol}$, are given in Higgs production for different polarization configurations with $|P_{e^-}| = 80\%$, $|P_{e^+}| = 60\%$ [12]; the scaling factors for the background processes are given in Table 3.1.

another factor of about 2 in background suppression. Background from ZZ is slightly suppressed with (R0) but not with (RL). To separate the Higgsstrahlung process from WW fusion right-polarized electron configurations are very suitable. Simultaneous left-handed polarized positrons suppress WW fusion and WW background, but enhance the ZZ background. Even in the case when the signal to background ratio, S/B, improves only slightly by simultaneous polarization of the e^- and e^+ beams with (80,60) one gets an improvement in $S/\sqrt{B}$ of about 20% in (Tables 3.4 and 3.1). Polarization of the positron beams is a powerful tool to suppress the single W background, $e^+e^- \to W^-e^+\nu$ and $e^+e^- \to W^+e^-\bar{\nu}$.

3.3.3 Determination of general $ZZ\Phi$ and $Z\gamma\Phi$ couplings

In [16] it has been worked with which accuracy the general coupling between Z–, Vector– and Higgsboson can be determined at the ILC using optimal observables [17]. The study was made for $\sqrt{s} = 500$ GeV and $\mathcal{L} = 300$ fb^{-1} and it turned out that beam polarisation is essential for fixing the $Z\gamma\Phi$ coupling. Simultaneous beam polarization of e^- and e^+ beams results in an further reduction of 20%–30% in the optimal errors compared to the case $(\pm 80, 0)$.

3.4 Supersymmetry

3.4.1 Determination of sfermion parameters

Summary: The advantages of having both beam polarised in sfermion production are – besides the unique test of the chiral quantum numbers, where polarised positrons are absolutely needed, see sect. 3.1 – given by a) larger cross sections by about a factor of 1.7 with $P_{e^-} = +90\%$, $P_{e^+} = -60\%$, b) error reduction by about 25% when determining the parameters, mass and mixing angle, and c) better suppression of possible background processes, see also sect. 3.2.1.

In this section phenomenological studies on the production of third generation sfermions in e^+e^- annihilation at $\sqrt{s} = 500$ GeV are summarised [72]. We take into account the effects of both e^- and e^+ beam polarizations. The main advantages of using polarized beams are: (i) larger cross sections can be obtained, (ii) background reactions can be suppressed, (iii) measurements of appropriate observables lead to additional information on the SUSY parameters. All calculations are performed within the Minimal Supersymmetric Standard Model (MSSM) with real parameters.

Sfermion Production

In the third generation, Yukawa terms give rise to mixing between the 'left' and 'right' states $\tilde{f}_L$ and $\tilde{f}_R$ ($\tilde{f} = \tilde{t}, \tilde{b}, \tilde{\tau}$). Neglecting the mixing between generations this mixing is described by a hermitian 2×2 mass matrix which depends on the soft SUSY–breaking mass parameters $M_{\tilde{Q}}$, $M_{\tilde{U}}$ etc., and the trilinear scalar coupling parameters A_t, A_b, A_τ. The mass eigenstates are $\tilde{f}_1 = \tilde{f}_L \cos\theta_{\tilde{f}} + \tilde{f}_R \sin\theta_{\tilde{f}}$, and $\tilde{f}_2 = \tilde{f}_R \cos\theta_{\tilde{f}} - \tilde{f}_L \sin\theta_{\tilde{f}}$, with $\theta_{\tilde{f}}$ the sfermion mixing angle.

Information on the sfermion mixing angle can be obtained from measuring production cross sections using different combinations of beam polarizations. It has be shown in [71–73] that beam polarisation may be crucial to resolve ambiguities, see as an example Fig. 4, where for the unpolarised case still two mixing angles $\cos 2\theta_{\tilde{\tau}}$ were consistent with the cross sections (red lines). However, using polarised beams projects out a single solution (green and blue line). The simultaneous polarisation of both beams is interesting for enhancing the P_{eff}, enhancing the signal and reducing systematics which might be rather important for $\tilde{\tau}/\tau$ analyses [71].

In the following in detail the production of light stops is discussed. The reaction $e^+e^- \to \tilde{f}_i\bar{\tilde{f}}_j$, $i = 1, 2$ proceeds via γ and Z exchange in the s–channel. The $\tilde{f}_i$ couplings depend on the sfermion mixing angle $\theta_{\tilde{f}}$. In Figs. 5 a, b contour lines of the cross section $\sigma(e^+e^- \to \tilde{t}_1\bar{\tilde{t}}_1)$ as a function of the e^- and e^+ beam polarizations $\mathcal{P}_-$ and $\mathcal{P}_+$ at $\sqrt{s} = 500$ GeV for $m_{\tilde{t}_1} = 200$ GeV and (a) $\cos\theta_{\tilde{t}} = 0.4$ and (b) $\cos\theta_{\tilde{t}} = 0.66$ are shown. Here the initial–state radiation (ISR) and SUSY–QCD corrections are included (for details see [72, 73]). The white windows show the range of polarizations $|P_{e^-}| < 0.9$ and $|P_{e^+}| < 0.6$. As can be seen, one can significantly increase the cross section by using the highest possible e^- and e^+ polarization available. Moreover, beam polarization strengthens the $\cos\theta_{\tilde{t}}$ dependence and can thus be essential for determining the mixing angle. Corresponding cross sections for the production of sbottoms, staus and τ–sneutrinos are

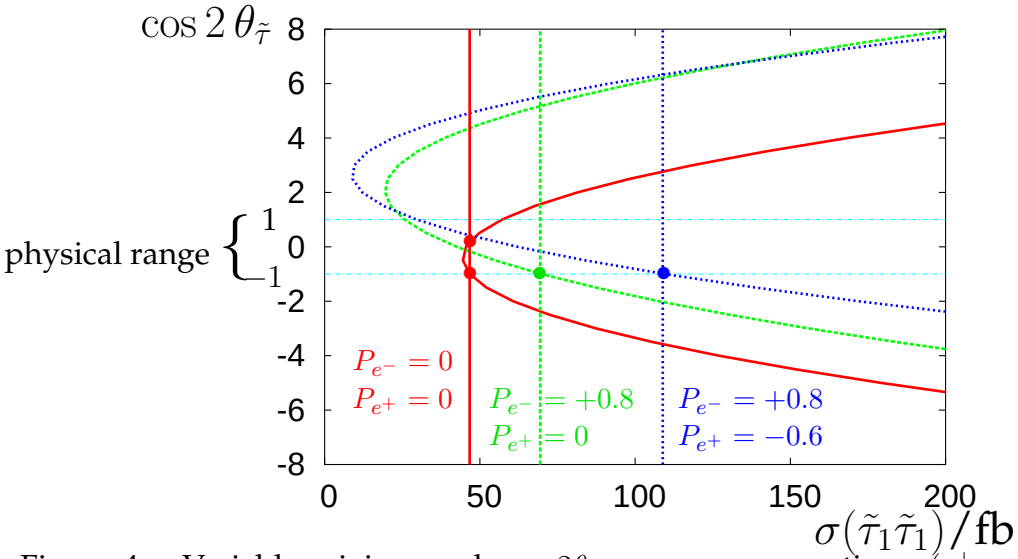

Figure 4: Variable mixing angle $\cos 2\theta_{\tilde{\tau}}$ versus cross section $\sigma(e^+e^- \to \tilde{\tau}_1\tilde{\tau}_1)$ at $\sqrt{s} = 500$ GeV for beam polarisations $P_{e^-} = +0.8$ and unpolarised positrons (green), $P_{e^-} = +0.8$ and $P_{e^+} = -0.6$ (blue) and the unpolarised case (red) for fixed $m_{\tilde{\tau}_1}$ as in the scenario RP. The vertical lines indicate the predicted cross sections in RP. For unpolarised beams one observes a two-fold ambiguity in $\cos 2\theta_{\tilde{\tau}}$ (red dots); for polarised beams, however, only one solution lies in the allowed range (green and blue dot) [71].

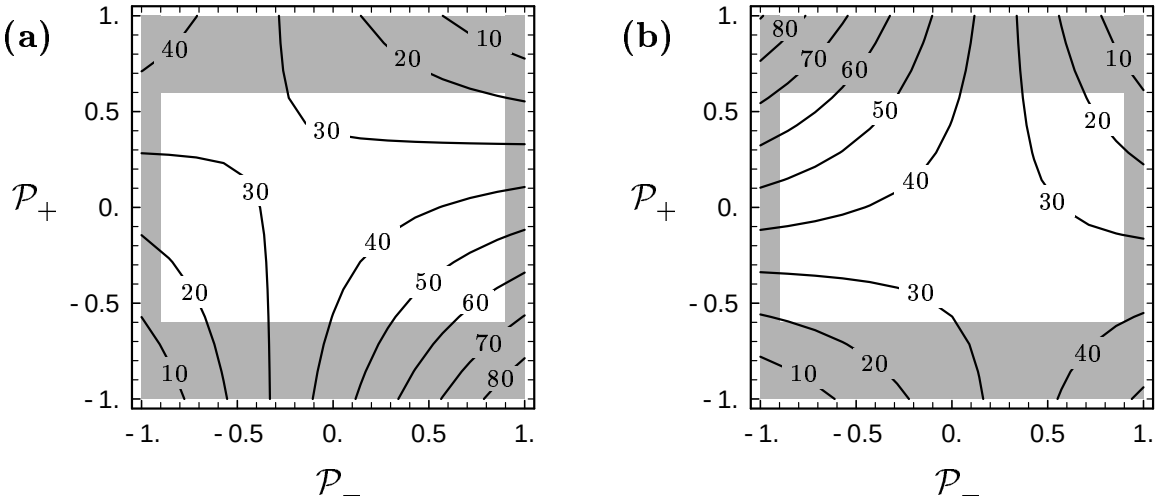

Figure 5: Dependence of $\sigma(e^+e^- \to \tilde{t}_1\bar{\tilde{t}}_1)$/fb on degree of electron and positron polarization at $\sqrt{s} = 500$ GeV, for $m_{\tilde{t}_1} = 200$ GeV, $\cos\theta_{\tilde{t}} = 0.4$ in (a) and $\cos\theta_{\tilde{t}} = 0.66$ in (b).

presented in [72].

Parameter Determination

The precision that one may obtain for the parameters of the $\tilde{t}$ sector from cross section measurements is estimated using the parameter point $m_{\tilde{t}_1} = 200$ GeV, $\cos\theta_{\tilde{t}} = -0.66$ as an illustrative example: For $P_{e^-} = -0.9$ we find $\sigma_L(\tilde{t}_1\bar{\tilde{t}}_1) = 44.88$ fb and for $P_{e^-} = 0.9$

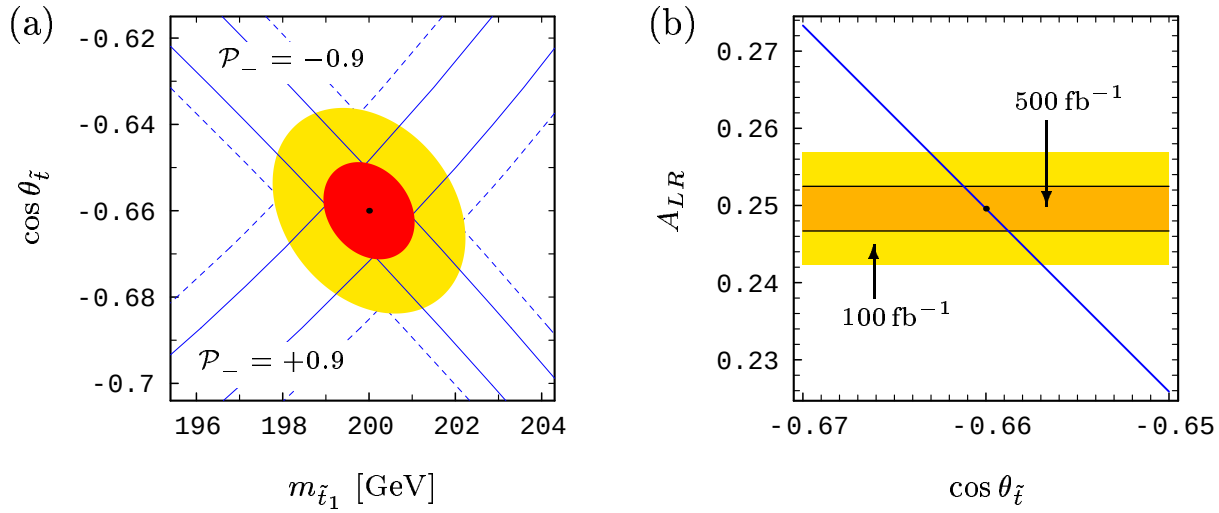

Figure 6: (a) Error bands and 68% CL error ellipse for determining $m_{\tilde{t}_1}$ and $\cos\theta_{\tilde{t}}$ from cross section measurements; the dashed lines are for $\mathcal{L} = 100$ fb^{-1} and the full lines for $\mathcal{L} = 500$ fb^{-1}. (b) Error bands for the determination of $\cos\theta_{\tilde{t}}$ from A_{LR}. In both plots $m_{\tilde{t}_1} = 200$ GeV, $\cos\theta_{\tilde{t}} = -0.66$, $\sqrt{s} = 500$ GeV, $P_{e^-} = \pm 0.9$, $P_{e^+} = 0$.

$\sigma_R(\tilde{t}_1\bar{\tilde{t}}_1) = 26.95$ fb (with $P_{e^+} = 0$) including SUSY–QCD, Yukawa coupling, and ISR corrections. According to the Monte Carlo study of [74] one can expect to measure the $\tilde{t}_1\bar{\tilde{t}}_1$ production cross sections with a statistical error of $\Delta\sigma_L/\sigma_L = 2.1\,\%$ and $\Delta\sigma_R/\sigma_R = 2.8\,\%$ in case of an integrated luminosity of $\mathcal{L} = 500$ fb^{-1} (i.e. $\mathcal{L} = 250$ fb^{-1} for each polarization). Scaling these values to $\mathcal{L} = 100$ fb^{-1} leads to $\Delta\sigma_L/\sigma_L = 4.7\,\%$ and $\Delta\sigma_R/\sigma_R = 6.3\,\%$. Figure 6 a shows the corresponding error bands and error ellipses in the $m_{\tilde{t}_1}$ – $\cos\theta_{\tilde{t}}$ plane. The resulting errors on the stop mass and mixing angle are: $\Delta m_{\tilde{t}_1} = 2.2$ GeV, $\Delta\cos\theta_{\tilde{t}} = 0.02$ ($\Delta m_{\tilde{t}_1} = 1.1$ GeV, $\Delta\cos\theta_{\tilde{t}} = 0.01$) for $\mathcal{L} = 100$ fb^{-1} ($\mathcal{L} = 500$ fb^{-1}). If in addition the e^+ beam is 60% polarized these values can be improved by $\sim 25\%$.

For the determination of the mixing angle, one can also make use of the left–right asymmetry $A_{LR} \equiv [\sigma(-|P_{e^-}|, |P_{e^+}|) - \sigma(|P_{e^-}|, -|P_{e^+}|)]/[\sigma(-|P_{e^-}|, |P_{e^+}|) + \sigma(|P_{e^-}|, -|P_{e^+}|)]$. We get $A_{LR}(e^+e^- \to \tilde{t}_1\bar{\tilde{t}}_1) = 0.2496$ for $m_{\tilde{t}_1} = 200$ GeV, $\cos\theta_{\tilde{t}} = -0.66$, $\sqrt{s} = 500$ GeV, $P_{e^-} = 0.9$, and $P_{e^+} = 0$. Taking into account experimental errors as determined in [74], a theoretical uncertainty of 1%, and $\Delta P/P = 10^{-2}$ we get $\Delta A_{LR} = 2.92\%$ (1.16%) for $\mathcal{L} = 100\,\text{fb}^{-1}$ ($500\,\text{fb}^{-1}$). This corresponds to $\Delta\cos\theta_{\tilde{t}} = 0.0031$ (0.0012). This is most likely the most precise method to determine the stop mixing angle. The corresponding error bands are shown in Fig. 6 b.

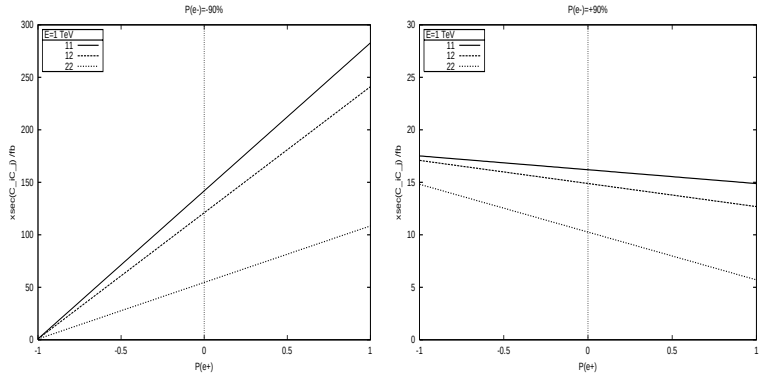

Figure 7: Chargino production: cross sections for $e^+e^- \to \tilde{\chi}_i^- \tilde{\chi}_j^+$ at $\sqrt{s} = 1$ TeV for fixed electron polarization $P_{e^-} = \pm 90\%$ as a function of positron polarization. (SPS1a scenario)

3.4.2 Polarisation effects in the chargino production

Summary: Chargino pairs are produced via (γ,) Z exchange in the annihilation channel and via only left coupling $\tilde{\nu}_e$ exchange in the scattering channel. At high energy the scattering channel is dominant. Therefore one gains almost a facor 2 when using both beam polarised compared to the case with only polarised electrons. Furthermore with both beams polarised a larger amount of observables is available what is crucial for the model-independent determination of the Susy parameters.

Chargino pairs at e^+e^- colliders are produced via s–channel γ and Z exchanges and via t–channel $\tilde{\nu}_e$ exchange. As can be seen in Fig.7 (for the SPS1a scenario) beam polarization can greatly enhance the signal, and therefore increase the $S/\sqrt{B}$ ratio. Measurements of the production cross sections at different beam polarizations can be used to reconstruct completely the chargino system [36]. Moreover, polarized beams can be used to disentangle the chargino and sneutrino parameters exploiting the fact that the $\tilde{\nu}_e$ exchange affects only the amplitude with left-chiral electrons (and right-chiral positrons). If the incoming beams were 100% polarized, one could switch on and off the $\tilde{\nu}_e$ exchange, and analyse the chargino system alone or with $\tilde{\nu}_e$ included, and thus perform an independent determination of chargino and $\tilde{\nu}_e$ parameters. With realistic beam polarization the $\tilde{\nu}_e$ exchange affects all amplitudes depending on the degree of polarization. Nevertheless, the positron polarization, in addition to electron polarization, provides a very powerfull analyzing tool.

3.4.3 Polarisation effects in the neutralino sector

Summary: Neutralino production occurs via (V-A) interaction. However, a complicated interplay between the effects of the neutralino mixing character and the masses of the virtual particles happens. One could gain up to an enhancing factor of about 1.8 for the cross sections with both beams polarised compared to only polarised electrons. To determine the fundamental parameters model independently it is needed to observe cross sections with different polarised beams. It is shown that it can happen that the cross sections do not differ if only polarised electrons were available and both beams polarised are crucial.

Both chargino and neutralino production occurs via gauge boson exchange in the direct channel and via scalar Susy particle exchange in the crossed channel. To perceive the kind of interaction in the crossed channel one has to apply suitable Fierz transformations and afterwards it is obvious that in both processes only pure (V-A) interaction couplings occur. Therefore 'only' the polarisation configuration LR and RL appear. The cross sections in the configurations LL and RR, however, are not vanishing since one has not completely polarised beams. In particular since the neutralinos are mixtures of gauginos (which couple to scalar Susy partners of the left and right electrons) and higgsinos (which couple to the Z boson) interesting features occur when applying all possible polarisation configurations.

Even in the minimal supersymmetric model a huge amount of new free parameter, about 105, occur if no assumptions on a specific Susy breaking scheme and unification assumptions are made. To reveal the structure of the underlying physics and to determine the model it is therefore important to determine the Susy parameters with less as possible model assumptions as possible. Beam polarization may be crucial for the determination of the parameters and the couplings, e.g. from the neutralino sector of supersymmetric models.

Beam polarisation can significantly enhance the signal and therefore improve the ratios S/B and $S/\sqrt{B}$. As can be seen in Figure 8a for a typical mSUGRA type scenario the cross section of the pairs can be enhanced by a factor 1.6 for $(-90, +60)$ compared to the case $(-90, 0)$. For right–polarised electrons similar results are obtained e.g. for $\sigma(\tilde{\chi}^0_3\tilde{\chi}^0_4)$, Figure 8b. In this configuration an even greater advantage of polarizing both beams with different signs is the suppression of the dominant WW background.

Particular interesting is the behaviour of the $\tilde{\chi}^0_2\tilde{\chi}^0_2$ pair, which is enhanced by a factor of 1.6 even for the exceptional configuration $(+90, +60)$ compared to the case $(+90, 0)$! This effect is due to the mixing state of $\tilde{\chi}^0_2 \sim \tilde{W}$, which is not completely suppressed for only $(+90, +60)$. In case of completely polarised beams in the (RR) the cross section for $\tilde{\chi}^0_2\tilde{\chi}^0_2$ would vanish, since – as mentioned before – only (V-A) interaction occurs in this process.

This example shows already that one may use all possible polarisation configuration as observables for determining the Susy parameters. Regarding the large amount of parameters in such a new physics model it is obvious that the interplay with both beams polarised may be extremely helpful and extends the physics potential considerably.

Let us now turn to a further effect when studying polarised cross sections. In lowest order neutralino production occurs via Z, $\tilde{e}_L$ and $\tilde{e}_R$ exchange, so it is sensitive to the chiral couplings and the masses of $\tilde{e}_L$, $\tilde{e}_R$.

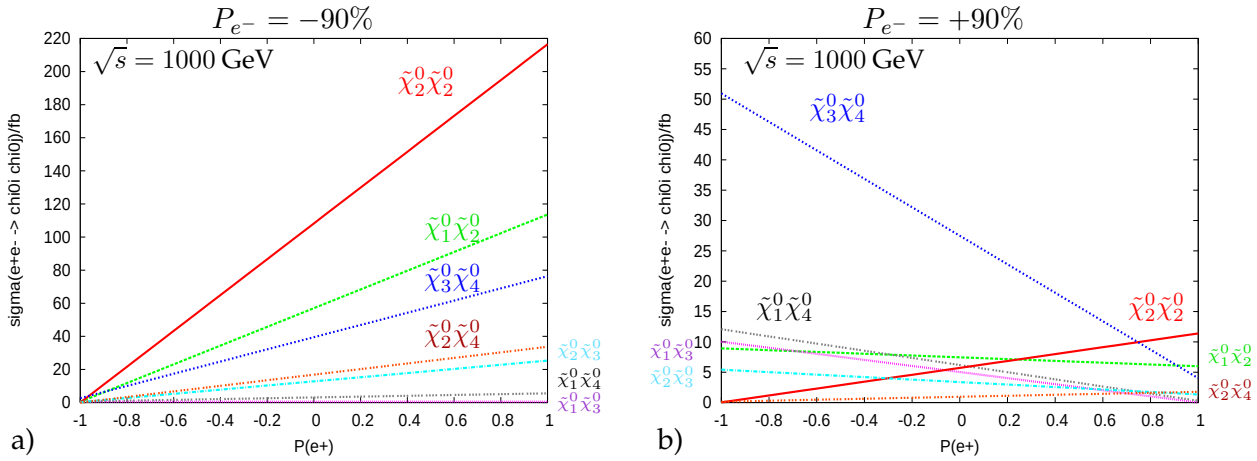

Figure 8: Neutralino production: Cross sections for $e^+e^- \to \tilde{\chi}_i^0\tilde{\chi}_j^0$ [fb] at $\sqrt{s} = 1000$ GeV in our reference scenario SPS1a, where the two lightest neutralinos are gaugino-like and the two heavier neutralinos higgsino-like, are shown for fixed electron polarization, in a) for $P_{e^-} = -90\%$ and in b) for $P_{e^-} = +90\%$, and variable positron polarization, P_{e^+}.

The ordering of the cross sections for different polarization configurations depends on the character of the neutralinos as well as on the masses of the exchanged virtual particles:

- Pure higgsino:

$$\sigma^{LR} > \sigma^{RL} > \sigma^{L0} > \sigma^{00} > \sigma^{R0} > \sigma^{LL} > \sigma^{RR} \tag{2}$$

- Pure gaugino and $m_{\tilde{e}_L} \gg m_{\tilde{e}_R}$:

$$\sigma^{RL} > \sigma^{R0} > \sigma^{00} > \sigma^{RR} > \sigma^{LL} > \sigma^{L0} > \sigma^{LR} \tag{3}$$

- Pure gaugino and $m_{\tilde{e}_L} \ll m_{\tilde{e}_R}$:

$$\sigma^{LR} > \sigma^{L0} > \sigma^{00} > \sigma^{LL} > \sigma^{RR} > \sigma^{R0} > \sigma^{RL} \tag{4}$$

If only the electron is polarized then the orderings of the cross sections for the cases (2) and (4) are equal. If, however, both beams are simultaneously polarized the three cases could be distinguished [65].

To demonstrate once more the complicated interplay between mixing character of the neutralinos, the masses of exchanged Susy particles and beam polarisation we take another Susy example, where the lightest neutralino has 79% gaugino-like, but the second lightest neutralino is about 68% higgsino-like, so that we get an interesting mixture in the cross section. In order to determine the fundamental Susy parameters the observation, i.e. the cross sections of two lightest neutralinos and the lightest chargino are sufficient [49], however the sleptons masses have to be known and different polarised cross sections should be accessible. In case that the slepton masses are unknown more observables have to be accessible. It may be not unnatural in some Susy models, 'split supersymmetry', that the sleptons are much heavier than the light gaugino/higgsino particles.

We now study the cross sections $\sigma(e^+e^- \to \tilde{\chi}_1^0\tilde{\chi}_2^0)$ for all beam polarisation configurations with $|P_{e^-}| = 90\%$, $|P_{e^+}| = 60\%$ for different slepton masses $m_{\tilde{e}_L}$, $m_{\tilde{e}_R}$ for the scenario $M_1 = 90$ GeV, $M_2 = 350$ GeV, $\mu = 140$ GeV, $\tan\beta = 20$, see Table 3.5. These parameters result in the masses for the lightest neutralinos $m_{\tilde{\chi}_1^0} = 76$ GeV, $m_{\tilde{\chi}_2^0} = 142$ GeV and the charginos $m_{\tilde{\chi}_1^\pm} = 130$ GeV, $m_{\tilde{\chi}_2^\pm} = 372$ GeV.

$(m_{\tilde{e}_L}, m_{\tilde{e}_R})$ [GeV]	$\sigma(e^+e^- \to \tilde{\chi}_1^0\tilde{\chi}_2^0)$/fb unpolarised	$\sigma^{\text{pol}}/\sigma^{\text{unpol}}$					
		$(-0.9, 0)$	$(+0.9, 0)$	$(-0.9, +0.6)$	$(+0.9, -0.6)$	$(-0.9, -0.6)$	$(+0.9, +0.6)$
(200, 200)	102	0.4	1.6	0.6	2.5	0.3	0.7
(500, 500)	29	0.5	1.5	0.7	2.4	0.3	0.6
(1000, 1000)	7.4	0.7	1.3	1.1	2.0	0.4	0.6
(1500, 1500)	4.0	0.9	1.1	1.3	1.8	0.4	0.5
(2000, 2000)	2.9	1.0	1.0	1.5	1.6	0.5	0.5
(500, 1500)	8.7	1.4	0.6	2.3	0.8	0.6	0.3
(1500, 500)	24	0.2	1.8	0.3	2.8	0.2	0.7

Table 3.5: Polarised cross sections $\sigma(e^+e^- \to \tilde{\chi}_1^0\tilde{\chi}_2^0)$/fb at $\sqrt{s} = 500$ GeV with all possible beam polarisation configurations for ($P_{e^-} = \pm 90\%$, $P_{e^+} = \pm 60\%$) and for different selectron masses $m_{\tilde{e}_{L,R}}$. The Susy parameters are given by $M_1 = 90$ GeV, $M_2 = 350$ GeV, $\mu = 140$ GeV, $\tan\beta = 20$ and the resulting masses are $m_{\tilde{\chi}_1^0} = 76$ GeV, $m_{\tilde{\chi}_2^0} = 142$ GeV.

3.4.4 CP asymmetries in neutralino and chargino production and decay

Summary: Sensitive observables for CP violation are T-odd asymmetries, builded by triple products between initial and two outgoing leptons or CP-odd asymmetries, given by the polarisation of final leptons. In the chargino/neutralino sector the value of the T-odd as well as the CP-odd asymmetries might be only slightly enhanced by simultaneously polarised positrons if highly longitudinally polarised electrons are available. However, the cross section is enhanced by about a factor of two. Therefore the measurability of the asymmetries is enhanced by about a factor of 1.3 compared to the case with only polarised electrons.

Particularly interesting in supersymmetry is the study of new additional CP violating sources. In the following we show a suitable observable for verifying CP violation in the gaugino/higgsino sector.

In the neutralino and chargino sectors of the Minimal Supersymmetric Standard Model (MSSM) [51], the gaugino mass parameter M_1, the higgsino mass parameter μ, and the trilinear coupling parameter A_τ in the stau sector, can be complex. The physical phases φ_{M_1}, φ_μ and φ_{A_τ} of these parameters can cause large CP-violating effects already at tree level [53–61, 66]. In the following we focus on the dependence on the beam polarisations of these CP-violating effects in neutralino production and decay.

In neutralino production

$$e^- + e^+ \;\; \rightarrow \;\; \tilde{\chi}_i^0 + \tilde{\chi}_j^0 \tag{5}$$

and the subsequent leptonic two-body decays

$$\tilde{\chi}_i^0 \;\; \rightarrow \;\; \tilde{\ell} + \ell_1 \quad \text{and} \quad \tilde{\ell} \rightarrow \tilde{\chi}_1^0 + \ell_2, \tag{6}$$

as well as the subsequent leptonic three-body decays

$$\tilde{\chi}_2^0 \longrightarrow \tilde{\chi}_1^0 + l_1 + l_2, \tag{7}$$

where $\ell_{1,2} = e, \mu, \tau$, the neutralino spin correlations allow the definition of several CP-odd asymmetries. The amplitude squared of the combined processes of production, Eq. (5), and decays, Eq. (6) and (7), can be written as

$$|T|^2 = PD + \Sigma_P^a \Sigma_D^a, \tag{8}$$

where P and D describe production and decay without spin correlation and Σ_P^a and Σ_D^a ($a = 1, 2, 3$) are the terms with spin correlation [69]. In Σ_P^a and Σ_D^a products like $i\epsilon_{\mu\nu\rho\sigma} p_i^\mu p_j^\nu p_k^\rho p_l^\sigma$ appear. This leads to CP-violating effects already at tree level.

We introduce the triple product $\mathcal{T} = (\vec{p}_{e^-} \times \vec{p}_{\ell_2}) \cdot \vec{p}_{\ell_1}$, where $\vec{p}_{e^-}, \vec{p}_{l_1}$ and $\vec{p}_{l_2}$ are the momenta of initial e^- beam and the two final leptons l_1 and l_2, respectively. We define a *T-odd* asymmetry of the cross section σ for the processes (5)–(7):

$$\mathcal{A}_{\mathrm{T}} = \frac{\sigma(\mathcal{T} > 0) - \sigma(\mathcal{T} < 0)}{\sigma(\mathcal{T} > 0) + \sigma(\mathcal{T} < 0)} = \frac{\int \mathrm{sign}\{\mathcal{T}\} |T|^2 d\mathrm{lips}}{\int |T|^2 d\mathrm{lips}}. \tag{9}$$

If absorptive phases from final state interactions and finite-widths effects are neglected, $\mathcal{A}_{\mathrm{T}}$ is CP-odd due to CPT invariance. $\mathcal{A}_{\mathrm{T}}$ is proportional to the difference of the number

of events with the final lepton l_1 above and below the plane spanned by $\vec{p}_{e^-}$ and $\vec{p}_{l_2}$. The dependence of $\mathcal{A}_{\rm T}$ on φ_{M_1} and φ_μ has been analysed in [53–55, 61].

In the case the neutralino decays into a τ-lepton, $\tilde{\chi}_i^0 \to \tilde{\tau}_k^\pm \tau^\mp$, $k = 1, 2$, the T-odd transverse τ^- and τ^+ polarisations P_2 and $\bar{P}_2$, respectively, give rise to the *CP-odd* observable

$$\mathcal{A}_{\rm CP} = \frac{1}{2}(P_2 - \bar{P}_2), \tag{10}$$

which is also sensitive to φ_{A_τ}. For several MSSM scenarios, $\mathcal{A}_{\rm CP}$ has been discussed in [59].

For measuring the asymmetries $\mathcal{A}_{\rm T}$ and $\mathcal{A}_{\rm CP}$ it is crucial to have both large asymmetries and large cross sections σ. In the following we study the impact of longitudinally polarised e^+ and e^- beams of a future linear collider in the 500 GeV range on $\mathcal{A}_{\rm T}$, $\mathcal{A}_{\rm CP}$ and σ.

Numerical results for two-body decays

We present numerical results for $e^+e^- \to \tilde{\chi}_1^0\tilde{\chi}_2^0$ with the subsequent leptonic two-body decay of $\tilde{\chi}_2^0$ for a linear collider with $\sqrt{s} = 500$ GeV. For $\mathcal{A}_{\rm T}$, Eq. (9), we study the neutralino decay into the right selectron and right smuon, $\tilde{\chi}_2^0 \to \tilde{\ell}_R \ell_1$, $\ell = e, \mu$ and for $\mathcal{A}_{\rm CP}$, Eq. (10), that into the lightest scalar tau, $\tilde{\chi}_2^0 \to \tilde{\tau}_1 \tau$. We study the dependence of the asymmetries and the cross sections on the beam polarisations P_{e^-} and P_{e^+} for fixed parameters $\mu = |\mu|\, e^{i\,\varphi_\mu}$, $M_1 = |M_1|\, e^{i\,\varphi_{M_1}}$, $A_\tau = |A_\tau|\, e^{i\,\varphi_{A_\tau}}$, M_2 and $\tan\beta$. We assume $|M_1| = 5/3 M_2 \tan^2\theta_W$ and use the renormalization group equations [62] for the selectron and smuon masses, $m^2_{\tilde{\ell}_R} = m_0^2 + 0.23 M_2^2 - m_Z^2 \cos 2\beta \sin^2\theta_W$ with $m_0 = 100$ GeV. The interaction Lagrangians and details on stau mixing can be found in [55].

In Fig. 9a we show the dependence of $\mathcal{A}_{\rm T}$ on the beam polarisation for $\varphi_{M_1} = 0.2\,\pi$ and $\varphi_{A_\tau} = \varphi_\mu = 0$. A small value of φ_μ is suggested by constraints on electron and neutron electric dipole moments (EDMs) [63] for a typical SUSY scale of the order of a few 100 GeV. It is remarkable that in our scenario the asymmetry can be close to 10% even for the small value of $\varphi_{M_1} = 0.2\,\pi$ and for $\varphi_\mu = 0$. The cross section $\sigma = \sigma(e^+e^- \to \tilde{\chi}_1^0\tilde{\chi}_2^0) \times {\rm BR}(\tilde{\chi}_2^0 \to \tilde{\ell}_R\ell_1) \times {\rm BR}(\tilde{\ell}_R \to \tilde{\chi}_1^0\ell_2)$ is shown in Fig. 9b. For our scenario with $|A_\tau| = 250$ GeV and $\varphi_{A_\tau} = 0$, the neutralino branching ratio is ${\rm BR}(\tilde{\chi}_2^0 \to \tilde{\ell}_R\ell_1) = 0.63$ (summed over both signs of charge) and ${\rm BR}(\tilde{\ell}_R \to \tilde{\chi}_1^0\ell_2) = 1$. Note that the asymmetry $\mathcal{A}_{\rm T}$ and the cross section σ are both considerably enhanced for negative positron and positive electron beam polarisation. This choice of polarisation enhances the contributions of the right slepton exchange in the neutralino production, Eq. (5), and reduces that of left slepton exchange [64, 65]. While the contributions of right and left slepton exchange enter σ with the same sign, they enter $\mathcal{A}_{\rm T}$ with opposite sign, which accounts for the sign change of $\mathcal{A}_{\rm T}$.

In Fig. 10a we show the contour lines of the τ polarisation asymmetry $\mathcal{A}_{\rm CP}$, Eq. (10), for $\varphi_{A_\tau} = 0.5\pi$ and $\varphi_{M_1} = \varphi_\mu = 0$ in the P_{e^-}-P_{e^+} plane. We have chosen a large value of $|A_\tau| = 1500$ GeV because $\mathcal{A}_{\rm CP}$ increases with increasing $|A_\tau| \gg |\mu| \tan\beta$ [59]. For unpolarised beams the asymmetry is 1%. However, it reaches values of more than $\pm 13\%$ if the e^+ and e^- beams are polarised with the opposite sign. If at least one of the beams is polarised (e.g. $P_{e^-} = 0.8$, $P_{e^+} = 0.6$), the asymmetries are somewhat smaller ($\sim 10\%$). The reason for this dependence is again the enhancement of either the right or the left selectron exchange contributions in the production process. The cross section $\sigma = \sigma(e^+e^- \to \tilde{\chi}_1^0\tilde{\chi}_2^0) \times {\rm BR}(\tilde{\chi}_2^0 \to$

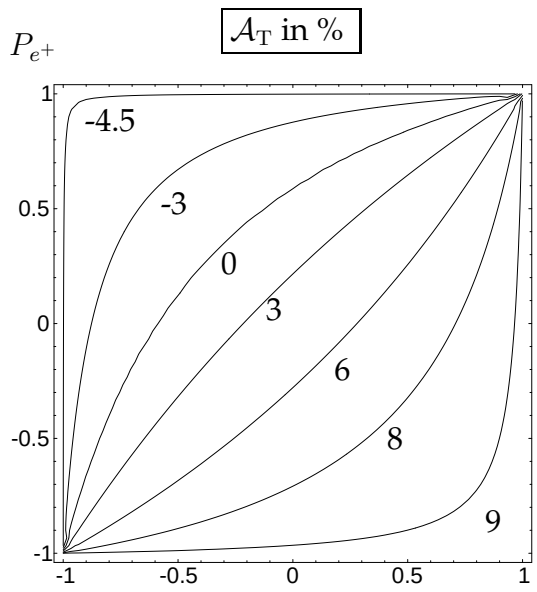

Fig. 9a

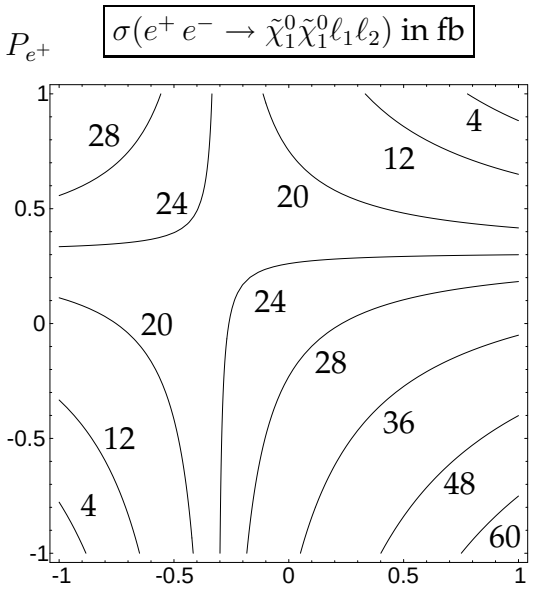

Fig. 9b

Figure 9: Contour lines of $\mathcal{A}_{\rm T}$ and σ for $\varphi_{M_1} = 0.2\pi$, $\varphi_\mu = 0$, $|\mu| = 240$ GeV, $M_2 = 400$ GeV, $\tan\beta = 10$ and $m_0 = 100$ GeV.

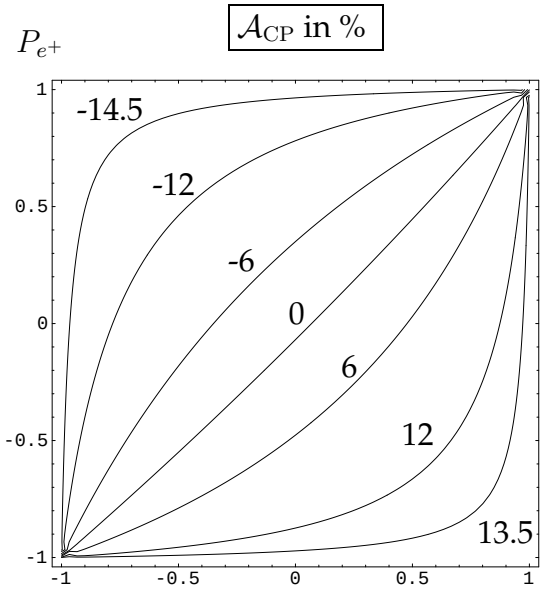

Fig. 10a

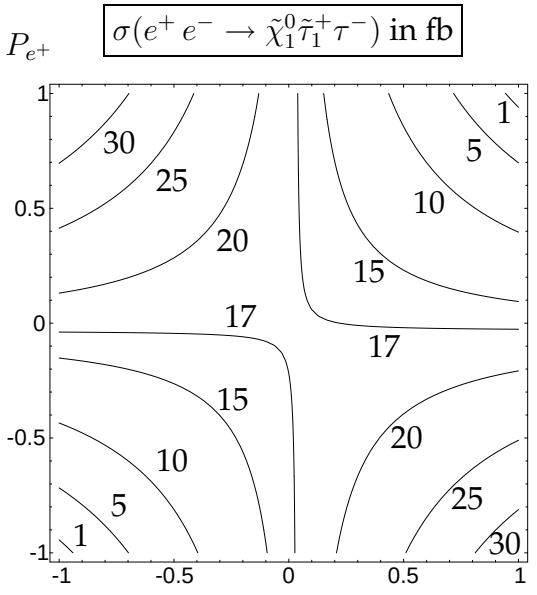

Fig. 10b

Figure 10: Contour lines of $\mathcal{A}_{\rm CP}$ and σ for $\varphi_{A_\tau} = 0.5\pi$, $|A_\tau| = 1500$ GeV, $\varphi_{M_1} = \varphi_\mu = 0$, $|\mu| = 250$ GeV, $M_2 = 200$ GeV, $\tan\beta = 5$ and $m_0 = 100$ GeV.

$\tilde{\tau}_1^+\tau^-$) is shown in Fig. 10b with $\mathrm{BR}(\tilde{\chi}_2^0 \to \tilde{\tau}_1^+\tau^-) = 0.22$. Also σ is very sensitive to variations of the beam polarisation and varies between 1 fb and 30 fb.

Since the asymmetry $\mathcal{A}_{\rm CP}$ is also very sensitive to the phases φ_{M_1} and φ_μ we show for $\varphi_{M_1} = 0.2\pi$ and $\varphi_\mu = \varphi_{A_\tau} = 0$, the dependence of $\mathcal{A}_{\rm CP}$ and $\sigma = \sigma(e^+e^- \to \tilde{\chi}_1^0\tilde{\chi}_2^0)\times\mathrm{BR}(\tilde{\chi}_2^0 \to \tilde{\tau}_1^+\tau^-)$ on the beam polarisation in Figs. 11a, b, respectively. The neutralino branching ratio is $\mathrm{BR}(\tilde{\chi}_2^0 \to \tilde{\tau}_1^+\tau^-) = 0.19$ for our scenario. Despite the small phases, $\mathcal{A}_{\rm CP}$ reaches

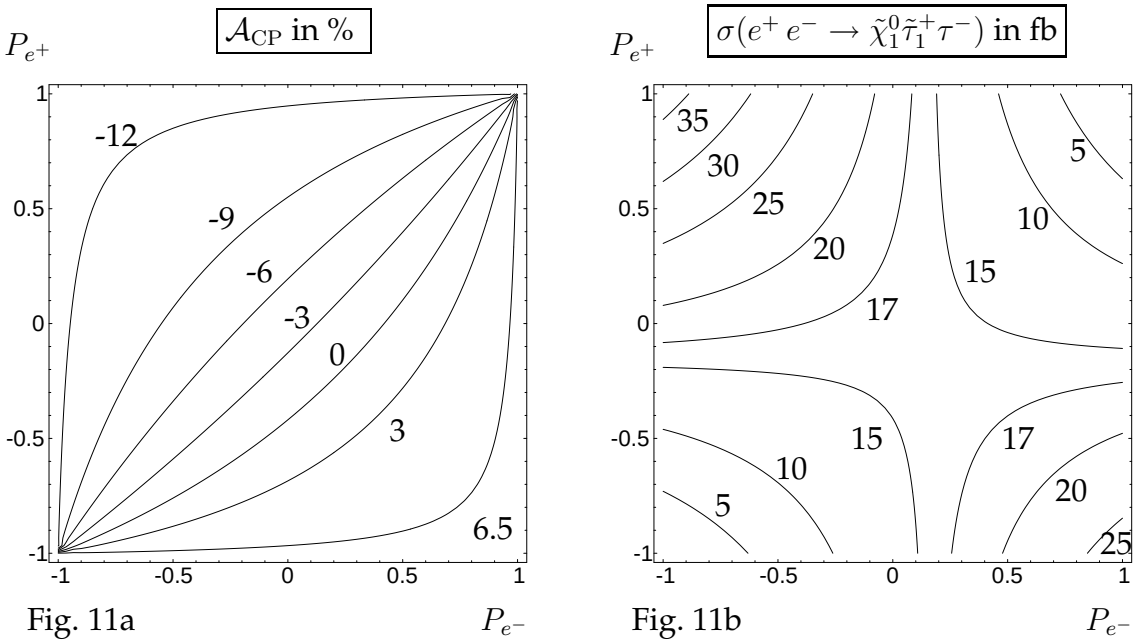

Fig. 11a Fig. 11b

Figure 11: Contour lines of $\mathcal{A}_{\rm CP}$ and σ for $\varphi_{M_1} = 0.2\pi$, $\varphi_\mu = 0$, $|\mu| = 250$ GeV, $M_2 = 200$ GeV, $\varphi_{A_\tau} = 0$, $|A_\tau| = 250$ GeV, $\tan\beta = 5$ and $m_0 = 100$ GeV.

values up to -12% for negative e^- and positive e^+ beam polarisations.

Numerical results for three-body decays

In this subsection we analyse numerically the influence of longitudinal e^- and e^+ beam polarisations on the T-odd asymmetry $\mathcal{A}_{\rm T}$, Eq. (9), for $e^+e^- \to \tilde{\chi}_i^0\tilde{\chi}_2^0$, $i = 1, 3$ and subsequent leptonic three-body decay $\tilde{\chi}_2^0 \to \tilde{\chi}_1^0\ell^-\ell^+$, $\ell = e, \mu$ (i.e. $\ell_1 = \ell^-$, $\ell_2 = \ell^+$, $\mathcal{T} = (\vec{p}_{e^-} \times \vec{p}_{\ell^+}) \cdot \vec{p}_{\ell^-}$). We fix the centre of mass energy $\sqrt{s} = 500$ GeV and the phases $\varphi_{M_1} = 0.2\pi$ and $\varphi_\mu = 0$. In Figs. 12(a) and (b) we show $\mathcal{A}_{\rm T}$ as a function of the e^- beam polarisation P_{e^-} for different e^+ beam polarisations P_{e^+}, $-0.6 \le P_{e^+} \le +0.6$, in the scenario $|M_1| = 150$ GeV, $M_2 = 300$ GeV, $|\mu| = 200$ GeV, $\tan\beta = 10$, $m_{\tilde{\ell}_L} = 267.6$ GeV, $m_{\tilde{\ell}_R} = 224.4$ GeV with large mixing between the gaugino and higgsino components of $\tilde{\chi}_1^0$, $\tilde{\chi}_2^0$ and $\tilde{\chi}_3^0$. In this scenario $|\mathcal{A}_{\rm T}|$ is maximal for $\varphi_{M_1} = 0.2\pi$ [61]. For both production processes $\mathcal{A}_{\rm T}$ is positive (negative) for $P_{e^-} \to -1$ ($P_{e^-} \to +1$). For these polarisations the $\tilde{e}_L$ ($\tilde{e}_R$) contributions to the spin density matrix are dominating. For $(P_{e^-}, P_{e^+}) = (-0.9, 0)$ ($(P_{e^-}, P_{e^+}) = (+0.9, 0)$) one gets $\mathcal{A}_{\rm T} = +9.0\,\%$ ($\mathcal{A}_{\rm T} = -6.2\,\%$) for $\tilde{\chi}_1^0\tilde{\chi}_2^0$ production and $\mathcal{A}_{\rm T} = +8.3\,\%$ ($\mathcal{A}_{\rm T} = -4.8\,\%$) for $\tilde{\chi}_3^0\tilde{\chi}_2^0$ production, respectively. An additional positron beam polarisation of opposite sign only slightly enhances these asymmetries. However, it considerably enhances the corresponding cross section σ of the combined production and decay process and hence the expected rate to measure $\mathcal{A}_{\rm T}$ by a factor of about 1.5 (see Figs. 12(c) and (d)).

The relative statistical error of $\mathcal{A}_{\rm T}$ is given by $\delta\mathcal{A}_{\rm T} = \Delta\mathcal{A}_{\rm T}/\mathcal{A}_{\rm T} = S/(\mathcal{A}_{\rm T}\sqrt{N})$ with S standard deviation and the number of events $N = \sigma\mathcal{L}$ for a total integrated luminosity $\mathcal{L}$. Assuming $\delta\mathcal{A}_{\rm T} \approx 1$ for $\mathcal{A}_{\rm T}$ to be measurable it follows $S \approx |\mathcal{A}_{\rm T}|\sqrt{\sigma\mathcal{L}}$ [55]. In Table 3.6 we give $\mathcal{A}_{\rm T}$, σ and the corresponding standard deviations S of $\mathcal{A}_{\rm T}$ for $\mathcal{L} = 500$ fb^{-1} and several sets of beam polarisations. For $\tilde{\chi}_1^0\tilde{\chi}_2^0$ production S raises from $S = 1.0$ for $(P_{e^-}, P_{e^+}) =$

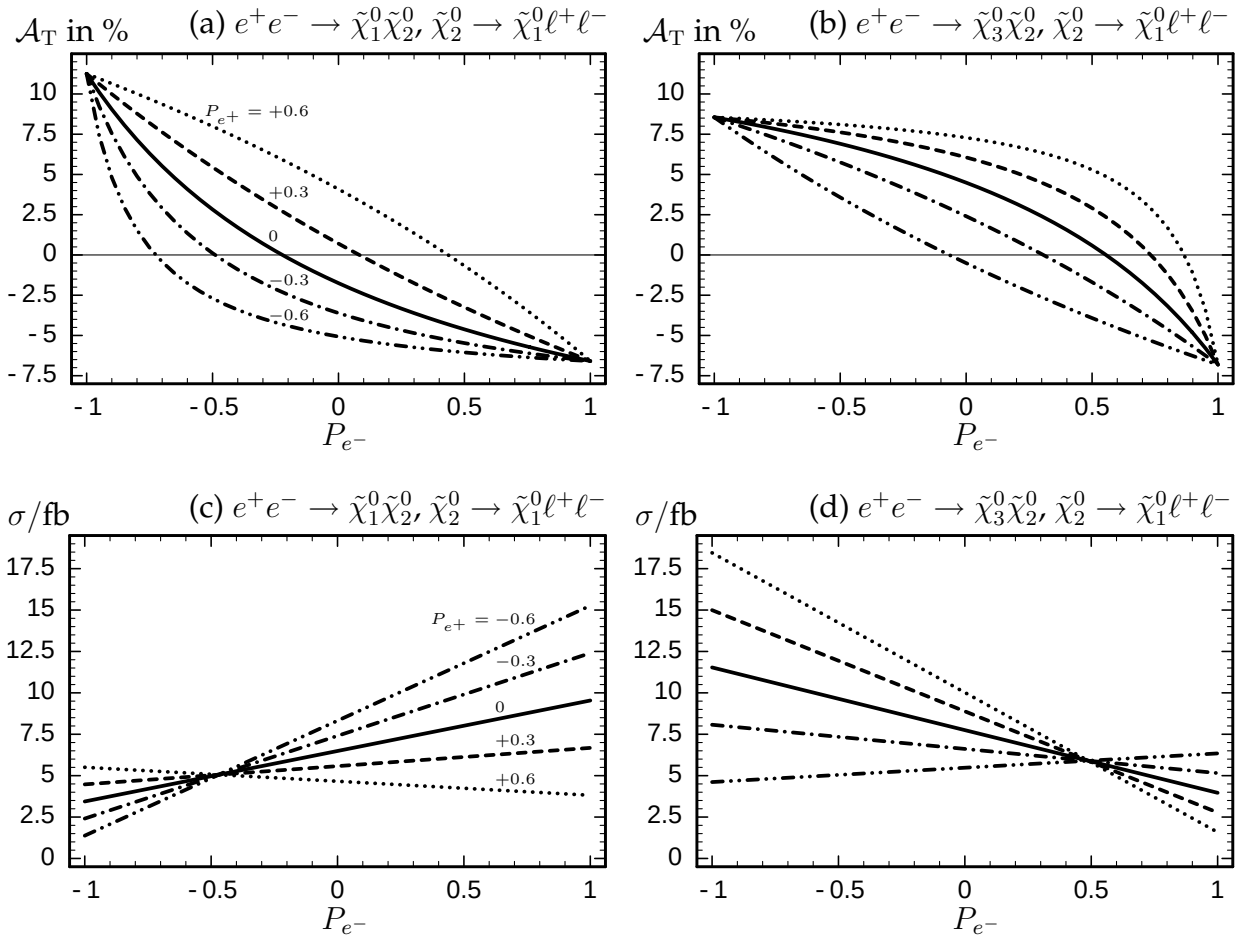

Figure 12: (a),(b) T-odd asymmetry $\mathcal{A}_{\rm T}$, Eq. (9), for $e^+e^- \to \tilde\chi_i^0\tilde\chi_2^0$, (a) $i = 1$ and (b) $i = 3$, with subsequent leptonic three-body decay $\tilde\chi_2^0 \to \tilde\chi_1^0\ell^+\ell^-$, and (c), (d) the corresponding cross section $\sigma = \sigma(e^+e^- \to \tilde\chi_i^0\tilde\chi_2^0)\cdot{\rm BR}(\tilde\chi_2^0 \to \tilde\chi_1^0\ell^+\ell^-)$, (c) $i = 1$ and (d) $i = 3$, summed over $\ell = e, \mu$, in the scenario $|M_1| = 150$ GeV, $\varphi_{M_1} = 0.2\pi$, $M_2 = 300$ GeV, $|\mu| = 200$ GeV, $\varphi_\mu = 0$, $\tan\beta = 10$, $m_{\tilde\ell_L} = 267.6$ GeV, $m_{\tilde\ell_R} = 224.4$ GeV as a function of the e^- beam polarisation P_{e^-} for different e^+ beam polarisations P_{e^+} and $\sqrt{s} = 500$ GeV.

$(0, 0)$ to $S = 4.2$ for $(P_{e^-}, P_{e^+}) = (+0.9, 0)$ and with additional positron beam polarisation to $S = 5.6$ for $(P_{e^-}, P_{e^+}) = (+0.9, -0.6)$. For $\tilde\chi_3^0\tilde\chi_2^0$ production the largest values for S arise for negative electron beam polarisation. The values are $S = 2.8$ for $(P_{e^-}, P_{e^+}) = (0, 0)$, $S = 6.2$ for $(P_{e^-}, P_{e^+}) = (-0.9, 0)$ and $S = 8.0$ for $(P_{e^-}, P_{e^+}) = (-0.9, +0.6)$.

Summary and conclusion

Within the MSSM we have analysed the dependence on the beam polarisation of CP-odd asymmetries in $e^+e^- \to \tilde\chi_i^0\tilde\chi_2^0$, $i = 1, 3$, and the subsequent leptonic two-body and three-body decays of $\tilde\chi_2^0$. For the process $e^+e^- \to \tilde\chi_1^0\tilde\chi_2^0$, $\tilde\chi_2^0 \to \tilde\ell_R\ell_1$, $\tilde\ell_R \to \tilde\chi_1^0\ell_2$ with $\ell_{1,2} = e, \mu$, we have found that the asymmetry $\mathcal{A}_{\rm T}$ of the triple product $(\vec p_{e^-} \times \vec p_{\ell_2}) \cdot \vec p_{\ell_1}$, which is sensitive to φ_{M_1} and φ_μ, can be twice as large if polarised beams are used, with e.g. $P_{e^-} = 0.8$ and $P_{e^+} = -0.6$. Also for these polarisations the cross section can be enhanced up to a factor of 2. For the neutralino decay, $\tilde\chi_2^0 \to \tilde\tau_1^\mp\tau^\pm$, we have given numerical

	$e^+e^- \to \tilde{\chi}_1^0\tilde{\chi}_2^0,\ \tilde{\chi}_2^0 \to \tilde{\chi}_1^0\ell^+\ell^-$					$e^+e^- \to \tilde{\chi}_3^0\tilde{\chi}_2^0,\ \tilde{\chi}_2^0 \to \tilde{\chi}_1^0\ell^+\ell^-$				
(P_{e^-}, P_{e^+})	$(0,0)$	$(-,0)$	$(-,+)$	$(+,0)$	$(+,-)$	$(0,0)$	$(-,0)$	$(-,+)$	$(+,0)$	$(+,-)$
$\mathcal{A}_{\rm T}$ in %	-1.8	9.0	10.6	-6.2	-6.5	4.5	8.3	8.5	-4.8	-6.3
σ/fb	6.5	3.7	5.4	9.2	14.6	7.8	11.2	17.6	4.3	6.3
S	1.0	3.9	5.5	4.2	5.6	2.8	6.2	8.0	2.2	3.5

Table 3.6: T-odd asymmetry $\mathcal{A}_{\rm T}$, Eq. (9), for $e^+e^- \to \tilde{\chi}_i^0\tilde{\chi}_2^0$, $i = 1, 3$, with subsequent leptonic three-body decay $\tilde{\chi}_2^0 \to \tilde{\chi}_1^0\ell^+\ell^-$, the corresponding cross section $\sigma = \sigma(e^+e^- \to \tilde{\chi}_i^0\tilde{\chi}_2^0) \cdot {\rm BR}(\tilde{\chi}_2^0 \to \tilde{\chi}_1^0\ell^+\ell^-)$, summed over $\ell = e, \mu$, and the standard deviations $S = |\mathcal{A}_{\rm T}|\sqrt{\sigma\mathcal{L}}$ for $\mathcal{L} = 500\,{\rm fb}^{-1}$ in the scenario $|M_1| = 150$ GeV, $\varphi_{M_1} = 0.2\pi$, $M_2 = 300$ GeV, $|\mu| = 200$ GeV, $\varphi_\mu = 0$, $\tan\beta = 10$, $m_{\tilde{\ell}_L} = 267.6$ GeV, $m_{\tilde{\ell}_R} = 224.4$ GeV for $\sqrt{s} = 500$ GeV and several beam polarisations (P_{e^-}, P_{e^+}) with $(\pm, \pm) \equiv (\pm 0.9, \pm 0.6)$.

examples for the beam polarisation dependence of the CP-odd τ polarisation asymmetry $\mathcal{A}_{\rm CP}$, which is also sensitive to φ_{A_τ}. Both $\mathcal{A}_{\rm CP}$ and the cross section depend sensitively on the beam polarisations and can be enhanced by a factor between 2 and 3. We have further analysed the dependence on longitudinal beam polarisations of the CP asymmetry $\mathcal{A}_{\rm T}$ in neutralino production with subsequent leptonic three-body decay. For the process $e^+e^- \to \tilde{\chi}_i^0\tilde{\chi}_2^0$, $\tilde{\chi}_2^0 \to \tilde{\chi}_1^0\ell^+\ell^-$, $i = 1$ ($i = 3$) the asymmetry $\mathcal{A}_{\rm T}$ is enhanced by a factor 3.6 (1.9) and the cross section by a factor 2.2 (2.3) for beam polarisations $P_{e^-} = +0.9$ and $P_{e^+} = -0.6$ ($P_{e^-} = -0.9$ and $P_{e^+} = +0.6$) in comparison to the unpolarised case. This set of beam polarisations results in the largest value $S = 5.6$ ($S = 8.0$) of the expected standard deviations in the measurement of $\mathcal{A}_{\rm T}$.

3.4.5 Polarisation effects in extended MSSM models

3.4.5.1 Production of singlino-like neutralinos

Summary: Nonminimal extensions of the MSSM, e.g. by adding an additional Higgs singlet or new gauge bosons, enlarges also the neutralino sector. Singlino dominated production results in extremely small cross sections. It has been shown that polarisation of both beams may be crucial for a) observing singlino dominated signals and b) for distinguishing between the MSSM and the extended model. Both beams polarised enhances the rates by about a factor 1.6 as well as the accessibility of the singlet vev by about a factor 1.3 compared to the case with only polarised electrons. Furthermore the produced light neutralinos may show exactly opposite polarisation so that a model distinction is possible.

Nonminimal extensions of the Minimal Supersymmetric Standard Model (MSSM) are characterized by an additional singlet superfield with vacuum expectation value x. The singlino character of these singlino-dominated neutralinos crucially depend on the parameter x. In the Next-to-Minimal Supersymmetric Standard Model (NMSSM) [37–40] or an E_6 inspired model with one extra neutral gauge boson Z' and one additional singlet superfield [41], neutralinos with a dominant singlet higgsino (singlino) component exist for large values $x \gtrsim 1$ TeV. Beam polarisation may be crucial either for a) observing singlino dominated neutralino poduction and b) for distinguishing between the MSSM and the extended model.

a) Production of singlino-dominated neutralinos

Since the singlino component does not couple to gauge bosons, gauginos, (scalar) leptons and (scalar) quarks, cross sections for the production of the exotic neutralinos are generally small [42–45]. However, they may be produced at a high luminosity e^+e^- linear collider with cross sections sufficient for detection, which can even be enhanced by the use of one or both polarised beams. Regions of x were analyzed where the associated production of the singlino-dominated neutralino yields detectable cross sections for different beam polarisations in scenarios where the MSSM-like neutralinos have similar masses and mixing character as in the 'typical mSUGRA' scenario, the reference scenario SPS, defined in [46, 47].

In the NMSSM the parameters (for details see [37]) $M_1 = 99$ GeV, $M_2 = 193$ GeV, $\tan\beta = 10$, the effective μ parameter $\mu_{\text{eff}} = \lambda x = 352$ GeV and the selectron masses $m_{\tilde{e}_R} = 143$ GeV and $m_{\tilde{e}_L} = 202$ GeV are chosen according to the scenario SPS 1a. For large $x \gg |M_2|$ a singlino-dominated neutralino $\tilde{\chi}^0_S$ with mass $\approx 2\kappa x$ in zeroth approximation decouples in the neutralino mixing matrix while the other four neutralinos $\tilde{\chi}^0_{1,\ldots,4}$ have MSSM character as in SPS 1a with masses 96 GeV, 177 GeV, 359 GeV and 378 GeV.

Further, an E_6 inspired model with one extra neutral gauge boson Z' and one additional singlet superfield is studied which contains six neutralinos [41]. Again the MSSM parameters and masses of the MSSM-like neutralinos are fixed according to the scenario SPS 1a, while a nearly pure light singlino-like neutralino $\tilde{\chi}^0_S$ with mass $\approx 0.18\, x^2/|M'|$, where M' is the mass parameter of the additional gauge boson, in zeroth approximation exists for very large values $|M'| \gg x$ [48]. The sign of M' is fixed by requiring relative sign $+1$ between the mass eigenvalues of $\tilde{\chi}^0_S$ and $\tilde{\chi}^0_1$ [42].

x reach	NMSSM		E6	
$(\sigma \geq 1fb)$	$m_{\tilde{S}} = 70$ GeV	$m_{\tilde{S}} = 120$ GeV	$m_{\tilde{S}} = 70$ GeV	$m_{\tilde{S}} = 120$ GeV
unpolarised beams	< 7.4 TeV	< 9.7 TeV	< 8.5 TeV	< 6.4 TeV
$P_{e^-} = +80\%$, unpol. e^+	< 10.0 TeV	< 12.3 TeV	< 11.4 TeV	< 7.9 TeV
$P_{e^-} = +80\%$, $P_{e^-} = -60\%$	< 12.6 TeV	< 15.5 TeV	< 14.4 TeV	< 10.0 TeV

Table 3.7: Range of accessible region of the singlet vacuum expectation value x under the discovery assumption of $\sigma(e^+e^- \to \tilde{S}\tilde{\chi}_i^0) \geq 1$ fb.

In Fig. 13 the associated production of the singlino-dominated $\tilde{\chi}_S^0$ together with the lightest MSSM-like neutralino $\tilde{\chi}_1^0$ is shown for unpolarized beams and beam polarizations $P_{e^-} = +0.8$, $P_{e^+} = 0$ and $P_{e^-} = +0.8$, $P_{e^+} = -0.6$ for two masses 70 and 120 GeV of $\tilde{\chi}_S^0$, where the singlino-dominated neutralino is the LSP and NLSP, respectively. Electron beam polarisation $P_{e^-} = +0.8$ enhances the cross section by a factor 1.5 to 1.8, while additional positron beam polarisation $P_{e^+} = -0.6$ gives a further enhancement factor of about 1.6. The cross sections are decreasing in good approximation as $1/x^2$ governed by the gaugino content of $\tilde{\chi}_S^0$ [42, 43]. Assuming a cross section of 1 fb to be sufficient for discovery, the singlino-dominated neutralino can be detected with unpolarized beams for $x < 7.4$ TeV (9.7 TeV) in the NMSSM with $m_{\tilde{\chi}_S^0} = 70$ GeV (120 GeV) and for $x < 8.5$ TeV (6.4 TeV) in the E_6 model. For polarized electron beam the reach in x is enhanced to $x < 10.0$ TeV (12.3 TeV) in the NMSSM and $x < 11.4$ TeV (7.9 TeV) in the E_6 model, whereas for both beams polarized to $x < 12.6$ TeV (15.5 TeV) in the NMSSM and $x < 14.4$ TeV (10.0 TeV) in the E_6 model, see Table 3.7. Direct experimental evidence of a fifth neutralino would be an explicit proof for an extended SUSY model and is also crucial to apply sum rules in order to test the closure of the neutralino system [49].

b) Distinction between MSSM and NMSSM

It may not only even be involved to detect the NMSSM itself, there are parts of the parameter space where aso the distinction between the MSSM and the NMSSM are very difficult. It is generally believed that either the Higgs sector May divide the models uniquely. However, it may happen that the kinematically accessible Higgs sector at the LHC as well as at the ILC do not indicate that it is not the MSSM model that is realised in nature. A next step is the analysis of the neutralino sector. If the complete neutralino sector is accessible sum rules for the production cross sections show a different energy dependence in the MSSM and the NMSSM [49]. If however, only a part of the spectrum is accessible, polarisation effects may play the crucial role. We show an example, where only the two lightest neutralinos are reachable at $\sqrt{s} = 500$ GeV, with, however, very low cross sections in the MSSM as well as in the NMSSM. Only with polarised beams the cross sections are sufficiently enhanced too be detectable and, furthermore, show different polarisation dependence and distinguish the models, see Table 3.8. The cross sections are enhanced by a factor of 1.6 compared to the case of only polarised electrons, respectively.

Conclusion

The production of singlino-dominated neutralinos in the NMSSM and an E_6 inspired model at a linear collider with polarized beams have been studied. With both beams po-

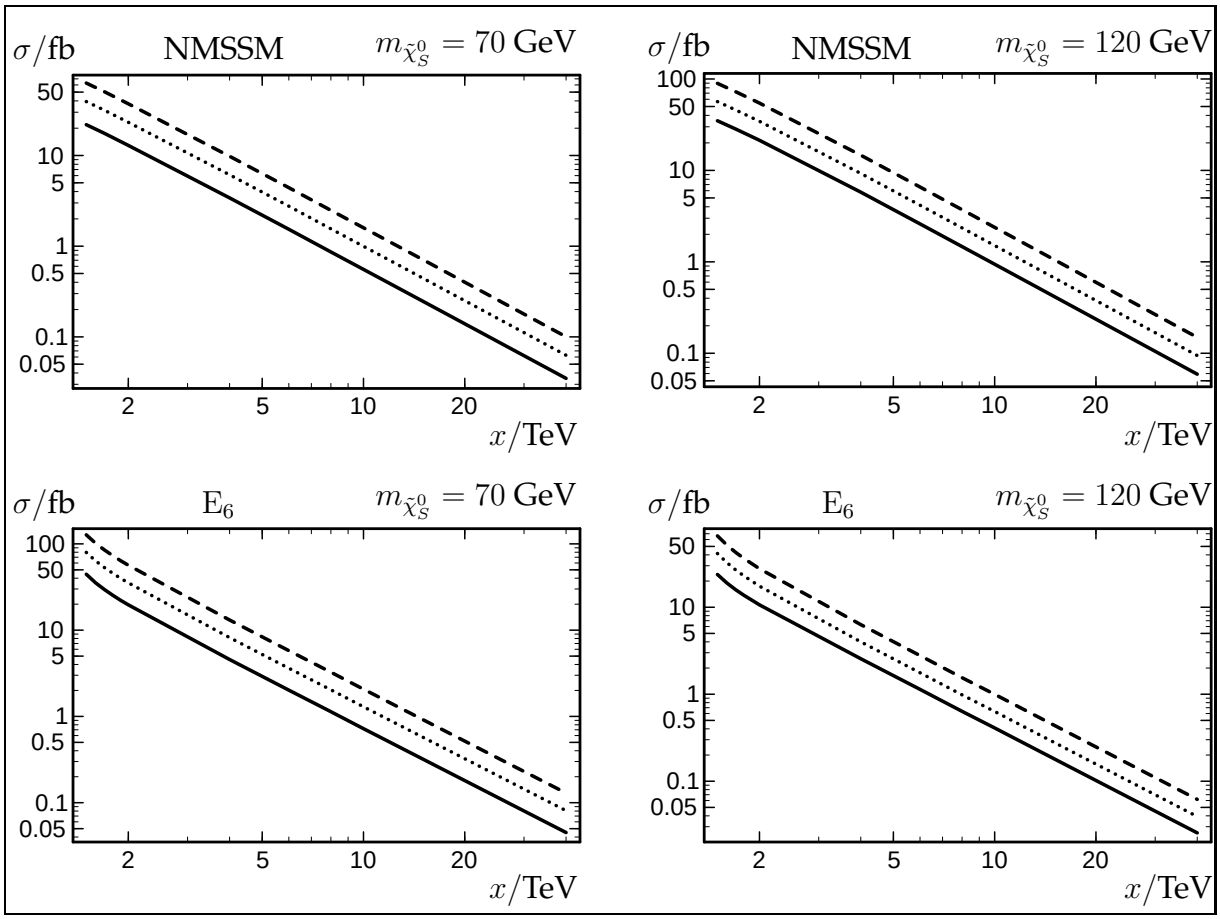

Figure 13: Cross sections for the production of a singlino-dominated neutralino $\tilde{\chi}^0_S$ via $e^+e^- \to \tilde{\chi}^0_S\tilde{\chi}^0_1$ for $\sqrt{s} = 500$ GeV in the SPS 1a inspired scenarios in the NMSSM and E_6 model with $M_1 = 99$ GeV, $M_2 = 193$ GeV, $\tan\beta = 10$ and $\mu_{\text{eff}} = \lambda x = 352$ GeV with unpolarized beams (solid) and beam polarizations $P_{e^-} = +0.8$, $P_{e^+} = 0$ (dotted) and $P_{e^-} = +0.8$, $P_{e^+} = -0.6$ (dashed). The mass of $\tilde{\chi}^0_S$ is fixed at 70 GeV and 120 GeV by the parameters κ (NMSSM) and M' (E_6 model).

$\sigma(\tilde{\chi}^0_1\tilde{\chi}^0_2)$ [fb]	unpolarised	$(-90, 0)$	$(+90, 0)$	$(-90, +60)$	$(+90, -60)$
MSSM	0.6	0.8	0.5	1.3	0.7
NMSSM	0.5	0.1	0.8	0.1	1.4

Table 3.8: Polarised cross section for the process $e^+e^- \to \tilde{\chi}^0_1\tilde{\chi}^0_2$ at $\sqrt{s} = 500$ GeV in a MSSM scenario ($M_1 = 195$ GeV, $M_2 = 300$ GeV, $\mu = 350$ GeV, $\tan\beta = 20$) and a NMSSM scenario ($M_1 = 270$ GeV, $M_2 = 381$ GeV, $\mu_{eff} = 350$ GeV, $\tan\beta = 20$ and $\kappa = 0.152$). The beam polarisation configuration is denoted by (P_{e^-}, P_{e^+}). The light neutralino masses are in both models given by $m_{\tilde{\chi}^0_1} = 189$ GeV, $m_{\tilde{\chi}^0_2} = 267$ GeV. The heavy neutralinos, the sleptons and the light chargino are kinematically not accessible.

larized the cross sections are enhanced by a factor 2.4 – 2.9 in comparison to unpolarized beams, depending on the scenario. This enhances the reach for the singlino-dominated neutralinos to singlet vacuum expectation valueas as large as 15 TeV.

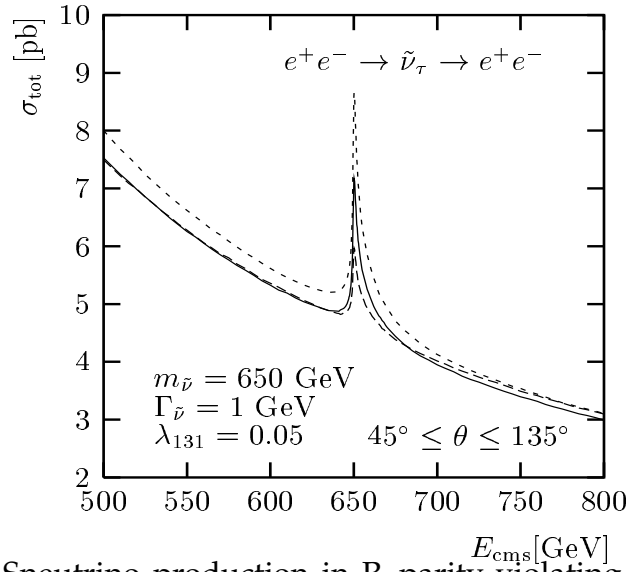

Figure 14: SUSY – Sneutrino production in R–parity violating model: Resonance production of $e^+e^- \to \tilde{\nu}$ interfering with Bhabha scattering for different configurations of beam polarization: unpolarized case (solid), $P_{e^-} = -80\%$ and $P_{e^+} = +60\%$ (hatched), $P_{e^-} = -80\%$ and $P_{e^+} = -60\%$ (dotted) [50].

3.4.5.2 Polarisation effects in R–parity violating SUSY

Summary: With both beams polarised one is directly sensitive to spin-zero resonances in the s-channel without applying an involved final-state analysis. In case that e.g. the Susy quantum number R–parity is not conserved scalar particles, sneutrinos, are produced in the s-channel. With left-polarised electrons and left-polarised positrons the signal indicates uniquely the production of a spin-zero particle and could immediately be distinguished from possible Z' signals.

In R–parity violating SUSY, processes can occur which prefer the extraordinary (LL) or (RR) polarization configurations. An interesting example is $e^+e^- \to \tilde{\nu} \to e^+e^-$. The main background to this process is Bhabha scattering. Polarizing both electrons and positrons can strongly enhance the signal. A study [50] was made for $m_{\tilde{\nu}} = 650$ GeV, $\Gamma_{\tilde{\nu}} = 1$ GeV, with an angle cut of $45^0 \leq \Theta \leq 135^0$ and a lepton–number violating coupling $\lambda_{131} = 0.05$ in the R–parity violating Langrangian $\mathcal{L}_{\not R} \sim \sum_{i,j,k} \lambda_{ijk} L_i L_j E_k$. Here $L_{i,j}$ denotes the left–handed lepton and squark superfield and E_k the corresponding right–handed field [50].

The resonance curve for the process, including the complete SM–background is given in Figure 14. The event rates at the peak are given in Table 3.9. Electron polarization with $P_{e^-} = -80\%$ enhances the signal only slightly by about 2%, whereas the simultaneous polarization of both beams with $P_{e^-} = -80\%$, $P_{e^+} = -60\%$ produces a further increase by about 20%. The background changes only slightly due to the t–channel (LL) contributions from γ and Z exchange.

This configuration of beam polarizations, which strongly suppresses pure SM processes, allows one to perform fast diagnostics for this R–parity violating process. For example the process $e^+e^- \to Z'$ could lead to a similar resonance peak, but with different polarization dependence. Here only the 'normal' configurations LR and RL play a role and this process will be strongly suppressed by LL. Therefore such a resonance curve, Figure 14, with different beam polarizations would uniquely identify an an R–parity violating SUSY process.

	$\sigma(e^+e^- \to e^+e^-)$ with $\sigma(e^+e^- \to \tilde{\nu} \to e^+e^-)$	Bhabha–background
unpolarized	7.17 pb	4.50 pb
$P_{e^-} = -80\%$	7.32 pb	4.63 pb
$P_{e^-} = -80\%$, $P_{e^+} = -60\%$	8.66 pb	4.69 pb
$P_{e^-} = -80\%$, $P_{e^+} = +60\%$	5.97 pb	4.58 pb

Table 3.9: SUSY – Sneutrino production in R–parity violating SUSY: Cross sections of $e^+e^- \to \tilde{\nu} \to e^+e^-$ for unpolarized beams, $P_{e^-} = -80\%$ and unpolarized positrons and $P_{e^-} = -80\%$, $P_{e^+} = -60\%$. The study was made for $m_{\tilde{\nu}} = 650$ GeV, $\Gamma_{\tilde{\nu}} = 1$ GeV, an angle cut of $45^0 \leq \theta \leq 135^0$ and the R–parity violating coupling $\lambda_{131} = 0.05$ [50].

3.4.6 Production of heavy Higgs bosons in weak boson fusion

Summary: The searches for heavy Susy Higgs particles can be very intriguing for both future colliders, the LHC as well as the LC. Exploiting single Higgs production in $e^+e^\to\nu\bar{\nu}H$ enlarges the kinematical range considerably. In the decoupling region, however, the properties of the heavy Higgs lead to very small rates. A very high luminosity together with a further enhancement of the signal of about a factor 1.6 with $P_{e^-} = -80\%$, $P_{e^+} = +60\%$ compared to the case with only a polarised electron beam might be crucial to detect the signal in such challenging scenario.

The search for rather heavy Higgs bosons might be very intriguing for searches at the LC as well as at the LHC. The possibility to enhance cross sections by using beam polarization can be very important for detecting processes with a very low rate. In Ref. [35] the production of the heavy neutral $\mathcal{CP}$-even Higgs boson H of the MSSM was studied. Since for large values of the $\mathcal{CP}$-odd Higgs boson mass M_A the heavy Higgs bosons A and H are approximately mass degenerate, $M_A \approx M_H$, the pair production channel $e^+e^- \to HA$ is limited by kinematics to the region $M_H < \sqrt{s}/2$. The kinematic limit of the LC can in principle be extended by single Higgs production in the process $e^+e^- \to \nu\bar{\nu}H$. However, due to the decoupling properties of the heavy Higgs bosons for $M_A \gg M_Z$ the VVH coupling ($V = W^\pm, Z$) is very small, so that the process $e^+e^- \to \nu\bar{\nu}H$ has only a very low rate.

In Ref. [35] it was shown that higher-order contributions to this Higgs-boson production process can remedy this situation, making the process potentially accessible at the LC. This requires a high integrated luminosity and polarized beams. The cross section becomes enhanced for left-handedly polarized electrons and right-handedly polarized positrons. While an 80% polarization of the electron beam alone results in a cross section that is enhanced by a factor 1.8, the polarization of both beams, i.e. 80% polarization for electrons and 60% polarization for positrons, would yield roughly an enhancement by a factor of 2.9. With an anticipated integrated luminosity of the LC running at high energy of $\mathcal{O}(2\text{ab}^{-1})$ ($\mathcal{L} = 500$ fb^{-1}/year) the enhancement in the cross section due to the beam polarization can extend the kinematic reach of the LC by roughly 100 GeV, see Fig. 15 (right) compared to the case of unpolarized beams, Fig. 15 (left).

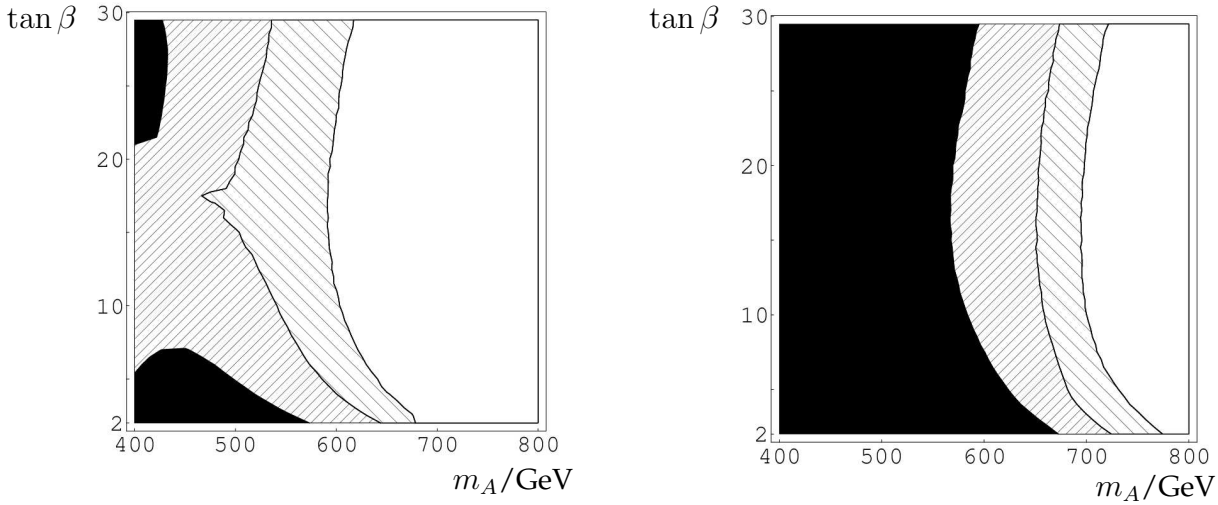

Figure 15: Cross section of heavy Higgs production with $\sigma(e^+e^- \to HA) > 0.5$ fb (black region), > 0.2 fb (right dashed) and > 0.1 fb (left dashed) for unpolarised beams (left) and with both beams polarised, $P_{e^-} = -80\%$, $P_{e^+} = +60\%$ (right) at $\sqrt{s} = 500$ GeV and with an integrated luminosity of $\mathcal{L} = 2$ ab^{-1}.

3.5 New physics searches in fermion pair production

3.5.1 Model-independent analysis of contact-interactions

Summary: With contact interactions non-Standard Model dynamics can be parametrised in general and indirect bounds on a new physics scale can be derived. Longitudinal beam polarisation is decisive to derive model-independent bounds on the different possible couplings. Using both beams polarised reduces the error in P_{eff} and enhances considerably the accuracy of the A_{LR} measurement so that the sensitivity to the new physics scale can be enlarged by up to about 1.3 compared to the case with only polarised electrons. A similar gain is reached for the resolution power for Z' studies in different models.

Although the production of SM fermion-pairs is not primarily devoted to the search for new phenomena, it guarantees – due to its clear signature of the final states in the detector and high statistics – a good sensitivity to deviations from the SM expectations. Physics beyond the SM could so be found at a LC operating far below the production threshold of new particles.

Generally, contact interactions (CI) represent an effective expression of a non-standard dynamics characterized by one (or more) new and very large mass scale exchanges, valid in quark and lepton reactions at the "low" energies $\sqrt{s} \ll \Lambda$ attainable by current and future accelerators. In this case, the new interactions and dynamical mass scales can manifest themselves only indirectly, through deviations of the measured cross sections from the Standard Model (SM) predictions that, being dimensionally suppressed by some power of $\sqrt{s}/\Lambda$, are expected to be quite small.

The fermion pair production process

$$e^+ + e^- \to f + \bar{f}, \tag{11}$$

with $f \neq t$, has to be studied at an electron-positron Linear Collider (LC) with polarized electron and positron beams, for the general, $SU(3)\times SU(2)\times U(1)$ symmetric $eeff$ dimension $D = 6$ contact-interaction Lagrangian, with helicity-conserving and flavor-diagonal fermion currents [78]:

$$\mathcal{L}_{\rm CI} = \frac{1}{1+\delta_{ef}} \sum_{i,j} g^2_{\rm eff}\, \epsilon_{ij}\, (\bar{e}_i \gamma_\mu e_i)\left(\bar{f}_j \gamma^\mu f_j\right). \tag{12}$$

In Eq. (12): $i, j = \mathrm{L}, \mathrm{R}$ denote left- or right-handed helicities, generation and color indices have been suppressed, and the CI coupling constants are parameterized in terms of corresponding mass scales as $\epsilon_{ij} = \eta_{ij}/\Lambda^2_{ij}$ with $\eta_{ij} = \pm 1, 0$ depending on the chiral structure of the individual interactions. Also, conventionally $g^2_{\rm eff} = 4\pi$, as a reminder that, in the case of compositeness, the new interaction would become strong at $\sqrt{s}$ of the order of Λ_{ij}. Obviously, deviations from the SM and upper bounds or exclusion ranges for the CI couplings can be equivalently expressed as lower bounds and exclusion ranges for the corresponding mass scales Λ_{ij}.

A general, model-independent analysis of the process (11) must account for all CI couplings as free, non-vanishing, parameters.

A simplifying procedure is to assume non-zero values for only one of the couplings (or one specific combination of them) at a time with all others set to zero, to test *specific* CI models only.

With longitudinally polarized beams the analysis of contact-interactions uses the observables integrated over the polar scattering angle: the (unpolarized) total cross section $\sigma_{\rm unpol}$ and forward-backward asymmetry $A_{\rm FB}$, the left-right asymmetry $A_{\rm LR}$ and left-right forward-backward asymmetry $A_{\rm LR,FB}$. These are defined in the notation of, e.g., Ref. [84], which differs from the denotation in eqn. (2)-(5), (9), (10) in section 2.1: the first and second subscripts refer to the helicities of the incoming and outgoing fermion respectively. Therefore the components are denoted with $\hat{\sigma}$, respectively.

$$\sigma_{\rm unpol} = \frac{1}{4}\left[\hat{\sigma}_{\rm LL} + \hat{\sigma}_{\rm LR} + \hat{\sigma}_{\rm RR} + \hat{\sigma}_{\rm RL}\right], \tag{13}$$

$$A_{\rm FB} = \frac{3}{4}\,\frac{\hat{\sigma}_{\rm LL} - \hat{\sigma}_{\rm LR} + \hat{\sigma}_{\rm RR} - \hat{\sigma}_{\rm RL}}{\hat{\sigma}_{\rm LL} + \hat{\sigma}_{\rm LR} + \hat{\sigma}_{\rm RR} + \hat{\sigma}_{\rm RL}}, \tag{14}$$

$$A_{\rm LR} = \frac{\hat{\sigma}_{\rm LL} + \hat{\sigma}_{\rm LR} - \hat{\sigma}_{\rm RR} - \hat{\sigma}_{\rm RL}}{\hat{\sigma}_{\rm LL} + \hat{\sigma}_{\rm LR} + \hat{\sigma}_{\rm RR} + \hat{\sigma}_{\rm RL}}, \tag{15}$$

and

$$A_{\rm LR,FB} = \frac{3}{4}\,\frac{\hat{\sigma}_{\rm LL} - \hat{\sigma}_{\rm RR} + \hat{\sigma}_{\rm RL} - \hat{\sigma}_{\rm LR}}{\hat{\sigma}_{\rm LL} + \hat{\sigma}_{\rm RR} + \hat{\sigma}_{\rm RL} + \hat{\sigma}_{\rm LR}}. \tag{16}$$

The deviations of measurements of these observables from the SM predictions are expressed in terms of the CI, ϵ_{ij}, of Eq. (12).

It can be seen from Eqs. (13) and (14), that with unpolarised beams the CI couplings could not be individually constrained within finite ranges, but only mutual correlations could be derived. With longitudinal beam polarization, two additional physical observables, (15) and (16), are available to obtain finite, model-independent, bounds on all CI couplings [79–81].

In principle, the polarisation of the electron beam alone would be sufficient to achieve model-independent results. The polarisation of both beams increases the cross sections (see section 1.3). This improves the sensitivity to new parameters which in general scales for these dimension d=6 operators with

$$\frac{m_X}{g_X} \sim \sqrt{\Delta_{stat}\sigma} \sim (\mathcal{L}_{int}\cdot s)^{1/4} \tag{17}$$

taking into account statistical errors only. Further, with both beams polarized the error of the effective polarisation, P_{eff} (cf. also section 1.3), is substantially reduced and involves a higher accuracy of the A_{LR} measurement:

$$\Delta A_{LR} = \sqrt{(\Delta_{stat}A_{LR})^2 + (\Delta_{sys}A_{LR})^2} = \sqrt{\frac{1 - P_{eff}^2 A_{LR}^2}{N P_{eff}^2} + A_{LR}^2(\frac{\Delta P_{eff}}{P_{eff}})^2}. \tag{18}$$

3.5.1.1 Expected Sensitivities to Contact Interactions

The analysis of contact interactions in Ref. [79] demonstrates the sensitivity to Λ depending on the collider parameters. The authors consider $b\bar{b}$ and $c\bar{c}$ final states, and take into account the particle identification efficiencies [87]: 60% and 35%, respectively. To assess

the relative roles of statistical and systematic uncertainties, the time-integrated luminosity $\mathcal{L}_{\rm int}$ is varied from 50 to 500 fb^{-1} with uncertainty $\delta\mathcal{L}_{\rm int}/\mathcal{L}_{\rm int} = 0.5\%$, and an experimental angular range of $|\cos\theta| \leq 0.99$ is assumed. The polarisation of electron and positron beams is considered as $|P_e| = 0.8$; $|P_{\bar{e}}| = 0.0, \text{and } 0.6$, with the uncertainties $\delta P_e/P_e = \delta P_{\bar{e}}/P_{\bar{e}} = 0.5$ %. The model-independent bounds on the mass scales Λ_{ij} at the 95% C.L. allowed by these experimental uncertainties are shown in Fig. 16. In this figure, heavy curves correspond to $|P_e| = 0.8, |P_{\bar{e}}| = 0.6$ while thin curves correspond to $|P_e| = 0.8, |P_{\bar{e}}| = 0.0$.

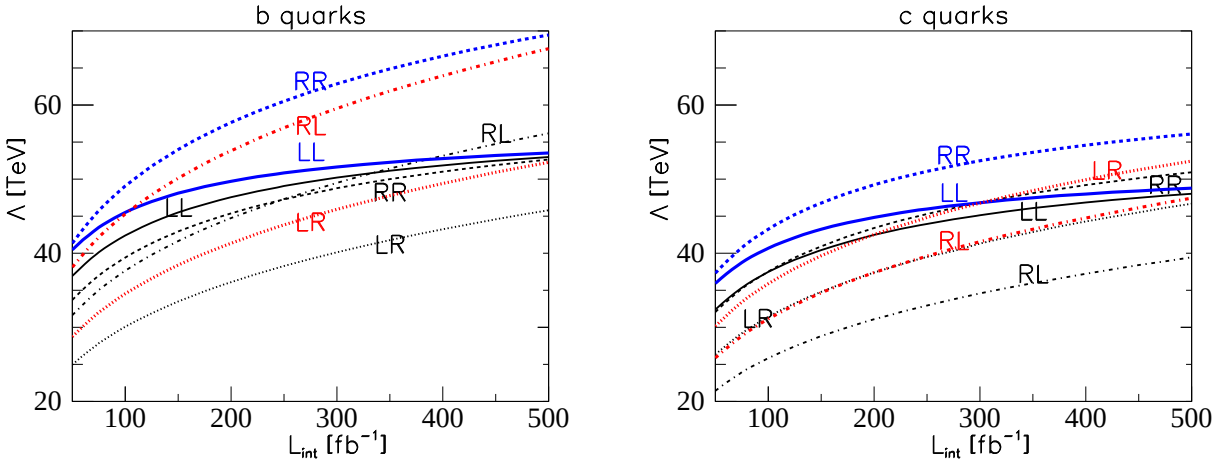

Figure 16: Lower bounds (95% C.L.) on the scale of contact-interaction, Λ, vs. the integrated luminosity, $\mathcal{L}_{\rm int}$, for $b\bar{b}$ and $c\bar{c}$ final states taking into account the four helicity combinations. Thin lines: $P_e = 0.8$, $P_{\bar{e}} = 0$, thick lines: $P_e = 0.8$, $P_{\bar{e}} = 0.6$.

In Figs. 17 the expected sensitivities for different models of contact interactions in $e^+e^- \to b\bar{b}, c\bar{c}$ are shown including systematic ($\Delta sys = 0\%, 0.5\%, 1.0\%$), luminosity ($\Delta L = 0.2\%, 0.5\%$) and polarisation uncertainties ($\Delta P/P = 0\%, 0.5\%$). It can clearly be seen that the reduction of systematic errors will be decisive. The study was done for $\sqrt{s} = 800$ GeV [33].

3.5.1.2 CI analysis in Bhabha scattering

With $\delta_{ef} = 1$ the four-fermion contact interaction Lagrangian of Eq. (12) is relevant to the Bhabha scattering process

$$e^+ + e^- \to e^+ + e^- \tag{19}$$

where γ and Z bosons are exchanged in both, s- and t-channel. It turns out that modifications of the pure t-channel contribution to the cross section, $\sigma_{{\rm LR},t}$, depend on the single contact interaction parameter ($\epsilon_{\rm LR} = \epsilon_{\rm RL}$), while the combinations of helicity cross sections, d$\sigma_{\rm R}$ and d$\sigma_{\rm L}$, contribute to the s-channel exchange in the processes (19) and depend on *pairs* of parameters, ($\epsilon_{\rm RR}$,$\epsilon_{\rm LR}$) and ($\epsilon_{\rm LL}$,$\epsilon_{\rm LR}$), respectively.

The change of the polarization of each beam pulse-by-pulse will allow separate measurements of the polarized differential cross sections dσ_{++}, dσ_{+-} and dσ_{-+}, corresponding to the configurations of beam polarizations $(P_e, P_{\bar{e}}) = (P_1, P_2), (P_1, -P_2)$ and $(-P_1, P_2)$, respectively, with $P_{1,2} > 0$ [88]. These differential cross sections represent a system of linear equations of the helicity cross sections d$\sigma_{\rm R}$, d$\sigma_{\rm L}$ and $\sigma_{{\rm LR},t}$ and allow to disentangle

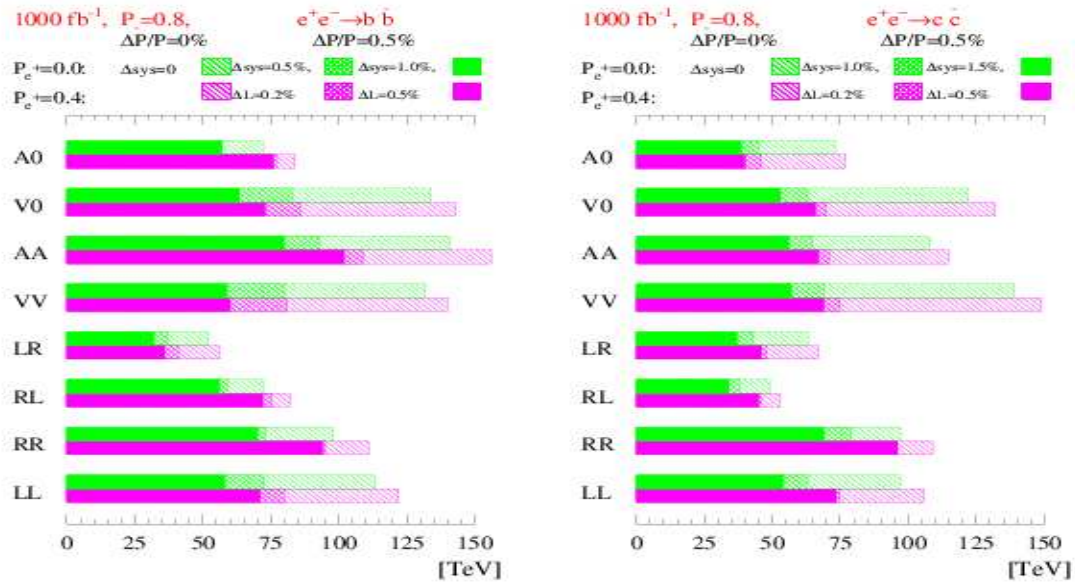

Figure 17: Left: Limits on contact interactions from $\mathrm{e^+e^-} \to \mathrm{b\bar{b}}$ and $e^+e^- \to c\bar{c}$ without positron polarization and with 40% polarization including different uncertainty scenarios [33].

the CI couplings ϵ_{LL}, ϵ_{RR} and ϵ_{LR}. Fig. 18 shows as example the result of a χ^2 analysis assuming that no deviation from the SM within the experimental uncertainty (statistical and systematic) is measured in $\mathrm{d}\sigma_{\mathrm{L}}$, $\mathrm{d}\sigma_{\mathrm{R}}$ and $\mathrm{d}\sigma_{\mathrm{LR},t}$ ($\mathcal{L}_{\mathrm{int}}(e^+e^-) = 50$ fb^{-1}, $P_1 = 0.8$, $P_2 = 0.6$, $\delta\mathcal{L}_{\mathrm{int}}/\mathcal{L}_{\mathrm{int}} = \delta P_1/P_1 = \delta P_2/P_2 = 0.5\%$). It is evident that only with *both* electron *and* positron polarization this model-independent analysis can be performed. A compar-

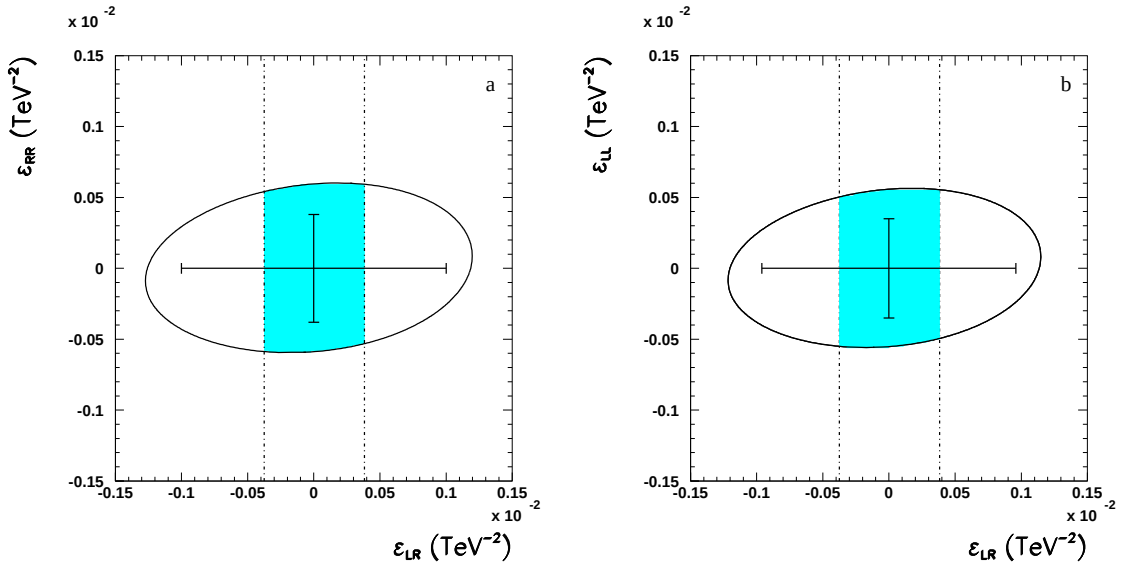

Figure 18: Allowed areas at 95% C.L. in the planes $(\epsilon_{\mathrm{LR}}, \epsilon_{\mathrm{RR}})$ and $(\epsilon_{\mathrm{LR}}, \epsilon_{\mathrm{LL}})$ obtained from σ_{R} and σ_{L} in $e^+e^- \to e^+e^-$ at $\sqrt{s} = 0.5$ TeV, $\mathcal{L}_{\mathrm{int}}(e^+e^-) = 50$ fb^{-1}, $|P_e| = 0.8$, $|P_{\bar{e}}| = 0.6$. Vertical dashed lines indicate the range allowed to ϵ_{LR} by $\sigma_{\mathrm{LR},t}$.The crosses indicate the constraints obtained by taking only one non-zero parameter at a time instead of two simultaneously non-zero and independent parameters.

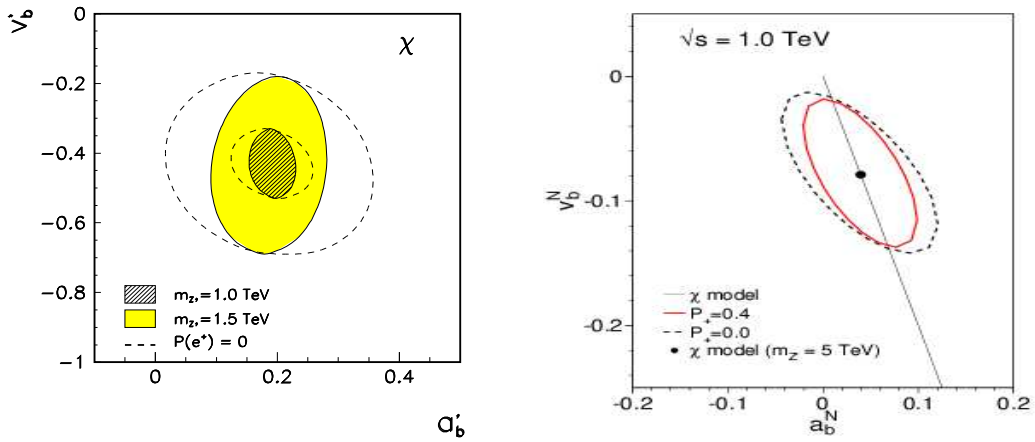

Figure 19: Left: 95% CL contours for (a'_b, v'_b) for $M_{Z'} = 1$, 1.5 TeV in the χ model and $\sqrt{s} = 500$ GeV and $\mathcal{L} = 500$ fb^{-1}. The dash lines correspond to $P_{e^+} = 0$ [34]; Right: Expected resolution power (95% CL) to reconstruct a Z' ($m_{Z'} = 5$ TeV) realised in the χ model without positron polarisation and with 40% polarisation based on the measurement of $b\bar{b}$ final states. The Z' mass is assumed to be unknown in this case [33].

ison with Moeller scattering, [79], shows that only in case that $\mathcal{L}_{\rm int}(e^-e^-)$ is not too low, Bhabha and Moeller scattering are complementary concerning the sensitivity to individual couplings in a model-independent data analysis.

3.5.1.3 Sensitivity to neutral extra gauge bosons

Extra neutral gauge bosons Z' can be probed by its virtual effects on cross sections and asymmetries by approaching $\epsilon_{ij} \to g'_i g'_i/(s - M^2_{Z'})$. Below a Z' resonance measurements of fermion-pair production are sensitive only to this ratio of Z' couplings and Z' mass. Therefore, limits on the Z' mass can be obtained only in dependence on a model with given Z' couplings. For the well-known E6 and LR models, e.g., mass sensitivities between $4 \cdot \sqrt{s}$ and $14 \cdot \sqrt{s}$ are reached. Thus, a LC operating at $\sqrt{s} = 800$ GeV may exceed the sensitivity of the LHC (which is about 4-5 TeV) to a potential Z' in some models. If a Z' will be detected at LHC its origin can be found by determining the Z' couplings, see Fig. 19a [34]. Positron beam polarisation improves only slightly the resolution power for Z' models in case of leptonic final states, but it will be quite important for the measurement of the Z' couplings to fermions. The crucial point in the analyses are the systematic errors, which can be significantly reduced with the use of both beams polarised [33,34].

3.5.2 Identification of graviton exchange effects

Summary: Effects from spin-2 graviton effects in models with large extra dimensions can also be probed indirectly in the framework of contact interactions. The identification reach for the new mass scale is improved by about 10% with both beams longitudinally polarised compared to the case with polarised electrons only, see also sect. 3.2.2.

Effects from large extra dimensions in the ADD [89] or Randall-Sundrum(RS) [131] scenarios can also be probed by virtual effects in the framework of contact interactions,

by the effective Lagrangian [91]

$$\mathcal{L} = i\frac{4\lambda}{M_H^4} T_{\mu\nu} T^{\mu\nu}, \tag{20}$$

where $T_{\mu\nu}$ is the energy-momentum tensor and λ is a sign factor ($\lambda = \pm 1$). In contrast to the previous contact-interaction Lagrangian (12), being induced by a dimension $D = 8$ operator the KK graviton exchange is suppressed by the much higher power $(\sqrt{s}/M_H)^4$, so that a lower reach on M_H can be expected in comparison to the constraints obtainable, at the same c.m.s., on the Λ's.

The scaling law for the search reach scales correspondingly as

$$m_H \sim [s^{(d-5)} \mathcal{L}_{int}]^{1/(2d-8)} = (s^3 \cdot \mathcal{L}_{int})^{1/8}. \tag{21}$$

The exchange of spin-2 fields modifies the Standard Model helicity amplitudes angular dependent [91,133] different from contact interactions represented by (12).

Assuming massless fermions and allowing for the possibility of spin-2 particle exchange in the $e^+e^- \to f\bar{f}$ process the relevant helicity amplitudes are given by [93,133]

$$\begin{aligned} T_{+-}^{+-} &= [f_{LL} - f_g(2z-1)](1+z) \\ T_{+-}^{-+} &= [f_{LR} - f_g(2z+1)](1-z) \\ T_{-+}^{+-} &= [f_{RL} - f_g(2z+1)](1-z) \\ T_{-+}^{-+} &= [f_{RR} - f_g(2z-1)](1+z)\,. \end{aligned} \tag{22}$$

where $z = \cos\theta$, $f_{L,R}$ are combinations of the vector and axial vector couplings of eZ and f_g is a model-dependent quantity. In the usual ADD model, employing the convention of [128], one finds

$$f_g = \frac{\lambda s^2}{4\pi\alpha M_H^4}\,. \tag{23}$$

where M_H represents the cutoff scale in the KK graviton tower sum and $\lambda = \pm 1$. In the RS model the corresponding expression can be obtained through the replacement

$$\frac{\lambda}{M_H^4} \to \frac{-1}{8\Lambda_\pi^2} \sum_n \frac{1}{s - m_n^2 + i m_n \Gamma_n}\,. \tag{24}$$

where Λ_π is of order a few TeV and $m_n(\Gamma_n)$ are the masses(widths) of the TeV scale graviton KK excitations. It is assumed that their widths can be neglected in cross section calculations.

In the case of massive final state fermions, such as tops, the helicity amplitudes given above are slightly altered and new amplitudes $T_{+-}^{\pm\pm}$ and $T_{-+}^{\pm\pm}$ are also present.

It is evident that the spin-2 nature of these new exchanges would be easily identified through an examination of the resonances themselves. Most likely the energy at a linear collider is well below the threshold for the production of these resonances and the s-channel exchange of spin-2 fields has to be distinguished from 'conventional' contact interaction sources.

The sensitivity to new physics effects can be described by (a) the discovery reach which gives values on Λ or M_H up to them a deviation from the Standard Model predictions can be obtained, and (b) the identification reach corresponding to values on Λ or

M_H up to them special models can be differentiated. If at least one beam is longitudinally polarised, a clear signature in the differential distributions of a cross sections or left-right asymmetries arises from graviton exchange (see, *e.g.*, [33, 91, 92]). In Table 3.10 (left) values on the mass scale M_H are shown, indicated as a 5σ identification reach corresponding to the resolution power between graviton effects (22) and the contact interaction of Equ. (12). The results include the combination of the channels $f = \mu, \tau, b, c$ [92].

3.5.3 Use of transversely polarised beams for graviton searches

Summary: Applying both beams transversely polarised one can define additional azimuthal asymmetries which indicate spin-2 graviton exchange. The identification reach for the new scale M_H is similar to the corresponding discovery reach when applying longitudinally polarised beams. However, with transversely polarised beams specific azimuthal asymmetries can be defined which allow to separate uniquely the extra dimension models ADD and RS model in such indirect searches.

3.5.3.1 Introduction

The observables in Equ. 16 are derived taking into account longitudinal polarisation. A potential contribution of transverse polarised electrons and positrons is eliminated by integrating over the full azimuthal angular range.

In general, a modulation of the particle production is associated with the azimuthal angle formed by the directions of the $e^{\pm}$ polarisation and the plane of the momenta of the outgoing fermions in the $e^+e^- \to f\bar{f}$ process. This transverse polarization (TP) [135, 136] allows for new asymmetries to be constructed which are highly sensitive to the spins of the interacting particles.

Consider the process $e^+e^- \to f\bar{f}$ with the both electron and positron beams polarized. The longitudinal and transverse components of the $e^-(e^+)$ polarizations are denoted by $P_{L,T}(P'_{L,T})$. For simplicity it is assumed that the two transverse polarization vectors are parallel up to a sign. As introduced in sect. 2.1.1 the spin-averaged matrix element for this process can be written as

$$\begin{aligned} |\bar{\mathcal{M}}|^2 &= \frac{1}{4}(1 - P_L P'_L)(|T_+|^2 + |T_-|^2) + (P_L - P'_L)(|T_+|^2 - |T_-|^2) \\ &+ (2P_T P'_T)[\cos 2\phi \; Re(T_+ T_-^*) - \sin 2\phi \; Im(T_+ T_-^*)] \,, \end{aligned} \tag{25}$$

where ϕ is the azimuthal angle defined on an event-by-event basis described above. It should be noted from eq. (25) that the ϕ-dependent contributions are *only* accessible if both beams are transversely polarized.

In addition to the observables in Equ. (16) a differential distribution of an azimuthal asymmetry is defined by

$$\frac{1}{N}\frac{dA^T}{dz} = \left[\frac{\int_+ \frac{d\sigma}{dz d\phi} - \int_- \frac{d\sigma}{dz d\phi}}{\int d\sigma}\right], \tag{26}$$

where $\int_\pm$ are integrations over regions where $\cos 2\phi$ takes on $\pm$ values. This differential asymmetry can be used to resolve effects of graviton exchange in fermion pair production. It is shown for both the SM and in the ADD scenario in Fig. 20 at a 500 GeV LC for the

final states $f = \mu$ or τ, c and b. Usually, in an analysis the results are combined for the $f = \mu$ and τ final states to get added statistics. For concreteness it is assumed that the spin rotators are 100% efficient [137] so that $P_T = 0.8$ and $P'_T = 0.6$. As can be seen from Fig. 20 the spin-2 effects cause a strong asymmetric behaviour under $z \to -z$ exchange.

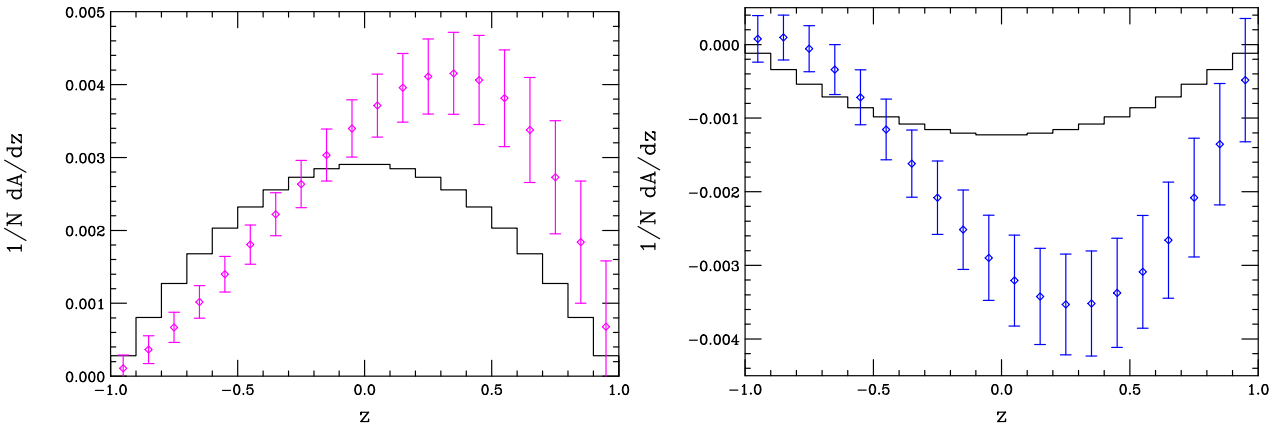

Figure 20: Differential azimuthal asymmetry distribution for $e^+e^- \to f\bar{f}$, i.e. $c\bar{c}$ (left) and $b\bar{b}$ (right), at a 500 GeV LC assuming a luminosity of $500\ fb^{-1}$. The histograms are the SM predictions while the data points assume the ADD model with $M_H = 1.5$ TeV. $P_T = 0.8$ and $P'_T = 0.6$ are assumed.

The differential asymmetry in Equ. (26) can be converted to an azimuthal forward-backward asymmetry sensitive to odd-z terms by separately integrating Equ. (26) over positive and negative values of z:

$$A_{FB}^T = \frac{1}{N}\left[\int_{z\geq 0} dz\, \frac{dA^T}{dz} - \int_{z\leq 0} dz\, \frac{dA^T}{dz}\right]. \tag{27}$$

In the SM and in any new physics specified in sections 3.5.1 one finds $A_{FB}^T = 0$ but in the case of spin-2 particle exchange A_{FB}^T is different from zero due to additional odd-z terms as given in Equ. (22).

3.5.3.2 Analysis of graviton effects with transverse polarised beams

In the following we concentrate on the ADD model; (almost) all limits on the expected sensitivity can be immediately translated to the case of the RS scenario.

To demonstrate the benefit of transverse polarized beams in the studies it is assumed that the individual polarizations are known with a precision $\delta P/P = 0.003$ and that the efficiencies of identifying the final state fermions are rather high: 100% for $f = \mu, \tau$, 60% for $f = c, t$, and 80% for $f = b$; systematic uncertainties of the particle identification are neglected, the effects of initial state radiation are included and a small angle cut of 100 mrad around the beam pipe has been used.

Analysing the observable A_{FB}^T with respect to deviations from the zero Standard Model expectation one derives the 5σ *identification* reach on M_H given in Table 3.10 (right). A comparison of left and right part of Table 3.10 shows that the identification reaches for M_H (5σ CL) using transverse beam polarisation and exploring A_{FB}^T are below that obtained with longitudinal polarisation [33, 92, 138].

M_H/TeV	$\mathcal{L}_{int}$/fb^{-1}		
$\sqrt{s} = 0.5$ TeV (long. pol.)	100	300	500
unpolarised beams	2.3	2.6	2.9
$P_{e^-} = +0.8$	2.5	2.8	3.05
$P_{e^-} = +0.8$, $P_{e^+} = -0.6$	2.45	3.0	3.25

M_H/TeV	$\mathcal{L}_{int}$/fb^{-1}			
(transv. pol.)	100	300	500	1000
$\sqrt{s} = 0.5$ TeV	1.6	1.9	2.0	2.2
$\sqrt{s} = 0.8$ TeV	2.4	2.6	2.8	3.1
$\sqrt{s} = 1.0$ TeV	2.8	3.2	3.4	3.8

Table 3.10: Left: 5σ identification reach on the mass scale M_H *vs.* integrated luminosity from the process $e^+e^- \to f\bar{f}$, with f summed over μ, τ, b, c, and for the energy 0.5 TeV [92] (cf. also [33], where the 95% CL sensitivy for M_H in $e^+e^- \to \mu\bar{\mu}, c\bar{c}, b\bar{b}$ has been simulated); Right: 5σ identification reach in M_H *vs.* integrated luminosity using A_{FB}^T as a function of the integrated luminosity from the process $e^+e^- \to f\bar{f}$, with f summed over μ, τ, b, c and t. Here $P_T = 0.8$ and $P_T' = 0.6$ are assumed. [142]

From Fig.20 it is apparent that modest values of M_H cause quite sizeable distortions in the $N^{-1}dA^T/dz$ distribution yielding a non-zero A_{FB}^T.

Instead of analysing A_{FB}^T an examination of the $N^{-1}dA^T/dz$ distributions allows a more sensitive distinction between a spin2/graviton exchange and the new physics effects (as, *e.g.*, Z′ or leptoquark exchange) specified by the contact interactions of Equ. (12). A fit to the $N^{-1}dA^T/dz$ distribution for fixed M_H assuming a Standard Model like shape ($N^{-1}dA^T/dz \propto 1 - z^2$) yields identification reaches as shown in Table 3.11 (left), 2nd column, including the μ, τ, c and b final states. The identification of M_H in the ADD model and the discrimination from models with 'conventional' contact interactions is possible up to $M_H \approx 10\sqrt{s}$. If systematic uncertainties are taken into account these values will be diminished in a detailed detector study since for luminosities above $100 - 200\ fb^{-1}$ the errors are completely dominated by systematic effects. Table 3.11 (left), 3rd column,shows the values up to them deviations from Standard Model predictions due to graviton/spin-2 exchange can be obtained: $M_H \geq 20\sqrt{s}$ (cf. also [140]).

A comparison of the results in Table 3.11 (left) with the corresponding studies based on longitudinal beam polarisation [142] shows that the *identification* reach of M_H exploring the $N^{-1}dA^T/dz$ distribution is numerically similar to the 95% CL *discovery* reach obtained using only singly longitudinally polarized beams [52, 138, 140] and considering the same process.

3.5.3.3 Distinguish models with graviton exchange

Here, we focus on the distinction between ADD and RS model scenarios below the KK production threshold with transvere polarisation. In the RS model, away from the Z and graviton KK poles the imaginary part of the amplitude proportional to $\sin 2\phi$ in see Equ. (25) becomes vanishingly small. However, as was recently pointed out by [141], the exchange of an essentially continuous spectrum of ADD gravitons leads to a finite, cutoff-independent *imaginary* part of the amplitude, which grows rapidly with increasing $\sqrt{s}$ and depends quite sensitively upon the number of extra dimensions. Thus, f_g gets an imaginary part, depending strongly on the number of extra dimensions. With a new asymmetry formed in analogy to that in Equ. (26) a sensitivity to the imaginary part of f_g is given - the terms proportional to real part, $\propto \cos 2\phi$, are found to cancel in these models:

$$\frac{1}{N}\frac{dA_i^T}{dz} = \left[\frac{\int_+ \frac{d\sigma}{dzd\phi} - \int_- \frac{d\sigma}{dzd\phi}}{\int d\sigma}\right], \tag{28}$$

E_{CM} [GeV]	ident. reach M_H [TeV]	95% CL disc. reach M_H [TeV]
500	5.4	10.2
800	8.8	17.0
1000	11.1	21.5
1200	13.3	26.0
1500	16.7	32.7

5 σ disc. reach M_H [TeV]	$\mathcal{L}_{int}$/fb^{-1}			
	100	300	500	1000
$\sqrt{s} = 0.5$ TeV	1.2	1.3	1.4	1.6
$\sqrt{s} = 0.8$ TeV	1.8	2.0	2.2	2.4
$\sqrt{s} = 1.0$ TeV	2.2	2.4	2.6	2.8

Table 3.11: Left: Identification reach for M_H in the ADD model exploring the distribution $N^{-1}dA^T/dz \sim 1 - z^2$ for the final states $f = \mu, \tau$, $f = b$ and $f = c$ for LC of different center of mass energies; the 95% CL discovery reach; Right: 5σ reach for the discovery of a nonzero value of the azimuthal asymmetry $N^{-1}dA_i^T/dz$ distribution as a function of the integrated luminosity at a LC for $\delta = 3$. $M_H = M_D$ is assumed throughout as is $P_T = 0.8$ and $P_T' = 0.6$.

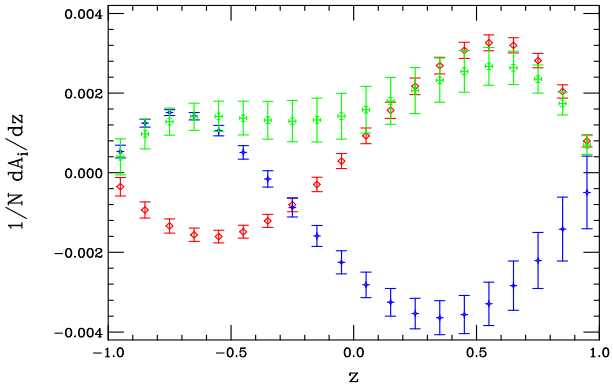

Figure 21: The $N^{-1}dA_i^T/dz$ distributions at a 500 GeV collider assuming $M_H = M_D = 1.5$ TeV and $\delta = 3$ with an integrated luminosity of 500 fb^{-1}. The plotted points from top to bottom in the center of the plot correspond to $f = b, \mu$ plus τ and c, respectively.

where now the $\int_\pm$ are integrations over regions where $\sin 2\phi$ takes on $\pm$ values and we integrate over all z and ϕ in the denominator. This new distribution is identically zero in both the SM as well as the RS model away from the Z and RS KK graviton poles. Thus, observing *any* non-zero value for this quantity is a signal for the ADD model. Table 3.11 (right) shows the 5σ discovery reach for these new asymmetry distributions at a 500 GeV LC assuming as before that $P_T = 0.8$ and $P_T' = 0.6$ and taking $\delta = 3$ for purposes of demonstration. In this analysis $M_H = M_D$ is assumed, for $M_H << M_D$ the sensitivity to the observable (28) is serious modified. In Table 3.11 (right) the resulting reaches at the 5σ level (for $\delta = 3$) are listed where the RS and the ADD model could be separated up to $M_H \sim (2.5 - 3)\sqrt{s}$. Although this number is not large in comparison to those obtained in the other analyses above they provide the first indication that these two scenarios can be distinguished at a collider via indirect measurements.

In the process $e^+e^- \to W^+W^-$ no obviously unique signature for a spin2/graviton exchange can be derived (see [142]).

3.6 CP sensitive observables within the SM particle sector

3.6.1 Searches for CP violation in $t\bar{t}$ with transversely polarised beams

Summary: (Pseudo-)Scalar or tensor interactions associated with a new physics scale Λ can lead to CP-odd observables from interference terms with the virtual γ, Z exchange in the annihilation channel. Only with transversely polarised these CP violating effects are measurable without an involved final state spin analysis. Exploiting such a CP-odd asymmetry that is only accessible with both beams transversely polarised, one is sensitive to a new scale up to 10 TeV in $t\bar{t}$ production.

Overview

Transverse polarization (TP) enables novel CP violation search in the inclusive process $e^+e^- \to A + X$ [94]. When the spin of A is unobserved and m_e is neglected, only (pseudo-)scalar or tensor currents associated with a new-physics scale Λ can lead to CP-odd observables at leading order in the presence of TP. They are due to the couplings in the interference terms between these new currents and the virtual γ and Z exchanges in the direct channel.

In order to test CP violation, one needs more than the momenta of particles to be measured in $e^+e^- \to f\bar{f}$. The presence of TP provides such a vector, without observing final state polarization. This leads, e.g., to gain in statistics. CP violation due to beyond the standard model interactions may be parametrized in terms of contact interactions in a model independent manner. When m_e is neglected, with only TP interactions that transform as V and A cannot interfere at leading order in the new interactions with the standard model interactions to yield CP odd correlations, which can be inferred from general results of [95]. The tensor and (pseudo-)scalar interactions are accessible only at a higher order of perturbation theory without TP, even if longitudinal polarization is available.

In our application example we have evaluated the contributions to the differential cross-section due to (pseudo)-scalar and tensor contact interactions at leading order in the interaction strengths for the process $e^+e^- \to t\bar{t}$. This is used to construct an effective up-down asymmetry and a polar angle integrated version of the same. By assuming that the coefficients of the effective interaction that is suppressed by the second power of the new-physics scale Λ, to be of order unity, we show that at $\sqrt{s} = 500$ GeV and with an integrated luminosity $\int dt\mathcal{L} = 500\,\mathrm{fb}^{-1}$, we find that at the 90% confidence level, the scale Λ can be bounded at about 10 TeV, with perfect TP.

Theoretical framework

The Lagrangian we will use for our calculations is:

$$\mathcal{L} = \mathcal{L}^{SM} + \frac{1}{\Lambda^2}\sum_i (\,\alpha_i \mathcal{O}_i + \mathrm{h.c.}\,), \tag{29}$$

where α_i are the coefficients which parameterize non-standard interactions, $\mathcal{O}_i$ are the effective dimension-six operators, and Λ is the scale of new physics.

After Fierz transformation the part of lagrangian containing the above four-Fermi operators can be rewritten as

$$\mathcal{L}^{4F} = \sum_{i,j=L,R} \Big[S_{ij}(\bar{e}P_i e)(\bar{t}P_j t) + V_{ij}(\bar{e}\gamma_\mu P_i e)(\bar{t}\gamma^\mu P_j t) + T_{ij}(\bar{e}\frac{\sigma_{\mu\nu}}{\sqrt{2}}P_i e)(\bar{t}\frac{\sigma^{\mu\nu}}{\sqrt{2}}P_j t) \Big], \qquad (30)$$

where

$$S_{RR} = S_{LL}^*, \quad S_{LR} = S_{RL} = 0, \quad \text{and} \quad V_{ij} = V_{ij}^*, \quad \text{and} \quad T_{RR} = T_{LL}^*, \quad T_{LR} = T_{RL} = 0.$$

The z axis is chosen along the direction of the e^-. The differential cross sections for $e^+e^- \to t\bar{t}$, with the superscripts denoting the respective signs of the e^- and e^+ TP, are

$$\frac{d\sigma^{\pm\pm}}{d\Omega} = \frac{d\sigma^{\pm\pm}_{SM}}{d\Omega} \mp \frac{3\alpha\beta^2}{4\pi}\frac{m_t\sqrt{s}}{s-m_Z^2}\left(c_V^t c_A^e \mathrm{Re}S\right)\sin\theta\cos\phi, \qquad (31)$$

$$\frac{d\sigma^{\pm\mp}}{d\Omega} = \frac{d\sigma^{\pm\mp}_{SM}}{d\Omega} \pm \frac{3\alpha\beta^2}{4\pi}\frac{m_t\sqrt{s}}{s-m_Z^2}\left(c_V^t c_A^e \mathrm{Im}S\right)\sin\theta\sin\phi, \qquad (32)$$

where

$$\begin{aligned}
\frac{d\sigma^{+\pm}_{SM}}{d\Omega} \;=\; & \frac{d\sigma^{-\mp}_{SM}}{d\Omega} = \frac{3\alpha^2\beta}{4s}\left[\frac{4}{9}\left\{1+\cos^2\theta+\frac{4m_t^2}{s}\sin^2\theta \pm \beta^2\sin^2\theta\cos 2\phi\right\}\right. \\
& - \frac{s}{s-m_Z^2}\frac{4}{3}\left\{c_V^e c_V^t(1+\cos^2\theta + \frac{4m_t^2}{s}\sin^2\theta \pm \beta^2\sin^2\theta\cos 2\phi)\right. \\
& \left.\left. + \; 2\, c_A^e c_A^t \beta\cos\theta\right\} + \frac{s^2}{(s-m_Z^2)^2}\left\{({c_V^e}^2 + {c_A^e}^2)\right. \right. \\
& \times\left[({c_V^t}^2 + {c_A^t}^2)\beta^2(1+\cos^2\theta) + {c_V^t}^2\frac{8m_t^2}{s}\right] + 8c_V^e c_A^e c_V^t c_A^t \beta\cos\theta \\
& \left.\left. \pm \; ({c_V^e}^2 - {c_A^e}^2)({c_V^t}^2 + {c_A^t}^2)\beta^2\sin^2\theta\cos 2\phi\right\}\right]
\end{aligned} \qquad (33)$$

The quantities $\sin\theta\sin\Phi$ and $\sin\theta\cos\Phi$ are CP-odd and CP-even. Here $\beta = \sqrt{1-4m_t^2/s}$, and we have defined

$$S \equiv S_{RR} + \frac{2c_A^t c_V^e}{c_V^t c_A^e}T_{RR}, \qquad (34)$$

where c_V^i, c_A^i are the couplings of Z to e^-e^+ and $t\bar{t}$, and where we have retained the new couplings to linear order only. In (34) the contribution of the tensor term relative to the scalar term is suppressed by a factor $2c_A^t c_V^e/c_V^t c_A^e \approx 0.36$. In what follows, we will consider only the combination S, and not S_{RR} and T_{RR} separately.

CP-odd asymmetries and numerical results

We construct the CP-odd asymmetry, which we call the up-down asymmetry as

$$A(\theta) = \frac{\displaystyle\int_0^\pi \frac{d\sigma^{+-}}{d\Omega}d\phi - \int_\pi^{2\pi}\frac{d\sigma^{+-}}{d\Omega}d\phi}{\displaystyle\int_0^\pi \frac{d\sigma^{+-}}{d\Omega}d\phi + \int_\pi^{2\pi}\frac{d\sigma^{+-}}{d\Omega}d\phi} \qquad (35)$$

and also the θ-integrated version,

$$A(\theta_0) = \frac{\int_{-\cos\theta_0}^{\cos\theta_0}\int_0^{\pi}\frac{d\sigma^{+-}}{d\Omega}d\cos\theta d\phi - \int_{-\cos\theta_0}^{\cos\theta_0}\int_{\pi}^{2\pi}\frac{d\sigma^{+-}}{d\Omega}d\cos\theta d\phi}{\int_{-\cos\theta_0}^{\cos\theta_0}\int_0^{\pi}\frac{d\sigma^{+-}}{d\Omega}d\cos\theta d\phi + \int_{-\cos\theta_0}^{\cos\theta_0}\int_{\pi}^{2\pi}\frac{d\sigma^{+-}}{d\Omega}d\cos\theta d\phi} \tag{36}$$

In the latter, a cut-off θ_0 angle has been introduced.

In a numerical study we put limits on the parameters using the integrated asymmetry $A(\theta_0)$. The figures are presented for $\sqrt{s} = 500$ GeV and the ideal condition of 100% beam polarizations for e^- as well as e^+. We will comment later on about the result for more realistic polarizations. As we can see from Fig. 22, the value of $A(\theta_0)$ increases with the

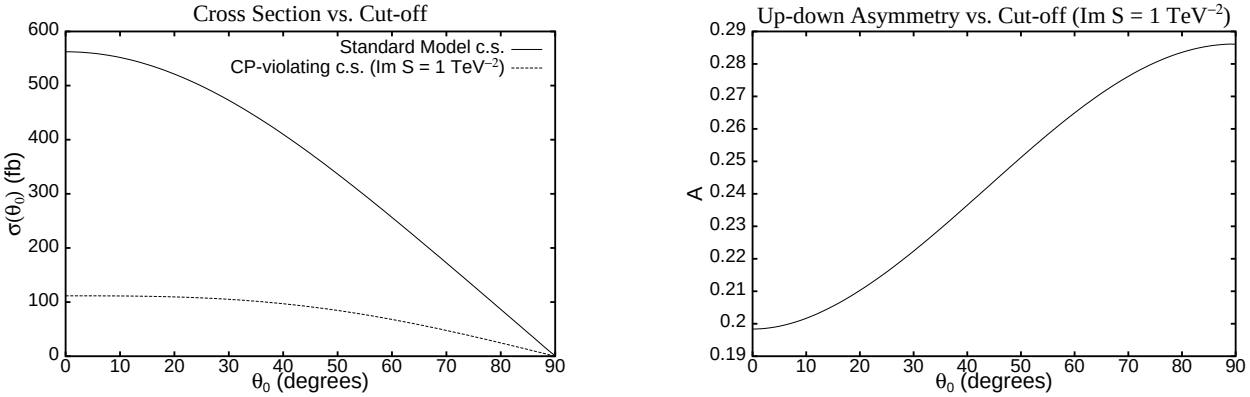

Figure 22: Left:The SM cross section (solid line) and the numerator of the asymmetry $A(\theta)$ in eq. (35) (broken line) as for the quantities integrated over θ with a cutoff θ_0, plotted as a function of θ_0; Right: The asymmetry $A(\theta_0)$ defined in eq. (36) plotted as a function of θ_0 for Im $S = 1$ TeV^{-2}.

cut-off, because the SM cross section in the denominator of eq. (36) decreases with cut-off faster than the numerator.

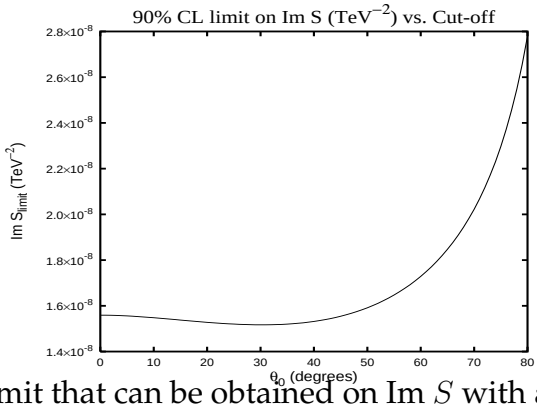

Figure 23: The 90% C.L. limit that can be obtained on Im S with an integrated luminosity of 500 fb^{-1} plotted as a function of the cut-off angle θ_0.

Fig. 23 shows the 90% confidence level (C.L.) limits that could be placed on $\mathrm{Im}S$ for an integrated luminosity of $L = 500$ fb^{-1}. The limit is the value of Im S which would give rise to an asymmetry $A_{\rm lim} = 1.64/\sqrt{L\Delta\sigma}$, where $\Delta\sigma$ is the SM cross section. This limit translates to a value of Λ of the order of 8 TeV, assuming that the coefficients α_i in

(29) are of order 1. The corresponding limit for $\sqrt{s}$ of 800 GeV with the same integrated luminosity is ~ 9.5 TeV.

Using realistic polarisation degrees of 80% and 60% for TP, the up-down asymmetry $A(\theta)$ or $A(\theta_0)$ gets multiplied by a factor $\frac{1}{2}(P_1 - P_2)$ for e^- and e^+ beams respectively. For $P_1 = 0.8$ and $P_2 = -0.6$, this means a reduction of the asymmetry by a factor of 0.7. Since the SM cross section does not change, this also means that the limit on the parameter Im S goes up by a factor of $1/0.7 \approx 1.4$, and the limit on Λ goes down by a factor of $\sqrt{0.7} \approx 0.84$, to about 6.7 TeV. If the positron beam is unpolarized, however, the sensitivity goes down further.

In summary, TP can be used to study CP-violating asymmetry arising from the interference of new-physics scalar and tensor interactions with the SM interactions. These interference terms cannot be seen with longitudinally polarized or unpolarized beams. Moreover, such an asymmetry would not be sensitive to new vector and axial-vector interactions (as for example, from an extra Z' neutral boson), or even electric or "weak" dipole interactions of heavy particles, since the asymmetry vanishes if $m_e \sim 0$.

3.6.2 Triple gauge boson couplings in WW production

Summary: In order to test the electroweak gauge group it is suitable to apply a general parametrisation of the gauge-boson self-interactions which lead to 14 complex parameters, 6 of them CP violating. Determining all of them in WW pair production presents a strong test of the SM which allows only 4 couplings (CP conserving) to be nonzero. With both beams polarised one gains up to a factor of 1.7 in the sensitivity compared to the case of using polarised electron beams only.

An important feature of the electroweak Standard Model (SM) is the non-Abelian nature of its gauge group, which gives rise to gauge boson self-interactions, in particular to the triple gauge couplings (TGCs) γWW and ZWW. The most general vertices contain altogether 14 complex parameters, six of them CP violating. The SM predicts only four CP conserving real couplings to be non-zero at tree level.

The triple gauge boson vertex WWV (V=Z or γ) can be described in a most general form by an effective Lagrangian [96]

$$\begin{aligned}\frac{\mathcal{L}^{WWV}}{ig_{WWV}} &= g_1^V V^\mu \left(W^-_{\mu\nu}W^{+\nu} - W^+_{\mu\nu}W^{-\nu}\right) + \kappa_V W^-_\mu W^+_\nu V^{\mu\nu} + \frac{\lambda_V}{M_W^2} V^{\mu\nu} W^{+\rho}_\mu W^-_{\rho\nu} \\ &- ig_4^V W^-_\mu W^+_\nu (\partial^\mu V^\nu + \partial^\nu V^\mu) \\ &+ ig_5^V \varepsilon^{\mu\nu\rho\sigma}\left[(\partial^\rho W^-_\mu)W^+_\nu - W^-_\mu(\partial^\rho W^+_\nu)\right] V_\sigma \\ &+ \frac{\tilde\kappa_V}{2} W^-_\mu W^+_\nu \varepsilon^{\mu\nu\rho\sigma} V_{\rho\sigma} + \frac{\tilde\lambda_V}{2M_W^2} W^-_{\rho\mu} W^{+\mu}{}_\nu \varepsilon^{\nu\rho\alpha\beta} V_{\alpha\beta},\end{aligned} \tag{37}$$

which is parametrised by seven real couplings for each vertex. Their behavior under charge (C) and parity (P) conjugation can be used to divide them into four groups. The three couplings g_1^V,κ_V and λ_V conserve C and P, while g_5^V violates C and P but conserves CP. The couplings g_4^V,$\tilde\kappa_V$ and $\tilde\lambda_V$ violate CP, but g_4^V conserves P, while $\tilde\kappa_V$ and $\tilde\lambda_V$ conserve C. In the SM at tree level the couplings are g_1^V=κ_V=1, while all other are set to zero. For convenience we introduce $\Delta g_1^\gamma = g_1^\gamma - 1$, $\Delta g_1^Z = g_1^Z - 1$, $\Delta\kappa_\gamma = \kappa_\gamma - 1$ and $\Delta\kappa_Z = \kappa_Z - 1$ thus we are only considering deviations from the standard model values.

Electro-magnetic gauge invariance requires g_1^γ=1 and reduces the number of C and P conserving couplings to 5. SU(2)$_L$ × U(1)$_Y$ gauge invariance introduces

$$\begin{aligned}\Delta\kappa_Z &= \Delta\kappa_\gamma \tan\theta_W + \Delta g_1^Z \\ \lambda_Z &= \lambda_\gamma\end{aligned} \tag{38}$$

for the C and P conserving couplings, where θ_W is the Weinberg angle, thus reducing the number of free couplings further.

A precision measurement of the TGCs at high energies will be a crucial test of the validity of the SM, given that a variety of new physics effects can manifest itself by deviations from the SM predictions (for references see e.g. [97]). Though no deviation from the SM has been found for the TGCs from LEP data [98], the bounds obtained are comparatively weak. The tightest bounds on the anomalous couplings, i.e. on the differences between a coupling and its SM value, are of order 0.05 for Δg_1^Z and λ_γ, of order 0.1 for $\Delta\kappa_\gamma$ and of order 0.1 to 0.6 for the real and imaginary parts of C and/or P violating couplings. These numbers correspond to fits where all anomalous couplings except one are

Table 3.12: 1σ statistical errors in units of 10^{-3} on the real parts of CP conserving TGCs in the presence of all anomalous couplings at $\sqrt{s} = 500$ GeV, with unpolarised beams and with different beam polarisations.

	$\mathrm{Re}\,\Delta g_1^\gamma$	$\mathrm{Re}\,\Delta g_1^Z$	$\mathrm{Re}\,\Delta\kappa_\gamma$	$\mathrm{Re}\,\Delta\kappa_Z$	$\mathrm{Re}\,\lambda_\gamma$	$\mathrm{Re}\,\lambda_Z$	$\mathrm{Re}\,g_5^\gamma$	$\mathrm{Re}\,g_5^Z$
no polarisation	6.5	5.2	1.3	1.4	2.3	1.8	4.4	3.3
$(P_l^-, P_l^+) = (\mp 80\%, 0)$	3.2	2.6	0.61	0.58	1.1	0.86	2.2	1.7
$(P_l^-, P_l^+) = (\mp 80\%, \pm 60\%)$	1.9	1.6	0.40	0.36	0.62	0.50	1.4	1.1
$(P_t^-, P_t^+) = (80\%, 60\%)$	2.8	2.4	0.69	0.82	0.69	0.55	2.5	1.9

set to zero. Moreover, many couplings, e.g. the imaginary parts of C and P conserving couplings, have been excluded from the analyses so far.

At a future linear e^+e^- collider one will be able to study these couplings with unprecedented accuracy. A process particularly suitable for this is W pair production where both the γWW and the ZWW couplings can be measured at the scale given by the c.m. energy $\sqrt{s}$.

Study of TGC with optimal observables

In [97] the prospects to measure the full set of 28 (real) TGCs is systematically investigated for unpolarised beams as well as for longitudinal beam polarisation using optimal observables. They are constructed to give the smallest possible statistical errors for a given event distribution [104]. In addition, they take advantage of the discrete symmetries of the differential cross section. In W pair production the covariance matrix of these observables consists of four blocks that correspond to CP even or CP odd TGCs and to their real or imaginary parts. Within each block all correlations between couplings are taken into account.

Table 3.12 shows the errors on the real parts of CP conserving TGCs at $\sqrt{s} = 500$ GeV with unpolarised beams and with different beam polarisations, assuming an integrated luminosity of 500 fb^{-1}. Here, only those events are considered where one W boson decays into a quark-antiquark pair and the other one into $e\nu$ and $\mu\nu$. It is further assumed that the two jets of the hadronic W decay cannot be identified as originating from the up- and down-type (anti)quark. In the case of longitudinal polarisation the luminosity is distributed equally on both directions of the polarisation vectors and the results are then combined. The errors with unpolarised beams are between 10^{-3} and 10^{-2} in the parameterisation using photon and Z couplings.

At 800 GeV all errors (with or without polarisation) are smaller, notably for $\mathrm{Re}\,\Delta\kappa_\gamma$. For both c.m. energies the errors on the couplings in the γ-Z-parameterisation decrease by about a factor 2 when going from unpolarised beams to longitudinal e^- polarisation and an unpolarised e^+ beam. Going from unpolarised beams to polarised e^- and e^+ this factor is between 3 and 4 for all couplings, except for $\mathrm{Re}\,\Delta\kappa_Z$ at 800 GeV where it is 4.7.

It has been emphasized [104] that the following linear combinations [96] can be measured with much smaller correlations than the γ-Z couplings:

$$\begin{aligned} g_1^L &= 4\sin^2\theta_W\, g_1^\gamma + (2 - 4\sin^2\theta_W)\,\xi\, g_1^Z, \\ g_1^R &= 4\sin^2\theta_W\, g_1^\gamma - 4\sin^2\theta_W\,\xi\, g_1^Z, \end{aligned} \tag{39}$$

Table 3.13: Same as Table 3.12, but for the imaginary parts and with the L-R-parameterisation.

	$\mathrm{Im}\, g_1^L$	$\mathrm{Im}\, \kappa_L$	$\mathrm{Im}\, \lambda_L$	$\mathrm{Im}\, g_5^L$	$\tilde{h}_-$	$\tilde{h}_+$	$\mathrm{Im}\, \lambda_R$	$\mathrm{Im}\, g_5^R$
no polarisation	2.7	1.7	0.48	2.5	11	—	3.1	17
$(P_l^-, P_l^+) = (\mp 80\%, 0)$	2.6	1.2	0.45	2.0	4.5	—	1.4	4.3
$(P_l^-, P_l^+) = (\mp 80\%, \pm 60\%)$	2.1	0.95	0.37	1.6	2.5	—	0.75	2.3
$(P_t^-, P_t^+) = (80\%, 60\%)$	2.6	1.2	0.46	2.0	3.7	3.2	0.98	4.4

where $\xi = s/(s - m_Z^2)$, and similarly for the other couplings. The L- and R-couplings respectively appear in the amplitudes for left- and right-handed initial e^-. Therefore this parameterisation seems to be more "natural" in the presence of beam polarisation than the conventional one. For detailed plots showing the sensitivity to the TGCs as a function of the degree of longitudinal polarisation we refer to [97]. There an extended optimal-observable method [105] has been used where correlations between TGCs are eliminated through appropriate energy- and polarisation-dependent reparameterisations.

For the imaginary parts of the CP conserving couplings, see Table 3.13, we further use the linear combinations $\tilde{h}_\pm = \mathrm{Im}(g_1^R \pm \kappa_R)/\sqrt{2}$ instead of $\mathrm{Im}\, g_1^R$ and $\mathrm{Im}\, \kappa_R$.

Sensitivity to TGCs at the LC in a true simulation

For comparison with a simulation of determining the charged current triple gauge couplings via a fit [106]. For the simulation we assume a luminosity of $500\,\mathrm{fb}^{-1}$ at a center-of-mass energy of $500\ \mathrm{GeV}$, which is the expected amount of data after one or two years of running. For $800\ \mathrm{GeV}$ this corresponds to a luminosity of $1000\,\mathrm{fb}^{-1}$. At both energies we expect roughly 4 millions W-pair events. This huge amount of events give us the possibility to do high precision measurements of the TGCs.

The semileptonic decay channel ($WW \to q\bar{q}\ell\bar{\nu}_\ell$) is used, because of the high branching ration of $43\,\%$ and the good event reconstruction.

There is only one ambiguity in the hadronic decay angles. From LEP analysis [99] we know that the background is very small. The background samples were generated by PYTHIA [146] also including ISR and beamstrahlung.

For the simulation of the proposed detector design we use the fast simulation program SIMDET (version 3.02 [100]), which is based on the proposed detector design, described in the TESLA CDR [101]. It includes a tracking and calorimeter simulation and a reconstruction of energy-flow objects. Concerning more details about data selection see [106].

We use a simple χ^2 fit and apply as input variables the normalized $\cos\theta_W$-distribution and the elements of the spin density matrix of W^+W^- pair. The total cross section is not used. In the case of unpolarized beams we expect a luminosity of $500\,\mathrm{fb}^{-1}$ at a center-of-mass energy of $500\ \mathrm{GeV}$ and $1000\,\mathrm{fb}^{-1}$ at $800\ \mathrm{GeV}$ in one or two years of running. We consider radiative corrections like initial state radiation (ISR) and beamstrahlung and uncertainties in other measurement like the W-mass and the beam energy, which might have an impact on this measurement.

In the case of polarised beams the total luminosity for one center-of-mass energy is split up equally on both polarizations. In the case of electron polarization this is for an energy of $500\ \mathrm{GeV}$ $250\,\mathrm{fb}^{-1}$ on left-handed (L) and $250\,\mathrm{fb}^{-1}$ on right-handed (R) electrons

with a polarization of $80\,\%$. In the case of additional polarized positrons the absolute value is $60\,\%$ with opposite polarization with respect to the electron polarization.

To get the maximal sensitivity for this measurement the data taken at both polarization combinations are fitted at the same time. Only this ensures that we can disentangle the WWZ- from the WWγ- couplings. To estimate the systematic error in the TGC measurement from the uncertainty in the polarization measurement the polarization is changed by $\Delta P = \pm 1\,\%$. We obtain that at an energy of 500 GeV all measurements are dominated by the polarization error. This error is $5 - 10$ times greater than the statistical error. At the higher energy the behavior is more mixed. Some couplings are almost not affected by the polarization error but others are. This is more pronounced in the case of electron and positron polarization. From this observations a polarization error of $\Delta P = 0.1 - 0.2\,\%$ is needed for a measurement which is not dominated by this polarization error. This translate into the following relative errors for electron polarization $\Delta\mathcal{P}^-/\mathcal{P}^- = 0.1 - 0.2\,\%$ and positron polarization $\Delta\mathcal{P}^+/\mathcal{P}^+ = 0.2 - 0.3\,\%$. One sees from Table 3.14 that the simulated results are in the same range as before.

unpolarised	Δg_1^Z	$\Delta\kappa_\gamma$	λ_γ	$\Delta\kappa_Z$	λ_Z	g_4^Z	g_5^Z	$\tilde{\kappa}_Z$	$\tilde{\lambda}_Z$
500 GeV	38.1	4.8	12.1	8.7	11.5	85.8	27.7	64.9	11.4
800 GeV	39.0	2.6	5.2	4.9	5.1	41.8	28.5	29.6	4.9

$\lvert P_{e^-}\rvert = 80\%$	Δg_1^Z	$\Delta\kappa_\gamma$	λ_γ	$\Delta\kappa_Z$	λ_Z	g_4^Z	g_5^Z	$\tilde{\kappa}_Z$	$\tilde{\lambda}_Z$
500 GeV	24.8	4.1	8.2	5.0	8.9	79.9	22.8	50.6	10.3
800 GeV	21.9	2.2	5.0	2.9	4.7	31.8	24.3	24.1	4.4

$\lvert P_{e^-}\rvert = 80\%$, $\lvert P_{e^+}\rvert = 60\%$	Δg_1^Z	$\Delta\kappa_\gamma$	λ_γ	$\Delta\kappa_Z$	λ_Z	g_4^Z	g_5^Z	$\tilde{\kappa}_Z$	$\tilde{\lambda}_Z$
500 GeV	15.5	3.3	5.9	3.2	6.7	45.9	16.5	39.0	7.5
800 GeV	12.6	1.9	3.3	1.9	3.0	18.3	14.4	14.3	3.0

Table 3.14: Expected sensitivity ($\times 10^{-4}$) for different couplings at a center-of-mass energy of 500 and 800 GeV and a luminosity of $500\,\mathrm{fb}^{-1}$ and $1000\,\mathrm{fb}^{-1}$. In the case of polarized beams the luminosity is split up equally on both combinations.

3.6.3 Use of transversely polarised beams for TGC's in WW production

Summary: Specific azimuthal asymmetries with transversely polarised beams may also be crucial for sensitive tests of TGC. It has been worked out that the imaginary part of one specific CP conserving coupling is only accessible with tranversely polarised beams but not with longitudinally polarised beams.

In [136] it has been pointed out that the use of transversely polarised beams may be an important tool for studying TGC and longitudinal W_L, in particular for measuring relative phases of the helicity amplitudes in WW production.

In [103] TGC were studied with optimal observables using transversely polarised beams, see Table 3.12. If both beams have transverse polarisation, the errors on most couplings are approximately of the same size as in the situation where only the e^- beam

has longitudinal polarisation. This resuls is confirmed by [102], where a first true simulation was done for studying TGC's in WW production and semileptonic decay with transversely polarised beams for the TESLA design using $\sqrt{s} = 500$ GeV, $\mathcal{L} = 500$ fb^{-1} and $|P_{e^-}| = 80\%$, $|P_{e^+}| = 60\%$ and including also ISR and beamstrahlung. For this simulation the program WHIZARD has been used. However, for one interesting coupling combination the use of transversely polarised beams is useful. The errors for $\mathrm{Re}\,\lambda_\gamma$, $\mathrm{Re}\,\lambda_Z$, $\mathrm{Re}\,\tilde{\lambda}_\gamma$ and $\mathrm{Re}\,\tilde{\lambda}_Z$ are they smaller with transversely polarised beams, viz. they are of the same size as with both beams longitudinally polarised. This is true for both energies.

If electron as well as positron polarisation is available we thus conclude that, regarding the 1σ-standard deviations on the TGCs (without assuming any coupling to be zero) *longitudinal* polarisation is the preferable choice, apart from one exception (see below). Note that we are better with longitudinal polarisation also for all CP violating couplings.

It has been shown in [97] that $\tilde{h}_+$ is not measurable from the normalised event distribution, neither with unpolarised beams nor with longitudinal polarisation. One can however measure this coupling with *transverse* beam polarisation with good sensitivity. In the γ-Z-parameterisation this means that the four couplings $\mathrm{Im}\,g_1^\gamma$, $\mathrm{Im}\,g_1^Z$, $\mathrm{Im}\,\kappa_\gamma$ and $\mathrm{Im}\,\kappa_Z$ are not simultaneously measurable without transverse polarisation.

Although for most couplings longitudinal polarisation of both beams is the advantageous choice, measurement of the full parameter space requires to spend part of the total luminosity of the collider on the transverse polarisation mode.

3.6.4 CP Violation in the 3 Jet and 4 Jet Decays of the Z Boson at GigaZ

Summary: An interesting channel to look for physics beyond the SM are CP-violating Z decays in heavy leptons and quarks. Both beam polarised with $|P_{e^-}| = 80\%$, $|P_{e^+}| = 60\%$ improves the sensitivity by about 20-30% compared to case with only polarised electrons. An efficiency of 100% has been used and statistical errors only have been taken into account. If systematics are also included, further strong improvements may even be expected.

An interesting topic is the test of the CP symmetry in Z decays. Here a flavor-diagonal Z decay where CP-violating effects within the Standard Model (SM) are estimated to be very small [107] is studied. Thus, looking for CP violation in such Z decays means looking for new physics beyond the SM. Of particular interest are Z decays involving heavy leptons or quarks. The process $Z \to b\bar{b}G$, which is sensitive to effective CP-violating couplings in the $Zb\bar{b}G$ vertex, has been analysed theoretically in [108] and experimentally in [109]. No significant deviation from the SM has been found.

If CP-violating couplings are introduced in the $Zb\bar{b}G$ vertex, they will, because of gauge invariance of QCD, appear in the $Zb\bar{b}GG$ vertex as well. But the $Zb\bar{b}GG$ vertex could in principle contain new coupling parameters. The analysis of the 4 jet decays of the Z boson involving b quarks looks into both, 4- and 5-point vertices. This has been investigated theoretically in [110] and experimentally in [111]. Also in this case no significant deviation from the SM has been found.

In the GigaZ scenario [52], these measurements which were performed at the electron-positron collider experiments at LEP could be redone with increased precision. In the following, the results of the calculations of the processes Z $\to$ 3 jets and Z $\to$ 4 jets including CP-violating couplings are reviewed. We require that at least two of the jets originate from a b or $\bar{b}$ quark. For the GigaZ scenario we allow for longitudinal beam polarisation of electrons and positrons. All details of the calculations for unpolarized e^+, e^- beams can be found in [108, 110], for polarized beams in [201]. For a model independent study of CP violation in 3 jet and 4 jet decays of the Z boson the effective Lagrangian approach as explained in [107] can be used. One adds to the SM Lagrangian $\mathcal{L}_{SM}$ a CP-violating term $\mathcal{L}_{CP}$

$$\mathcal{L}_{CP}(x) = [\, h_{Vb}\, \bar{b}(x)\, T^a\, \gamma^\nu\, b(x) + h_{Ab}\, \bar{b}(x)\, T^a\, \gamma^\nu\, \gamma_5\, b(x)\,]\; Z^\mu(x)\; G^a_{\mu\nu}(x) \quad , \tag{40}$$

where $b(x)$ denotes the b quark field, $Z^\mu(x)$ and $G^a_{\mu\nu}(x)$ represent the field of the Z boson and the field strength tensor of the gluon, respectively, and $T^a = \lambda^a/2$ are the generators of $SU(3)_C$. In (40) h_{Vb} and h_{Ab} are real CP-violating vector and axial vector chirality conserving coupling constants. Dimensionless coupling constants $\widehat{h}_{Vb,Ab}$ using the Z mass as the scale parameter can be defined by $h_{Vb,Ab} = e\, g_s\, \widehat{h}_{Vb,Ab}/(\sin\vartheta_W\, \cos\vartheta_W\, m_Z^2)$.

Chirality conserving CP-violating interactions as introduced (40) can arise at one loop level in multi-Higgs extensions of the Standard Model [114]. They can also possibly be generated in models with excited quarks which is further investigated here. Excitations of quarks would be natural in a scenario where quarks have substructure and participate in a new type of strong interaction. This type of models and effects from excited quarks at hadron colliders have for instance been discussed in [115]. In particular, here it is assumed that b quarks have excited partners b' of spin $\frac{1}{2}$ and mass $m_{b'}$. Due to higher order dimensional operators in composite models chirality-conserving $Zb'b$ couplings at

the scale of GigaZ energies are a priori possible (see e.g. [116]). Because of colour gauge invariance the $b'bG$ couplings can be expected to be chirality-flipping dipole couplings. Then, couplings $\widehat{h}_{Vb,Ab}$ as introduced in (40) can be generated by the following effective interactions of b' and b quarks, Z bosons and gluons:

$$\begin{aligned}\mathcal{L}'(x) = & - \frac{e}{2\,\sin\vartheta_W\,\cos\vartheta_W}\,Z_\mu(x)\,\bar{b}'(x)\,\gamma^\mu\,(g'_V - g'_A\gamma_5)\,b(x) \\ & - i\,\frac{g_s}{2m_{b'}}\,\hat{d}_c\,\bar{b}'(x)\,\sigma^{\mu\nu}\,\gamma_5\,T^a\,b(x)\,G^a_{\mu\nu}(x) + \text{h.c.} \end{aligned} \tag{41}$$

Here g'_V, g'_A and $\hat{d}_c$ are complex parameters, which can be expected to be of order one if the underlying dynamics is strongly interacting. In this model for $m_{b'} \gg m_Z$ one derives for the couplings [114] $\widehat{h}_{Vb} = m_Z^2\,\mathrm{Re}(\hat{d}_c\,g'^*_A)/(m^2_{b'})$ and $\widehat{h}_{Ab} = -m_Z^2\,\mathrm{Re}(\hat{d}_c\,g'^*_V)/(m^2_{b'})$

In this study it is assumed that one is able to flavor-tag the b quarks and to measure their momenta. This is justified due to the extremely good b-tagging capabilities foreseen at TESLA [52]. Then, the CP-violating couplings are analysed using CP-odd observables constructed from the momentum directions of the b and $\bar{b}$ quarks, $\widehat{\mathbf{k}}_b = \mathbf{k}_b/|\mathbf{k}_b|$ and $\widehat{\mathbf{k}}_{\bar{b}} = \mathbf{k}_{\bar{b}}/|\mathbf{k}_{\bar{b}}|$ (see [107,108]):

$$T_{33} = (\widehat{\mathbf{k}}_{\bar{b}} - \widehat{\mathbf{k}}_b)_3\,(\widehat{\mathbf{k}}_{\bar{b}} \times \widehat{\mathbf{k}}_b)_3\,, \tag{42}$$

$$V_3 = (\widehat{\mathbf{k}}_{\bar{b}} \times \widehat{\mathbf{k}}_b)_3\,. \tag{43}$$

The observable T_{33} transforms as tensor component, V_3 as vector component.

The expectation values of the observables (42), (43) have been calculated, using JADE cuts to define the jets, as function of $\widehat{h}_b = \widehat{h}_{Ab}g_{Vb} - \widehat{h}_{Vb}g_{Ab}$ and $\widetilde{h}_b = \widehat{h}_{Vb}g_{Vb} - \widehat{h}_{Ab}g_{Ab}$. For unpolarised e^+e^- beams a non-zero value $<\mathcal{O}> \neq 0$ for one of the CP-odd observables above is an unambiguous indicator of CP violation. For longitudinally polarised beams this holds if possible chirality flipping interactions at the e^+e^-Z vertex — which do not exist in the SM — are neglected. In very good approximation, it was found for Z $\to$ 3 jets and Z $\to$ 4 jets that the tensor observables are only sensitive to $\widehat{h}_b$ and the vector observables only to $\widetilde{h}_b$ [108,110].

Numerical results

The sensitivities $1/\delta\widehat{h}_b$, $1/\delta\widetilde{h}_b$ to $\widehat{h}_b$, $\widetilde{h}_b$ for the tensor (42), vector (43) observables have been calculated varying the jet resolution parameter y_{cut}. A total number of $N_{tot} = 10^9$ Z decays for unpolarized beams was assumed [52]. A measurement of $\widehat{h}_b$, $\widetilde{h}_b$ has to produce a mean value larger than $\delta\widehat{h}_b$, $\delta\widetilde{h}_b$ to be able to claim a non-zero effect at the 1 s. d. level. Comparing with optimal observables it was found for unpolarized beams [108,110] that these simple observables (42,43) reach nearly optimal sensitivities. Therefore optimal observables are not considered in the following.

The inverse sensitivities $\widehat{h}_b$, $\widetilde{h}_b$ are shown in Fig. 24 (left) for Z $\to$ 3 jets for different longitudinal beam polarisations. The results for Z $\to$ 4 jets can be found in [201]. The sensitivity decreases with increasing y_{cut} for all observables due to the decrease in number of events available.

Because the expectation value of the tensor observable does not depend on longitudinal polarisation, the differences in $\delta\widehat{h}_b$ for different polarisation choices reflect only the change in statistics. For $P_+ = 0.6$ and $P_- = -0.8$ the enhancement of the Z production rate

is largest. The differences in $\delta\widetilde{h}_b$ reflect both the change in statistics and the modification of the expectation value due to polarisation. For $P_+ = 0.6$ and $P_- = -0.8$ the sensitivity increases by more than a factor of six compared to unpolarized beams. A convenient choice of the polarisations can even lead to a better sensitivity of the vector observable to $\widetilde{h}_b$ than of the tensor observable to $\widehat{h}_b$. The improvement in sensitivity due to positron polarisation in addition to electron polarisation is relatively small.

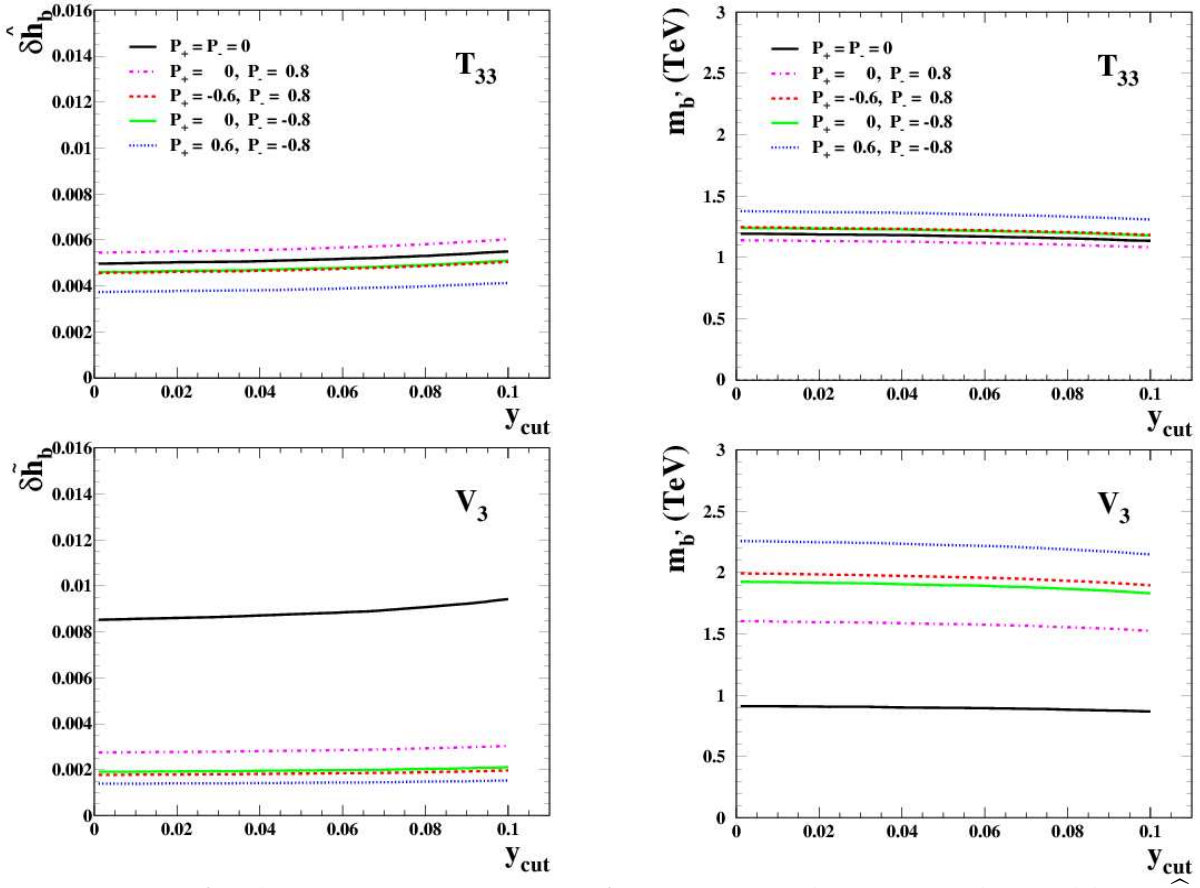

Figure 24: Left: The inverse sensitivities of tensor T_{33} and vector V_3 observables to $\widehat{h}_b$ and $\widetilde{h}_b$. Right: Lower limits on the excited quark mass $m_{b'}$ at the 1 s. d. level which can be derived from a measurement of those observables (couplings for the b' as discussed in the text are assumed). The results for Z $\rightarrow$ 3 jets are shown as function of the jet resolution parameter y_{cut} for different longitudinal polarizations of the e^+ and e^- beams.

If a measurement of $\widehat{h}_b$, $\widetilde{h}_b$ produces a mean value lower than $\delta\widehat{h}_b$, $\delta\widetilde{h}_b$ a non-zero effect at the 1 s. d. level cannot be claimed and therefore an upper limit on these couplings can be derived. As discussed above this can be translated into lower bounds on the excited quark mass $m_{b'}$. Assuming $\mathrm{Re}(\hat{d}_c\, g'^*_A) = \mathrm{Re}(\hat{d}_c\, g'^*_V) = 1$ these bounds are shown in Fig. 24 (right) for Z $\rightarrow$ 3 jets for different longitudinal beam polarisations. The results for Z $\rightarrow$ 4 jets can be found in [201].

Conclusions

If flavor tagging of b and $\mathrm{b\bar{b}}$ jets is available then, with a total number of 10^9 Z decays and choosing a cut parameter* $y_{cut} = 0.02$, the anomalous coupling constant $\widehat{h}_b$ can be determined with an accuracy of order 0.004 (Z $\rightarrow$ 3 jets) and 0.008 (Z $\rightarrow$ 4 jets) at 1 s. d. level using the tensor observable T_{33} (42) for the measurement. Here, $b - \mathrm{b\bar{b}}$ distinction is not necessary. These accuracies are close to the ones which already can be obtained with unpolarized beams. If in a measurement a non-zero effect at the 1 s. d. level is not observed excited quark masses $m_{b'}$ lower than 1.4 TeV (Z $\rightarrow$ 3 jets) and 0.94 TeV (Z $\rightarrow$ 4 jets) can be excluded if appropriate couplings are of a size characteristic of a strong interaction.

If $b - \mathrm{b\bar{b}}$ distinction is experimentally realizable, which should be the case at a future linear collider, the coupling constant $\widetilde{h}_b$ can be measured with an accuracy of order 0.0015 (Z $\rightarrow$ 3 jets) and 0.003 (Z $\rightarrow$ 4 jets) using the vector observable V_3 (43) and choosing $P_+ = 0.6$ and $P_- = -0.8$ as longitudinal polarisations of positrons and electrons, respectively. In case of a non-observation of an effect at the 1 s. d. level excited quark masses $m_{b'}$ lower than 2.2 TeV (Z $\rightarrow$ 3 jets) and 1.5 TeV (Z $\rightarrow$ 4 jets) can be excluded if the relevant couplings are of a size characteristic of a strong interaction.

Comparing 3 and 4 jet analyses [201] one finds that the sensitivity to the anomalous coupling $\widehat{h}_b$ is roughly constant as function of the cut parameter y_{cut} for $y_{cut} < 0.1$ in the 3 jet case. For the 4 jet case the sensitivity is found to increase as y_{cut} decreases. For $y_{cut} \approx 0.01$ the 4 jet sensitivity is found to become equal to that from 3 jets. Of course in an experimental analysis one should try to make both 3 and 4 jet analyses in order to extract the maximal possible information from the data.

In these theoretical investigations always 100% efficiencies are assumed and only the statistical errors are considered. Assuming systematic errors to be of the same size as the statistical ones, the accuracies in the determinations of $\widehat{h}_b$, $\widetilde{h}_b$ discussed above should indeed be better by more than one order of magnitude than those derived from LEP. As shown in [114] this will, for instance, give valuable information on the scalar sector in multi-Higgs extensions of the Standard Model. Moreover interesting information on models with excited quarks can be derived.

*This value of y_{cut} is, in fact, a relatively large number for a selection of events Z $\rightarrow$ 4 jets. So the numbers given in the following are conservative for this channel.

3.6.5 Transversely polarised beams for CP violation in γZ production

Summary: Anomalous CP-violating $\gamma\gamma Z$ vertex gives rise to a novel asymmetry which is accessible with transversely polarised beams in the process $e^+e^- \to \gamma Z$. This asymmetry, which is odd under naive time reversal, is proportional to the real part of the $\gamma\gamma Z$ CP-violating coupling and is not accessible with unpolarised or longitudinally polarised beams but could only be measured with transversely polarised beams. This is in contrast to the simple forward-backward asymmetry of the γ (or Z) with unpolarized or longitudinally polarized beams, which is even under naive time reversal, and is proportional to the imaginary part.

In γZ production a CP-violating contribution can arise if anomalous CP violating $\gamma\gamma Z$ and γZZ couplings are present. The interference of the contributions from these anomalous couplings with the SM contribution give rise to the polar-angle forward-backward asymmetry with longitudinally polarised beams [120], as well as new combinations of polar and azimuthal asymmetries in the presence of transversely polarised beams [117,118]. The parametrisation of the couplings was done in the most general form consistent with Lorentz invariance, gauge invariance and chirality conservation and include contact interactions as well as triple gauge vertices.

In general it was shown in [118] that longitudinal beam polarisation plays an important role in improving the sensitivity to absorptive parts of CP violating form factors, which are measurable even with unpolarised beams. However, transverse polarisation enables measurements of dispersive parts of certain form factors which are inaccessible with longitudinally or unpolarised beams.

Overview

The role of transverse polarization in the context of CP violation has been already studied in section 3.6.1 in the process $e^+e^- \to t\bar{t}$. Since transverse beam polarization provides an additional reference coordinat axis in addition to the e^+e^- beam direction, there is the possibility of studying the azimuthal distribution of a single final-state particle. This has the advantage that the polarization of the produced particle, and hence its decay distribution, need not be measured. In case that SM contribution occurs only via s-channel γ, Z exchange, CP violating effects could only happen from intereferences with (pseudo)scalar or tensor couplings.

This results gets somewhat modified if the possibility of t- and u-channel exchanges are also taken into account. In particular, the t- or u-channel exchange would introduce an extra dependence on the scattering (polar) angle θ. In a process where A is its own conjugate, there may be a consequent forward-backward asymmetry corresponding to $\theta \to \pi - \theta$, which is CP odd. It is well-known that such an asymmetry could arise without transverse polarization (see, for example, [119–121]). However, such a forward-backward asymmetry, in the absence of transverse polarization, is even under naive time reversal T (*i.e*, reversal of particle spins and momenta). Hence the CPT theorem implies that the contribution comes only from an absorptive part in one of the interfering amplitudes (see, for example, [122]). Thus, such a symmetry is only sensitive to the imaginary parts of the new-physics couplings.

However, if there is transverse polarization, a T-odd but CP-even azimuthal asymme-

try can be combined with the T-even but CP-odd forward-backward asymmetry to give an asymmetry which is both CP odd as well as T odd. In this case, the CPT theorem dictates that such an asymmetry measure the real part of the new-physics couplings.

In the following some details are given concerning the study of CP-violating triple gauge couplings [117], the extension to a set of general form factors has been done in [118].

Theoretical framework for the inclusion of CP-violating TGC's

The chosen process is $e^+e^- \to \gamma Z$, where the final-state particles are both self-conjugate. This process occurs at tree level in SM. A CP-violating contribution can arise if anomalous CP-violating $\gamma\gamma Z$ and γZZ couplings are present.

The interference of the contributions from these anomalous couplings with the SM contribution gives rise to the expected polar-angle forward-backward asymmetry, as well as new combinations of polar and azimuthal asymmetries. In particular, there is a CP-odd, T-odd asymmetry, which is proportional to the real part of the $\gamma\gamma Z$ coupling. This real part cannot be probed without transverse polarization.

The most general effective CP-violating Lagrangian for $\gamma\gamma Z$ and γZZ interactions, can be written as

$$\mathcal{L} = e\frac{\lambda_1}{2m_Z^2}F_{\mu\nu}\left(\partial^\mu Z^\lambda \partial_\lambda Z^\nu - \partial^\nu Z^\lambda \partial_\lambda Z^\mu\right) + \frac{e}{16 c_W s_W}\frac{\lambda_2}{m_Z^2}F_{\mu\nu}F^{\nu\lambda}\left(\partial^\mu Z_\lambda + \partial_\lambda Z^\mu\right), \qquad (44)$$

where $c_W = \cos\theta_W$ and $s_W = \sin\theta_W$ and θ_W is the weak mixing angle.

The differential cross section is given by

$$\frac{d\sigma}{d\Omega} = \mathcal{B}\left[\frac{1}{\sin^2\theta}\left(1 + \cos^2\theta + \frac{4\bar{s}}{(\bar{s}-1)^2} - P_e P_{\bar{e}}\frac{g_V^2 - g_A^2}{g_V^2 + g_A^2}\sin^2\theta\cos 2\phi\right) + C_A\cos\theta\right], \qquad (45)$$

where θ is the angle between photon and the e^- directions, and ϕ is the azimuthal angle of the photon, with e^- direction chosen as the z axis and the direction of its transverse polarization chosen as the x axis. The e^+ polarization direction is chosen parallel to the e^- polarization direction. P_e and $P_{\bar{e}}$ are respectively the degrees of polarization of the e^- and e^+. The following notations have been used:

$$\bar{s} \equiv \frac{s}{m_Z^2}, \qquad (46)$$

$$\mathcal{B} = \frac{\alpha^2}{16 s_W^2 m_W^2 \bar{s}}\left(1 - \frac{1}{\bar{s}}\right)(g_V^2 + g_A^2), \qquad (47)$$

$$C_A = \frac{\bar{s}-1}{4(g_V^2+g_A^2)}\left\{(g_V^2 + g_A^2 + (g_V^2 - g_A^2)P_e P_{\bar{e}}\cos 2\phi)\mathrm{Im}\lambda_1\right. \qquad (48)$$

$$\left. - g_V(1 + P_e P_{\bar{e}}\cos 2\phi)\mathrm{Im}\lambda_2 - g_A P_e P_{\bar{e}}\sin 2\phi\,\mathrm{Re}\lambda_2\right\}. \qquad (49)$$

Defining the following CP-odd asymmetries, which combine a forward-backward asymmetry with an appropriate asymmetry in ϕ, so as to isolate appropriate anomalous couplings:

$$A_1 = \tfrac{1}{\sigma_0}\textstyle\sum_{n=0}^{3}(-1)^n\left(\int_0^{\cos\theta_0} d\cos\theta \int_{\pi n/2}^{\pi(n+1)/2} d\phi\, \tfrac{d\sigma}{d\Omega} - \int_{-\cos\theta_0}^{0} d\cos\theta \int_{\pi n/2}^{\pi(n+1)/2} d\phi\, \tfrac{d\sigma}{d\Omega}\right) \qquad (50)$$

$$A_2 = \frac{1}{\sigma_0}\sum_{n=0}^{3}(-1)^n\left(\int_0^{\cos\theta_0} d\cos\theta\int_{\pi(2n-1)/4}^{\pi(2n+1)/4} d\phi\,\frac{d\sigma}{d\Omega} - \int_{-\cos\theta_0}^{0} d\cos\theta\int_{\pi(2n-1)/4}^{\pi(2n+1)/4} d\phi\,\frac{d\sigma}{d\Omega}\right) \quad (51)$$

$$\begin{aligned} A_3 = \frac{2}{\sigma_0}\Bigg\{&\int_0^{\cos\theta_0} d\cos\theta\left(\int_{-\pi/4}^{\pi/4} d\phi\,\frac{d\sigma}{d\Omega} + \int_{3\pi/4}^{5\pi/4} d\phi\,\frac{d\sigma}{d\Omega}\right) \\ &- \int_{-\cos\theta_0}^{0} d\cos\theta\left(\int_{-\pi/4}^{\pi/4} d\phi\,\frac{d\sigma}{d\Omega} + \int_{3\pi/4}^{5\pi/4} d\phi\,\frac{d\sigma}{d\Omega}\right)\Bigg\} \end{aligned} \quad (52)$$

with

$$\sigma_0 \equiv \sigma_0(\theta_0) = \int_{-\cos\theta_0}^{\cos\theta_0} d\cos\theta\int_0^{2\pi} d\phi\,\frac{d\sigma}{d\Omega}\,. \quad (53)$$

These are easily evaluated to be

$$A_1(\theta_0) = -\mathcal{B}'\,g_A\,P_eP_{\overline{e}}\,\mathrm{Re}\lambda_2 \quad , \quad (54)$$

$$A_2(\theta_0) = \mathcal{B}'\,P_eP_{\overline{e}}\,((g_V^2 - g_A^2)\,\mathrm{Im}\lambda_1 - g_V\,\mathrm{Im}\lambda_2) \quad (55)$$

$$A_3(\theta_0) = \mathcal{B}'\,\left[\frac{\pi}{2}((g_V^2 + g_A^2)\,\mathrm{Im}\lambda_1 - g_V\,\mathrm{Im}\lambda_2) + P_eP_{\overline{e}}((g_V^2 - g_A^2)\,\mathrm{Im}\lambda_1 - g_V\,\mathrm{Im}\lambda_2)\right]. \quad (56)$$

$$\sigma_0 = 4\pi\mathcal{B}\left[\left\{\frac{\bar{s}^2+1}{(\bar{s}-1)^2}\ln\left(\frac{1+\cos\theta_0}{1-\cos\theta_0}\right) - \cos\theta_0\right\}\right]\,. \quad (57)$$

In the above equations, we have defined

$$\mathcal{B}' = \frac{\mathcal{B}(\bar{s}-1)\cos^2\theta_0}{(g_V^2+g_A^2)\sigma_0(\theta_0)}. \quad (58)$$

It can be seen that $A_1(\theta_0)$ is proportional to $\mathrm{Re}\lambda_2$, and the other two asymmetries depend on $\mathrm{Im}\lambda_1$ and $\mathrm{Im}\lambda_2$. Moreover, the latter two measured simultaneously can be used to get limits on the two couplings $\mathrm{Im}\lambda_1$ and $\mathrm{Im}\lambda_2$.

It has been calculated 90% CL limits that can be obtained with a linear collider with $\sqrt{s} = 500$ GeV, $\int \mathcal{L}dt = 500$ fb^{-1}, $P_e = 0.8$, and $P_{\overline{e}} = 0.6$ making use of the asymmetries A_i. The limiting value λ^{lim} (i.e. the respective real or imaginary part of the coupling) is related to the value A of the asymmetry for unit value of the coupling constant by

$$\lambda^{\mathrm{lim}} = \frac{1.64}{A\sqrt{N_{SM}}}, \quad (59)$$

where N_{SM} is the number of SM events.

A_1 depends on Re λ_2 alone, and can therefore place an independent limit on Re λ_2. We emphasize once again that information on Re λ_2 cannot be obtained without transverse polarization. The best limits are summarized in Table 3.15.

Coupling	Individual limit from			Simultaneous limits
	A_1	A_2	A_3	
Re λ_2	1.38×10^{-2}			
Im λ_1		6.22×10^{-3}	3.82×10^{-3}	7.05×10^{-3}
Im λ_2		9.10×10^{-2}	3.01×10^{-2}	6.74×10^{-2}

Table 3.15: 90 % CL limits on the couplings from asymmetries A_i for a cut-off angle of 26°, $\sqrt{s} = 500$ GeV, and integrated luminosity of 500 fb^{-1}. The electron and positron transverse polarizations are assumed to be respectively 0.8 and 0.6.

3.7 Precision measurements of the electroweak theory at GigaZ

3.7.1 Measurement of $\sin^2\theta_{eff}$ – Application of the Blondel Scheme

Summary: The most sensitive test of the SM can be made with the Gigaz option of a Linear Collider, i.e. running with high luminosity at the Z-pole or at the WW threshold. Measuring accurately the left-right asymmetry enables to derive the electroweak mixing angle with highest precision. However, in order to exploit the gain in statistics at GigaZ, the uncertainty in the polarisation has to be kept under 0.1%. This precision cannot be provided by Compton polarimetry but with applying a modified Blondel Scheme, which requires both beams polarised. One gains about one order of magnitude when applying this scheme compared to the case of having only polarised electrons and using Compton polarimetry only.

The option GigaZ refers to running the LC at the Z resonance with to about 10^9 Z events and makes possible the most sensitive test of the SM ever made.

In the SM the left–right asymmetry A_{LR} depends only on the effective leptonic weak mixing angle:

$$A_{LR} = \frac{2(1-4\sin^2\Theta^l_{eff})}{1+(1-4\sin^2\Theta^l_{eff})^2}. \tag{60}$$

The statistical power of the data sample can be fully exploited only when $\delta(A_{LR}(pol)) < \delta(A_{LR}(stat))$. For $10^8 - 10^9$ Z's this occurs when $\delta(P_{eff}) < 0.1\%$. In this limit $\delta(\sin^2\theta_{eff}) \sim 10^{-5}$, which is an order–of–magnitude smaller than the present value of this error. Thus it will be crucial to minimize the error in the determination of the polarization. Although the improvements in Compton polarimetry achieving a precision $< 0.1\%$ may be difficult. The desired precision should, nevertheless, be attainable with the Blondel Scheme, where it is not necessary to know the beam polarization with such extreme accuracy, since A_{LR} can be directly expressed via cross sections for producing Z's with longitudinally polarized beams:

$$\sigma = \sigma_{unpol}[1 - P_{e^-}P_{e^+} + A_{LR}(P_{e^+} - P_{e^-})], \tag{61}$$

$$A_{LR} = \sqrt{\frac{(\sigma^{RR}+\sigma^{RL}-\sigma^{LR}-\sigma^{LL})(-\sigma^{RR}+\sigma^{RL}-\sigma^{LR}+\sigma^{LL})}{(\sigma^{RR}+\sigma^{RL}+\sigma^{LR}+\sigma^{LL})(-\sigma^{RR}+\sigma^{RL}+\sigma^{LR}-\sigma^{LL})}}. \tag{62}$$

In this formula the absolute polarisation values of the left- and the right-handed states are assumed to be the same. Corrections have to be determined experimentally by means of polarimetry techniques; however, only relative measurements are needed, so that the absolute calibration of the polarimeter cancels [21].

As can be seen from (62) the Blondel scheme also requires some luminosity for the less favoured combinations (LL, RR). However only about 10% of running time will be needed for these combinations to reach the desired accuracy for these high precision measurements. Fig. 25 shows the statistical error on A_{LR} as a function of the positron polarisation for $P_{e^-} = 80\%$. Already with 20% positron polarisation the goal of $\delta\sin^2\theta_{eff} \sim 10^{-5}$ can be reached. The comparison of different beam polarisation configurations and the gain for the A_{LR} Measurements see also [22].

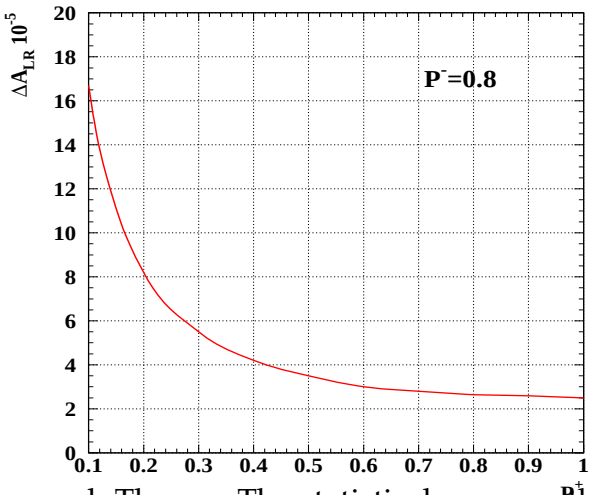

Figure 25: Test of Electroweak Theory: The statistical error on the left–right asymmetry A_{LR} of $e^+e^- \to Z \to \ell\bar{\ell}$ at GigaZ as a function of the positron polarization $P(e^+)$ for fixed electron polarization $P_{e^-} = \pm 80\%$ [21].

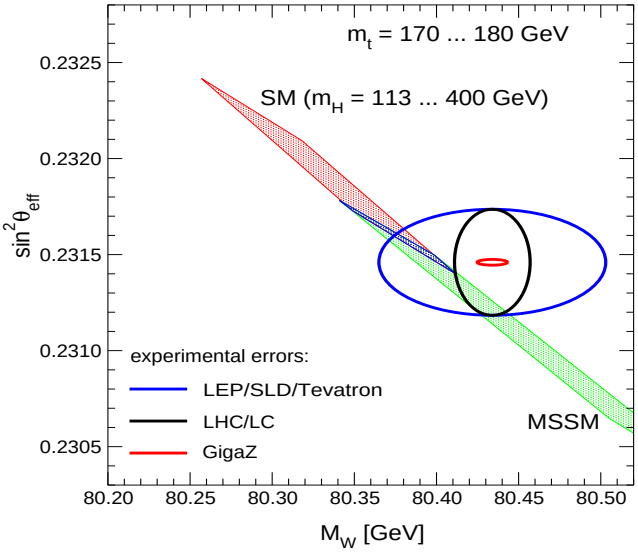

Figure 26: Test of Electroweak Theory: A high-precision measurement at GigaZ of the left–right asymmetry A_{LR} and consequently of $\sin^2\Theta^l_{eff}$ allows to test the electroweak theory at an unprecedented level. The allowed parameter space of the SM and the MSSM in the $\sin^2\Theta^l_{eff}$–M_W plane is shown together with the experimental accuracy reachable at GigaZ. For comparison, the present experimental accuracy (LEP/SLD/Tevatron) and the prospective accuracy at the LHC and a LC without GigaZ option (LHC/LC) are also shown [23,24].

As an example of the potential of the GigaZ $sin^2\theta_{eff}$ measurement Fig. 26 compares the present experimental accuracy on $sin^2\theta_{eff}$ and M_W from LEP/SLD/Tevatron and the prospective accuracy from the LHC and from a LC without GigaZ option with the predictions of the SM and the MSSM. With GigaZ a very sensitive test of the theory will be possible.

3.7.2 Higgsmass versus electroweak mixing angle

Summary: The gain of about one order of magnitude in the precise measurement of the leptonic electroweak mixing angle leads to a strong improvement for the prediction of the Higgs mass in the SM and in the MSSM. In the SM the Higgs mass is constraint up to a few GeV when applying both beam polarised, that means the constraints are about one order of magnitude better compared to the case of using polarised electrons only. In the MSSM the corresponding predicted range for the Higss mass m_h is reduced by about a factor of 7 when having both beams polarised.

The precise measurement of the effective leptonic weak mixing angle at the Z-boson resonance, $\sin^2\theta_{\rm eff}$, at GigaZ will allow a very sensitive test of the electroweak theory [24]. With both beams polarized, i.e. 80% polarization for electrons and 60% polarization for positrons, an accuracy of $\Delta \sin^2\theta_{\rm eff} = \pm 1.3 \times 10^{-5}$ can be achieved [25]. If only electron polarization were available, this would result in an accuracy of only about $\Delta \sin^2\theta_{\rm eff} = \pm 9.5 \times 10^{-5}$ [26].

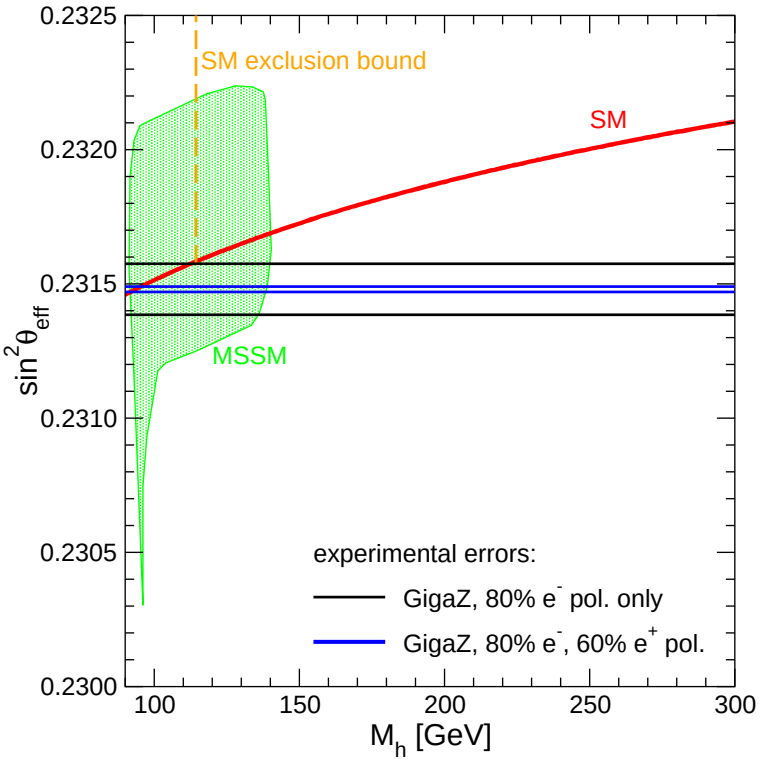

Figure 27: The predictions for $\sin^2\theta_{\rm eff}$ in the SM and the MSSM as a function of M_h, which corresponds to the Higgs-boson mass in the SM and the mass of the lightest $\mathcal{CP}$-even Higgs boson in the MSSM. The exclusion bound on the SM Higgs mass of $M_h > 114.4$ GeV [27] is indicated in the plot. The SM prediction is given for $m_t = 175 \pm 0.1$ GeV, while in the MSSM the SUSY parameters have been scanned. The theory predictions are compared with the experimental accuracies obtainable at GigaZ with an 80% polarized electron beam only and with the case of simultaneous polarization of both beams.

The impact of the more precise measurement for testing the electroweak theory is indicated in Fig. 27, where the experimental accuracy (using the current experimental central

value of $\sin^2\theta_{\text{eff}}$ [28]) is compared with the predictions in the SM and the MSSM. The theoretical predictions are shown as a function of M_h, which corresponds to the Higgs-boson mass in the SM and the mass of the lightest $\mathcal{CP}$-even Higgs boson in the MSSM. In the region where both models overlap, $M_h \lesssim 135\ \text{GeV}$ [29], the SM prediction corresponds to the MSSM result in the limit where all SUSY partners are heavy. The area corresponding to the MSSM prediction was obtained by varying all relevant SUSY parameters independently, taking into account the constraints from the direct search for SUSY particles and the LEP Higgs search. The MSSM predictions are based on the results described in Ref. [30], and the Higgs mass predictions have been obtained with *FeynHiggs2.0* [31].

Within the SM, the precision in $\sin^2\theta_{\text{eff}}$ achievable with both beams polarized constrains the Higgs-boson mass to an interval of few GeV (neglecting the uncertainties from unknown higher-order corrections), while the precision corresponding to electron polarization leaves an uncertainty of about $\pm 25\ \text{GeV}$ in M_h. Within the MSSM the parameter space in the M_h–$\sin^2\theta_{\text{eff}}$ plane is reduced by about a factor 7 with the $\sin^2\theta_{\text{eff}}$ measurement based on simultaneous polarization of both beams as compared to the case with electron polarization only. This puts sensitive constraints on the possible values of the underlying SUSY parameters. Combined with direct information on the SUSY spectrum the precise measurement of $\sin^2\theta_{\text{eff}}$ will allow a very stringent consistency test of the MSSM.

3.8 Summary of the Physics Cases

In the physics sections we have shown some advantages that one gets in case that the positron as well as the electron beam are simultaneously polarised. One can distinguish between several fields for applying both beams polarised: for direct and indirect searches for new particles and for precision tests of the Standard Model.

In **direct searches** one improves the physics potential of a LC qualtitatively as well as quantitatively when using both beams simultaneously polarised:

- the chiral structure of the interaction in the processes can be probed independently. This provides the possibility to probe quantum numbers of the interacting particles and test model assumptions; some of these tests are not possible with polarised electrons only;
- a larger number of observables are available which is crucial for determining the new physics parameters, particularly in a model independent approach;
- transversely polarised beams can be applied in order to construct new CP-odd observables and to enrich the amount of observables to determine the model parameters;
- rates can be further enhanced with suitable polarisation of both beams; This leads to a quick gain in luminosity and may be important for the observation of marginal signals of new physics;
- better control/suppression of SM background processes, which might also be crucial to find traces of new physics particles and determine their properties, e.g. in searches for graviton signatures and Susy partices.

In **indirect searches** for new physics the effect of having both beams simultaneousy polarised is mainly given quantitatively and strongly model dependent:

- enhancement of the effective polarisation and correspondingly the rates leading to a reduction of the statistical error;
- increase of sensitivity to the new physics scale and extension of the disvocery and identification range;
- increase of sensitivity to non-standard couplings;
- measuring the polarisation with better accuracy and reduction of the systematical error;
- increase of sensitivity to new tensor (e.g. graviton) - and (pseudo)scalar-interactions;
- application of transversely polarised beams lead to model distinction even in indirect searches for gravitons.

Exceptionel are the **precision tests** of the Standard Model. Here the use of simultaneously polarised beams improves significantly:

- at high $\sqrt{s}$: separation of the annihilation and scattering channel in W^+W^- production; leading to higher sensitivity in the determination of TG couplings;
- at GigaZ/W^+W^- threshold: higher accuracy in measuring the left-right asymmetry; crucial reduction of systematic errors which are caused by the polarisation measurement; for this purpose a Blondel Scheme has to be applied which definitly needs both beams polarised,

Only if both beams polarised are provided the option of using **transversely polarised beams** is given which enriches the physics potential in both, dierect as well as indirect searches. As already mentioned above, this option

- offers new observables in case of CP-violation;
- enhances the sensitivity to graviton interactions and enables distinction between different models even in indirect searches;
- enables the access to specific TGC which are not accessible with only longitudinally polarised beams;

In Table 3.16 are listed the qualitative (2nd column) and quantitative (3rd column) effects of both beams longitudinally polarised. The numbers in the 3rd column are extracted from the examples in the text with the corresponding polarisation degrees and compared with the case of using polarised electrons only. In most cases $|P_{e^-}| = 80\%$ and $|P_{e^+}| = 60\%$ are used, but in some cases also $|P_{e^-}| = 90\%$ as well as $|P_{e^+}| = 80\%$ or 40% have been used. As a rule of thumb one should keep in mind that one gains about a factor 2 (~ 1.8) concerning S/B and $S/\sqrt{B}$ when employing both beams polarised compared the case with polarised electrons only. But in cases of non-standard couplings even a factor of about 10 can be reached in the comparison. Since in some new physics models only very small rates are expected such a 'quick gain' in luminosity may be crucial to detect the signals. Concerning some examples, e.g. the test of quantum numbers of Susy particles, simultaneously polarised beams are absolutely needed, corresponding remarks are also given in the last column.

Indirect searches for new physics are a very important tool to find traces of physics beyond the SM if the new mass scale is far beyond the kinematical reach of present, future and next-generation collider experiments. Such indirect searches suffer from strong model dependence and it is difficult to give general statements concerning the quantitative physics gain when having both beams polarised. Since the discovery reach scales with the luminosity it is often enhanced by about 20% with both beams polarised compared to the case with only polarised electrons. However, one should keep in mind that the dominant error in these indirect searches may be the systematical error (which were not always taken into account in the given examples). Using both beams polarised reduces the systematical error caused by polarisation measurement.

Concerning e.g. the indirect searches for gravitons, examples have shown that one could even distinguish between different models in indirect searches if both beams polarised were available and transversely polarised beams were applied.

Furthermore the latter option is also particularly interesting concerning searches for CP violating interactions since it provides new observables, e.g. by exploiting the azimuthal dependence of the process in order to detect even marginal traces of new sources

of CP violation. Effects from transversely polarised beams are only present in ee processes if both beams are polarised. Therefore in Table 3.17 are only listed the qualitative effects that one obtains when using this option. One should keep in mind that still physics studies are ongoing and the listed examples can only be seen as a kind of status report up to now.

Table 3.16: The improvement factors indicate the gain if one uses longitudinally polarised e^- and e^+ beams compared to the case of applying polarised electrons only; the corresponding polarisation degrees are given in the text, respectively (B=background, S=signal).

Process	$P(e^+)$ Effects	$P(e^+)$ Improvement Factors
Direct searches for new physics particles		
Higgs:		
$e^+e^- \to H\bar{\nu}\nu$	Enhancement of $\frac{S}{B}$, $\frac{S}{\sqrt{B}}$, B=WW, ZZ, $Z\bar{\nu}\nu$	factor 1.2–1.3
$e^+e^- \to HZ$	better separation: $HZ \leftrightarrow H\bar{\nu}\nu$	factor 4 with RL
	suppression of $B = W^+\ell^-\nu$	factor 1.7
$e^+e^- \to HZ \to H\bar{f}f$	general HZV determination	error reduction by a factor 1.4
SUSY:		
$e^+e^- \to \tilde{e}\tilde{e}$	Test of quantum numbers L, R	$P(e^+)$ absolutely essential
$e^+e^- \to \tilde{\mu}\tilde{\mu}$	enhancement of S/B, $B = WW$	factor 5, may be decisive
	$\Rightarrow m_{\tilde{\mu}_{L,R}}$ in the continuum	
$e^+e^- \to HA$, $m_A > 500$ GeV	enhancement of S/B	factor 1.6, may be crucial
$e^+e^- \to \tilde{\chi}^+\tilde{\chi}^-$, $\tilde{\chi}^0\tilde{\chi}^0$	Enhancement of $\frac{S}{B}$, $\frac{S}{\sqrt{B}}$	factor 2–3
	separation between SUSY models	important, may be crucial
	larger # of observables	may be crucial
	'model independent' determination	
	better indirect $m_{\tilde{\nu}}$	
$\not{CP}$: $e^+e^- \to \tilde{\chi}_i\tilde{\chi}_j$ with	enhancement of CP-odd asymmetries	factor 1.3
$\tilde{\chi}_i \to \tilde{\ell}\tilde{\chi}_1^0$, $\ell_1\ell_2\tilde{\chi}_1^0$		
$\not{R}$: $e^+e^- \to \tilde{\nu}_\tau \to e^+e^-$	Enhancing S/B, $S/\sqrt{B}$	factor 10 with LL
	Test of spin quantum number	
ED:		
$e^+e^- \to G\gamma$	enhancement of S/B, $B = \gamma\nu\bar{\nu}$	factor 3
	Enhancement of discovery reach	factor 1.25, dependent on # of dimensions
Indirect searches for new physics scales		
$e^+e^- \to Z', W' \to f\bar{f}$	Reduction of systematic errors, access to both Z' mass and coupling	strong model dependence
	measurement of Z' couplings	factor 1.6
	discovery reach of W', Z'	enlarged by about $10\% - 20\%$
CI: $e^+e^- \to e^+e-$, $q\bar{q}$	enhancement of sensitivity	factor 1.3
	reduction of systematical errors	
	model distinction	
ED: $e^+e^- \to f\bar{f}$	Enhancement of sensitivity	enlarged by 10%, O(TeV)
Precision measurements of the Standard Model		
top threshold	improvement of A_{LR} measurement	factor 3.8
$e^+e^- \to t\bar{q}$	Enhancing of $\frac{S}{B}$, $(\frac{S}{\sqrt{B}})$, $B = Wq\bar{q}'$	factor 2.1 (1.7)
	FCNC top couplings	limits reduction by a factor 1.8
$e^+e^- \to W^+W^-$	Enhancing of $\frac{S}{B}$, $\frac{S}{\sqrt{B}}$	up to a factor 2
	error reduction of $\Delta\kappa_\gamma$, $\Delta\lambda_\gamma$, $\Delta\kappa_Z$, $\Delta\lambda_Z$	factor 1.7
Giga Z:		
$e^+e^- \to Z$	improve $\delta(P)$, A_{LR}	factor 10, 'Blondel Scheme': $P(e^+)$ essential

Table 3.17: Physics cases where the use of transversely polarised beams are needed. Effects from transversely polarised beams are only present in ee processes if both beam are simultaneously polarised.

Process	Effect of transversely polarised e^- and e^+ beams
$e^+e^- \to f\bar{f}$	ED: *Distinction(!)* between ADD and RS models below KK-modes (*indirect* searches)
$e^+e^- \to t\bar{t}$	$\not{C}\not{P}$: CP-odd asymmetries, sensitive to new (pseudo)S- and T-currents up to 10 TeV
$e^+e^- \to \tilde{\chi}_i\tilde{\chi}_j$	$\not{C}\not{P}$ in Susy: CP-odd observables without final state spin analysis
$e^+e^- \to W^+W^-$	$\not{C}\not{P}$: specific TGC *only* accessible via trans. beams
$e^+e^- \to \gamma Z$	$\not{C}\not{P}$: specific TGC *only* accessible via trans. beams

Chapter 4

Machine Issues

4.1 General remarks

Maybe useful: Remark concerning conventional e+ source

Although it is forseen that the baseline machine would have spin polarised electrons of $P_{e^-} \geq 80\%$ from the beginning, polarised positrons (with $P_{e^+} \geq 50\%$) are considered to be an option for a later upgrade, see [172].

When implementing polarised beams at a very high energy linear collider, one must check that no significant polarisation is lost during the transport of the polarised particles from the source to the interaction region and that any loss is well understood and under control. After the source and after the low-energy beam transport, the transport elements that might contribute to a loss of polarisation are the damping rings, the linac itself and the high energy beam delivery system. The interaction of the two beams at the interaction point(s) might also lower the polarisation.

Polarised sources at the LC:

Polarised electrons: The (now) standard source for polarised electrons is a DC gun with a strained photocathode. This design was already successfully used at the SLC and is used in CEBAF. For details, see section 4.2.

Polarised positrons: Two methods for generating polarised positrons are being discussed:

- Circularly polarised photons from a helical undulator are used to generate longitudinally polarised positrons in a target via $e^{\pm}$ pair production. For details see sections 4.3.1, 4.3.2. The feasibility of undulator–based polarised positron sources will be checked in the E-166 experiment which is being prepared at SLAC.

- Circularly polarised photons obtained by backscattering of a laser light off an electron beam are then used to generate longitudinally polarised positrons in a target as above. See section 4.3.3. This concept will be checked in an experiment being conducted at KEK.

  The design described in section 4.3.3 is for a warm technology linear collider. However, laser-based scheme is also applicable for ILC, a cold technology linear collider [169]. Two options of light sources are considered. One is CO_2 lasers like section 4.3.3 and the other is FELs. First, when we employ CO_2 lasers, the bunch

spacing must be short (a few nano seconds) to put about a hundred of bunches in a pulse of CO_2 laser. About 30 pulses is used to obtain 3000 bunches required for ILC. Repetition rate of both CO_2 lasers and target electron beam is about 300 Hz. Fast kickers are necessary to handle such bunches with short spacing when we put (take) them into (out from) a damping ring. Second, if we employ FELs for light source [170], we can directly provide positron beam of 3000 bunches with a few nano seconds, 10-20 seconds, or 300 nano seconds bunch spacing.

No loss of polarisation is expected on the way from the source to the first linac.

Low-energy beam transport:

After the positrons have been produced in the target they must be captured and accelerated. The design of the capture optics has still to be done but will probably include an adiabatic matching device and accelerating cavity, the beam will then pass via a transfer line to the damping rings. The acceleration will be carried out in a cavity with an embedded solenoid field for focussing, who's field will probably be tapered. Tracking of the particle spin will have to be carried out throughout this section and the parameters set to ensure that polarisation is preserved. Due to the low energy of the positrons the space-charge effect will also have to be considered. Accurate modelling of this section will be crucial in delivering a polarised beam for the machine.

Damping rings:

Since the divergence of a newly produced electron or positron beam is too large to allow acceleration in the main linac, the transverse motion must first be damped by exploiting the combined effects of energy loss and gain from, respectively, synchrotron radiation and accelerating cavities in damping rings.

In order to avoid immediate depolarisation, the spins must be rotated into the vertical at the entrance to a damping ring so that they are parallel to the vertical guide fields in the dipole magnets. This can be done with an appropriate combination of solenoid and dipole fields. The vertical spins can be brought back to the longitudinal direction with an analogous system of fields in the extraction line. Since damping rings run at relatively low energies and the particles remain in the ring for a very short time, it is unlikely that the depolarisation effects familiar in high energy storage rings will be significant. It would probably only be necessary to avoid first order depolarising resonances by a correct choice of energy [171]. Nevertheless a detailed simulation of depolarisation effects should be made. This is best carried out using a a Monte–Carlo simulation of the spin–orbit motion [173].

Main linac:

In a linac, the electric field and the particle velocity are essentially parallel. Then, according to the Thomas-BMT equation the electric field will cause essentially no spin precession. There should therefore be no loss of polarisation in the main linac even when the beam is accelerated to hundreds of GeV.

The beam delivery system:

After acceleration, the $e^{\pm}$ beams will be brought to collision with the aid of appropriate beam lines. Since these contain bending magnets and since, according to the Thomas–BMT equation, a beam deflection of $\delta\theta_b$ in a transverse field causes a spin rotation of $a\gamma\delta\theta_b \approx E(\text{GeV})/0.441(\text{GeV})$, care is needed to ensure that the polarisation is longitudinal at the interaction point. Thus it is desirable to design the spin rotators between the damping rings and the main linacs so that the direction of the polarisation can already be adjusted at low energy. The effect of synchrotron radiation in the dipoles on the polarisation and the beam at the high energy should also be checked.

Beam-beam interactions:

Further loss of polarisation can occur as the electron and positron bunches collide. Although a *detailed* study of the mechanism has not been carried out so far, one expects that a first estimate of polarisation loss can be obtained by looking at two mechanisms: a) spin rotation, according to the Thomas–BMT equation, of the spins in one bunch due to the electric and magnetic fields in the oncoming bunch, b) spin flip due to synchrotron emission, namely by the Sokolov-Ternov. The joint effect has been studied analytically [176] as well as numerically [177, 187]. The expected overall loss of polarization [177] of the a bunch is expected to be $\Delta P/P \simeq 1\%$, however, the effective loss up to the point of interaction (luminosity-weighted) is only $\simeq 0.25\%$. See section 5 for more detail. Simulations for the specific final design will have still to be done and in any case an evaluation of the validity of this kind of approach for the actual parameters of the bunches should be carried out.

4.2 Polarised Electrons for Linear Colliders

The SLC established that reliable electron beams with a polarization at high energy approaching 80% can be provided over periods of years. However, the beam structures planned for future colliders present new demands, and in addition higher polarization is desirable. The prospect for meeting these needs is outlined below. The electron beam for JLC/NLC is required to have a 270 ns macropulse at the IP consisting of 192 micropulses spaced 1.4 ns apart. At the IP each micropulse should have a charge of 0.75×10^{10} e^-. If a conventional dc-biased polarized electron gun based on GaAs-type photocathodes is used, it is assumed the gun must produce 1.5×10^{10} e^- for each micropulse, or a total of 2.9×10^{12} e^- in a single macropulse, which is over an order of magnitude more charge than produced for SLC. The problem is that as the current density in the macropulse increases beyond the SLC level, a dynamic barrier due to photoexcited electrons temporarily trapped in surface states limits the charge that can be extracted from the cathode. A satisfactory solution has been found that works well for conventional dc-biased guns: a very high dopant density at the GaAs surface promotes the tunneling of holes to the surface where efficient recombination rapidly disposes of the trapped electrons. Using this technique, macropulses (no micropulse structure) with current densities in excess of JLC/NLC requirements have recently been demonstrated. Although the charge in a single micropulse for TESLA is roughly twice that of JLC/NLC, the spacing between micropulses is 337 ns, which precludes a surface charge limit problem.

Highly polarized electrons are obtained from GaAs (or its tertiary and quaternary analogues) by directing a circularly-polarized laser beam tuned to the band-gap edge to a thin (typically 100 nm), strained epilayer of p-doped GaAs. Only a small fraction of the photons are absorbed in the epilayer. Electrons with zero momentum are promoted from the valence band maximum (VBM) to the conduction band minimum (CBM) upon the absorption of laser photons. A biaxial compressive strain produced by a lattice mismatch with the substrate or by the quantum confinement associated with short-period superlattice structures breaks the degeneracy of the heavy-hole (hh) and light-hole (lh) bands at the VBM. Hh-lh separations of 80 meV are readily achieved, which in carefully grown structures is sufficient to allow the selection of electrons from the hh band only. Because of angular momentum selection rules, this results in CB electrons of exclusively one spin state. A thin epilayer is chosen to minimize strain relaxation away from the heterojunction. As the CB electrons diffuse to the surface, they undergo some depolarization, primarily by interaction with holes. This effect can be considerably reduced by decreasing the dopant density (everywhere but the last few nanometers near the surface, often called 'gradient doping'). Near the surface, the energy levels for pdoped GaAs bend downwards. Most of the electrons reaching the surface are confined to this band-bending region (BBR) for a finite time until they are emitted to vacuum or lose sufficient energy to be trapped in surface states. The BBR is depleted of holes. However, the confined but still mobile electrons in the BBR lose energy by scattering from optical phonons, as a result of which the amplitude and phase of the spin precession vector is continuously reoriented, leading to a significant depolarization. The probability for electrons to escape to vacuum can be as high as 20% if the surface is properly activated with cesium and an oxide to create a negative electron affinity (NEA). Energy dispersion studies show that most of these electrons have energies below that of the CBM in the bulk, while time-resolved polarization measurements demonstrate that the polarization of the emitted electrons drops

continuously with time, consistent with the depolarization mechanism in the BBR described above.

The maximum polarization of the SLC beam was 78% at the source, produced using a 100 nm thick GaAsP/GaAs strained-layer photocathode. By decreasing the dopant density in the bulk, the polarization of this type of cathode was slightly improved for the initial run of a PV experiment (E158-I) at SLAC that required beam parameters similar to those for JLC/NLC. Higher polarization is an ongoing R&D endeavor. Several laboratories have demonstrated electron beams with polarization of 90% or even higher. The problem is that such high values are universally achieved only with a cathode surface having a relatively low quantum efficiency (QE), defined as number of photoemitted electrons per incident photon. Recent improvements in polarization while maintaining a high QE have been achieved with strained GaAsP/GaAs superlattice structures. Each layer of the superlattice (typically 4 nm) is considerably thinner than the critical thickness (10 nm) for the onset of strain relaxation, while the transport efficiency for electrons in the conduction band still can be high. In addition the effective band gap for such superlattices is larger than for GaAs alone, which improves the maximum NEA value and thus the surface escape probability. Today, 100 nm thick, gradient-doped GaAsP/GaAs superlattice photocathodes routinely yield at least 85% polarization at low energy with a maximized QE of 1%. This type of cathode was successfully used during the summer 2003 dedicated run at SLAC of E158-III, for which the polarization at high energy, measured by a Moller polarimeter, was (905% except for short periods following refreshment of the cathode QE (accomplished every few days by adding a small amount of Cs to the surface). This experience points to the possibility of a constant 90% polarization if a technique to control the minimum surface barrier can be developed without reintroducing the surface charge limit effect. Data for 2 SL photocathodes are compared with that for the strain-layer cathode in Table 1. The absolute accuracy of the polarimeters is on the order of 5%

The NLC ZDR describes a dc-biased polarized electron gun operating at 120 kV, i.e., very similar to that of the SLC polarized electron source. For JLC/NLC, because of space-charge effects, such a gun would have to produce first a 270 ns dc pulse. Before acceleration, the microstructure of the electron macropulse would then be generated by rf subharmonic bunchers, which will increase the rms normalized transverse emittance of the beam to the order of 10-4 m. Two alternatives are currently being investigated that would allow the micropulse structure to be generated by the laser itself: very high dc-bias and an rf gun. Advances in the technology of dc-guns may allow electric fields at the cathode as high as 20 MV/m or more, which is an order of magnitude higher than the SLC polarized electron source. The extracted beam should have a low transverse emittance, but since the energy is still quite low, the energy spread will be large so that after some acceleration the microbunches may need to be compressed. An rf gun offers the potential of a very low emittance beam (on the order of 10-6 m) at energies of several MeV so that additional bunch compression is not necessary. With either option the transport and accelerator capture efficiency will be improved so that the charge required for each micropulse would be significantly reduced. A low emittance beam will reduce damping ring requirements. It has not yet been demonstrated that the necessary surface properties of an activated GaAs photocathode will survive for a reasonable time in an operating rf gun.

Because of the large micropulse separation, the TESLA microstructure must be produced by the laser. The required 3 MHz (later 6 MHz), 3 W average power (during the

Cathode Structure	*Growth Method*	$P_e max$	λ_0 *(nm)*	$QE_{max}(\lambda_0)$	*Polarimeter*	*Ref*
1a GaAsP/GaAs strained SL	MOCVD	0.92	775 warm	0.005	Mott Nagoya	a
1b GaAsP/GaAs strained SL	MBE	0.86	783 warm	0.006	CTS Mott SLAC	b
		0.90	780 cold	0.008	Møller E158-III SLAC	c
2 GaAsP/GaAs strained-layer	MOCVD	0.82	805 warm	0.001	CTS Mott SLAC	d
		0.85	800 cold	0.004	Møller E158-I SLAC	e

Table 4.1: Comparison of the data for a 2 SL photocathodes and for the strain layer cathode .

1-ms macropulse) laser (assuming cathode QE of 1% and capture/acceleration efficiency of 50%) with a repetition rate of only a few hertz can in principle be used with either a low-voltage dc gun (each micropulse ¿0.5 ns), a high-voltage dc gun, or using a ¡100 ps pulsewidth with an L-band rf gun. The JLC/NLC micropulse structure can be produced by amplifying a shaped 300-ns string of 714 MHz oscillator micropulses to the level of just over 200 W using, for example, a regenerative amplifier with multiple pumps. Neither laser system has been demonstrated, but both appear to be reasonably doable. The SLC demonstrated that the longitudinally polarized electrons produced at the gun can be transported to the IP with virtually no loss of polarization. Because the JLC/NLC damping ring will operate at constant energy far from a resonance, the polarization of the virtually monoenergetic electron beam, with the spin vector flipped to vertical, will undergo no loss during damping. While there is also no loss of polarization during acceleration in a linac, a loss of 1% is expected in the 180-degree turnaround into the main linac at 8 GeV due to spin diffusion. In the SLC, the polarization vector in the linac had a transverse component to accommodate control of the flat beam. The spin vector was adjusted to longitudinal at the IP by use of spin bumps in the arcs that were independent of the controls for the orientation of the flat beam.

4.3 Positron Polarisation

4.3.1 Undulator-based polarised positron source

The coventional positron source is based on bremsstrahlung from electrons passing through a thick target, simultaneously generating the positrons. However, thick targets limit the maximum obtainable intensities due to multiple-scattering processes. The Linear Collider will work in a pulsed mode with a large number of bunches per pulse. The positron source must produce positrons with the same bunch structure, hence a high number of positron, about 10^{12}-10^{13} per bunch are required. However, a fundamental intensity limit for conventional positron sources is given by the thermal stress which builds up in the conversion target due to the energy deposition of the particles and which could even lead to target damage if the intensity limit is not respected [178]. The emittance of the positron beam exiting a thick target is also greater, making the post target positron capture optics more difficult and less efficient.

Polarised positrons are produced from circularly polarised photons of some MeV energy via pair production in a thin production target. The polarisation to the outgoing positron is transferred accordingly to the cross sections, calculated already by [174] in 1959.

In this section we present the following method to produce a polarised positron beams of the required intensity: a high-energy electron beam in combination with a helical undulator upwards of a 100 m in length is used to produce circularly polarised photons; the polarised photons are then converted in a thin target to polarised positrons via pair production [175].

a) Radiation of a helical undulator

In a helical undulator the electrons pass through a transverse magnetic field whose direction rotates around the beam axis. On axis, along the longitudinal (z) direction the field is,

$$B(z) = B[\cos(\frac{2\pi z}{\lambda_U}), \sin(\frac{2\pi z}{\lambda_U}), 0] \tag{1}$$

where λ_U is the period of the undulator and the electrons move in a spiral trajectory. The helical field may be produced by a pair of conducters wound to a double helix, see Fig. 5. When currents in opposite directions are passed through the two conductors the central axial magnetic field is cancelled leaving only the transverse components. With the dimensionless parameter K

$$K = \frac{2\pi e B_0 \lambda_U}{m_e c^2} = 0.09 B_0[T] \lambda_U[mm], \tag{2}$$

where B_0 is the peak, on-axis, transverse magnetic field of the undulator, the undulator radiation is given by

$$\frac{dN_\gamma}{dL} \frac{30.6}{\lambda_U[mm]} \frac{K^2}{1+K^2} \text{photons}/m/e^-. \tag{3}$$

The photon number spectrum is relatively flat up to the maximum energy E_{c10} of the first harmonic radiation

$$E_{c10} \approx \frac{2\gamma^2 hc/\lambda_U}{1+K^2}. \tag{4}$$

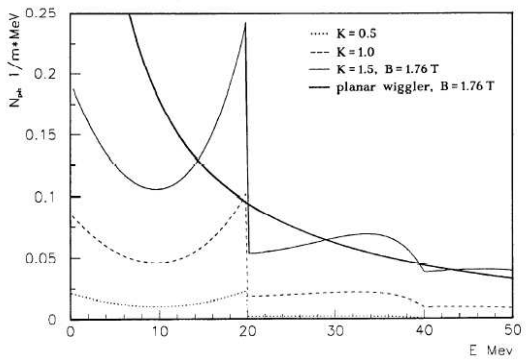

Figure 1: Photon number spectrum for helical undulators and a planar wiggler for different K factors [181].

The energy of the photons produced is related to the electron energy, the periodicty and the on-axis strength of the hleical field. Realistic values for these parameters mean that Polarised photons with energies of the order of 10 Mev are produced, see Fig. 1.

b) Production of polarised positrons

The probability for the production of positrons is roughly independent of the fractional energy E_{e^+}/E_γ in the pair-production process, so that positrons with all energies up to the photon energy are produced. Due to an interplay between energy loss via bremsstrahlung followed by a slight loss of polarisation, the polarisation of positrons of a given energy is highest in targets up to 0.5 radiation length.

Positrons with an energy close to the energy of the incoming photons are 100% longitudinally polarised, while positrons with a lower energy have a lower longitudinal polarisation. The on-axis photons of helical undulator radiation are completely circularly polarised, whereas the off-axis photons have a lower polarisation and a lower energy. The polarisation of the photon beam and the produced positron beam can be increased by scraping off-axis photons off, lengthening the undulator or using specific rescattering devices which means eliminating by this procedure the photons radiated at the second harmonic. Prototypes concerning the helical undulator design, see also [179].

Undulators with superconducting (SC) wires is more brightly exposed to work at high-energy primary beam such as $\geq$ 150 GeV. A SC undulator also allows operation with (relatively) large aperture about 6-8 mm which reduces incident photons on the vessel walls. Periods in the range 8-10 mm would give good operational safety margins. As a SC undulator would not be pulsed its functionality would not depend on the repetition rate [180]. Concerning possible materials about latest designs of SC undulators for a Lc see [182].

4.3.1.1 Demonstration experiment

The experiment E-166 at SLAC is to test the principle and feasibility of generating polarised positron sources via the undulator based scheme [183].

The international E-166 collaboration uses the 50 GeV beam of the Final Focus Test Beam, see Fig.2. The beam will pass through a 1 m long undulator to generate photons of energies up to 10 MeV. The pulsed undulator has a period length of only 2.4 mm and an

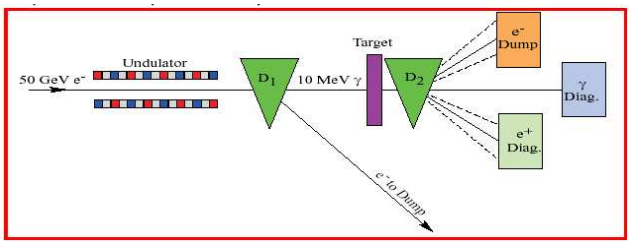

Figure 2: Conceptual layout of the experiment to demonstrate the production of polarised positrons in the SLAC FFTB. The 50-GeV e^- beam passes through an undulator, producing a beam of circular polarised photons of MeV energy. The electrons are deflected by the D_1 magnet. The photons are converted to electrons and positrons in a thin Ti target.The polarisation of the positrons and photons are measured in polarimeters based on Compton scattering of electrons in magnetised iron.

Parameter	TESLA	NLC	E-166
Beam Energy, E_e [GeV]	150-250	150	50
N_e/bunch	3×10^{10}	8×10^9	1×10^{10}
N_{bunch}/pulse	2820	190	1
Pulses/s [Hz]	5	120	30
Undulator Type	plan./helical	helical	helical
Und. Parameter, K	1	1	0.17
Und. Period, λ_u [cm]	1.4	1.0	0.24
Und. Length, L [m]	135	132	1
1^{st} Harmon., E_{c10} [MeV]	9-25	11	9.6
$\mathrm{d}N_\gamma/\mathrm{d}L$ [γ/m/e^-]	1	2.6	0.37
Target Material	Ti-alloy	Ti-alloy	Ti-alloy, W
Target Thickn. [rad. len.]	0.4	0.5	0.5

Table 4.2: TESLA, NLC, E-166 polarised positron parameters

inner diameter of 0.9 mm. The photons are converted into positrons in a thin target. As can be seen from Table 4.2 the photons produced in E-166 are in the same energy range and with the same polarisation characteristics as for a LC. Concerning the pair production process the same target thickness and material as in the LC are used, however, the positron intensity/pulse is lower by a factor 1/2000 compared to a positron source of a future LC. The generated positrons will be guided through a spectrometer and reconverted into photons. The polarisation of the reconverted photons will be measured finally in a transmission polarimeter.

4.3.1.2 Cost and Availability

Cost and availability issues associated with an undulator based positron source are discussed in *Chapter 7: Design Configuration Variants of the U.S. Linear Collider Technology Options Study* of [184]. In this study, a comparison is made between an undulator based versus a conventional source system. Whereas the detailed assumptions and quantitative results of the USLCTOS study are open to discussion, the general conclusions are reasonable: the cost difference between an undulator source and an upgrade from a conventional source is large in absolute terms but small ($\sim 1\%$) in comparison to the overall project cost; availability and schedule are impacted due to the requirement of high en-

ergy electrons for undulator based positron production. These issues need be addressed in future design studies. A brief summary of the discussion in [184] is presented below.

The cost to upgrade to positron polarisation depends of course upon the initial base line. One conclusion in [184] was that the overall LC cost would be reduced by approximately 2% if a conventional positron source were built instead of an undulator based system, but that a later upgrade to include a polarised positron source would be difficult. If the initial LC configuration included the space required in the linac to later install the components of the undulator-based source, the energy make-up in the linac, and the tunnel needed for the positron transfer line, then the total cost would be approximately the same as starting with an undulator source with no conventional source [184]. The cost to subsequently add the technical components for the upgrade from conventional to polarized positrons is likely to be an additional $\sim$1% (taken to be $\frac{1}{2}$ of the 'savings' for a conventional source), assuming the infrastructure (civil and utility) is in the initial construction.

Availability is of concern. Availability comparisons are made between an undulator e^+ source and a conventional e^+ source in Chapter 4 of [184]. The significant difference is that the undulator based source requires high energy electrons for positron production, while the conventional source does not. This difference changes the downtime from 15% for the undulator e^+ source to about 11% for the conventional e^+ source due to considerations of machine recovery times. More importantly, in the USLCTOS model [184], the time spent integrating luminosity increases from about 75% to over 85%. In addition, there is concern regarding the luminosity availability during commissioning as well as the impact on the project schedule if an undulator source adopted at the onset rather than a conventional source.

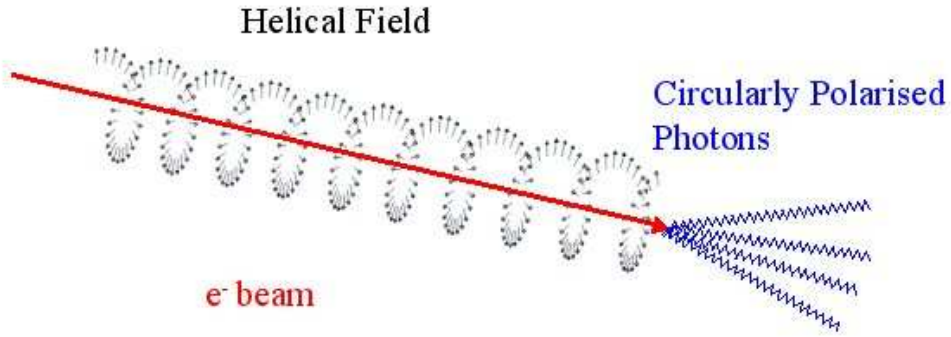

Figure 3: Helical field generating circularly polarised photons

4.3.2 Helical undulator design at Daresbury

ASTeC is involved in designing a helical undulator for the TESLA project.

One of the greatest challenges for any of the proposed Next Linear Colliders is efficient positron production. One of the possible schemes involves using radiation created by the main electron passing through a very long (100m) undulator. This radiation hits a special target in which electron and positron pairs are produced. The positrons can then be captured and accelerated down the main positron linac.

To create a polarised positron beam circularly polarised light from a helical undulator is needed. The transverse magnetic field of a helical undulator means that an electron would follow a helical trajectory through the device - emitting circularly polarised photons. (shown in Figure)

As the energy of the radiation increases so does the rate of electron positron production in the target - up to an energy of 20MeV. To create the highest radiation flux the period of the undulator needs to be as small as possible so that there are as many periods as possible in the available space (100m). These parameters along with the 250 GeV energy of the TESLA beam mean that for a particular undulator period the required on-axis field is easily defined. The shorter the period the higher the field required.

Required on axis field as a function of undulator period to produce 20MeV circularly polarised radiation with a 250 GeV electron beam.

After looking at many different designs including pure permanent magnet planar helical device and other novel magnetic arrangements two different solutions have been recommended.

The first is a super-conducting bi-filar wire. Here two s-c wires are wrapped in a double helix around the vacuum vessel. When current is passed through the wires the longitudinal components of the magnetic field cancel leaving only the rotating (helical) field required on axis.

Schematic of wires wrapped in helix around a former showing different current directions.

The second option is based on permanent magnet technology. Here a dipole field is create by a ring of permanent magnet blocks, with each blocks magnetisation vector rotated around the ring. Many rings are then stacked together so that along a period the

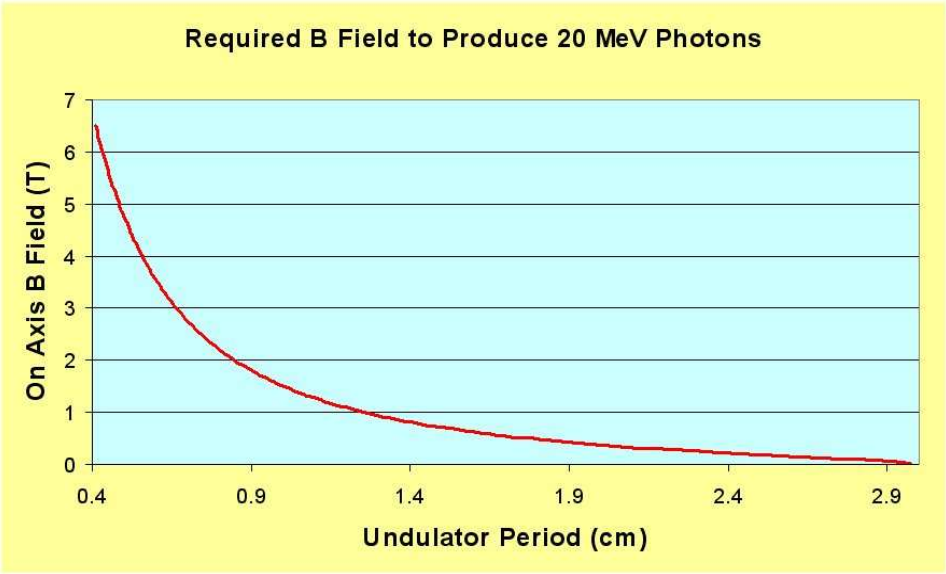

Figure 4: On-axis-B-field versus undulator period

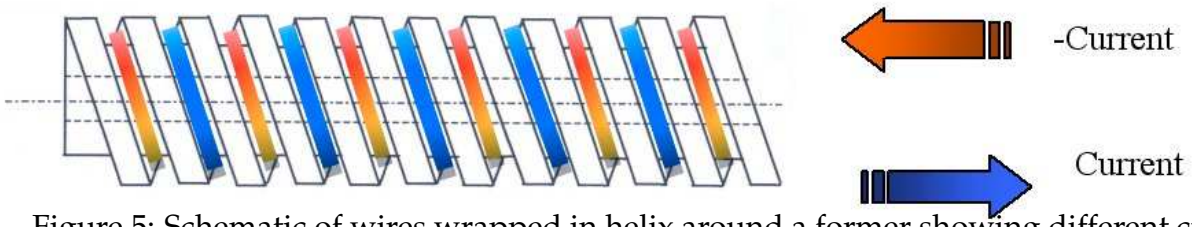

Figure 5: Schematic of wires wrapped in helix around a former showing different current directions.

Figure 6: Prototype

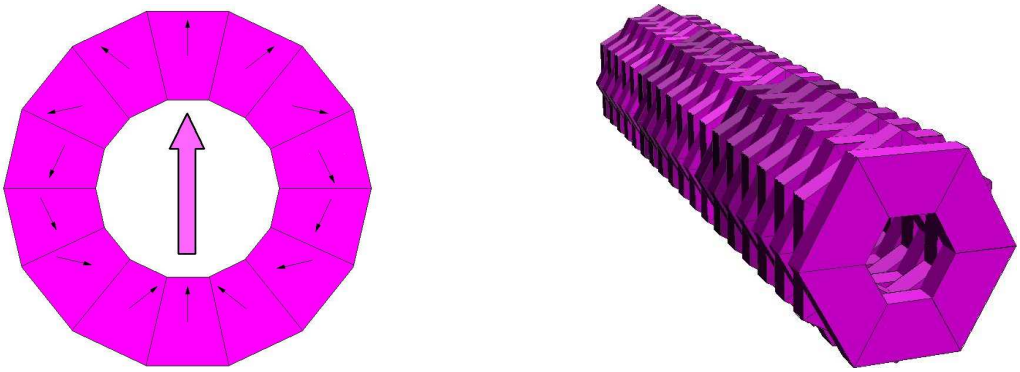

Figure 7: PPM design

Period	On-Axis Field	Magnet Aperture	Material	Current density	Length	Full Module
14 mm	0.85 T	6 mm	NbTi	1000 A/mm^2	30 cm	1-2 m

Table 4.3: SC helical undulator design at Daresbury

dipole field is rotated by 360 degrees. This type of arrangement is called a HALBACH helical undulator.

Dipole field created by many blocks arranged in a ring. Many rings are stacked together to create the helical field

The work done has shown that devices with a period of 14mm look feasible for both different types of technology. It is hoped that over the next year construction of prototypes of both different technologies will commence in order to provide a better understanding of the pros and cons of each design. Each prototype will be around ten or twenty periods long. They are to be used to measure the quality of the magnetic field on axis and to give an initial assessment of the engineering difficulties in constructing such devices, which have not widely been built. The following basic parameters for each device are to be used for the prototypes.

It has been decided that for the prototypes both devices will have a period of 14mm to allow for a good comparison between the two. As can be seen from the numbers modelling of the permanent magnet device suggests that it can produce a higher on axis field than is required so possibly the period could be reduced. However magnet inhomogenieties, magnetisation vector misalignments and engineering tolerances will mean that the measured on axis field will be less. How much is less is one of the reasons for building a prototype.

For the super-conducting device use of Niobium-Tin as a material could increase the on axis magnetic field and so allow for the period to be reduced. This material is relatively

Period	On-Axis Field	Magnet Aperture	Material	Length	Full Module
14 mm	0.83 T	4 mm	NbFeB (1.3 T)	15 cm	5 m

Table 4.4: PPM helical undulator design at Daresbury

new and difficult to work with and so has not been considered for the prototype. The use of iron poles to increase the flux density on-axis is also being considered - although this makes fabrication of the former more difficult.

There are still a number of technical issues that need to be solved and effects that are dependant on the beam properties of the machine that need to be calculated. It is hoped that in the near future a fully working proto-type module will be built. This will further test the engineering difficulties of the design and look at the emitted radiation characteristics.

4.3.3 Laser-Compton Based Polarized Positron Source

This chapter describes the design of a laser-Compton based polarized positron source [185]. In this design, the Compton scattering of circularly polarized laser light off a relativistic electron beam is utilized. Polarized γ-rays are created in the scattering, and then polarized positrons are produced in the subsequent pair-creation on a thin conversion target. Linear colliders usually require huge amount of positrons with multi-bunch/multi-train timing structure, but details of timing structure depend on design of main linacs. Here we assume the requirements of GLC design [186]. In order to meet this requirements, we employ 10 CO_2 lasers, a high current and low emittance electron beam, and multiple laser-electron collision points (see Fig. 8). The electron and laser beams have a multi-bunch structure. As for the time structure of the beam of the main linac, the choice in the polarized positron option is different from that in the standard GLC design, i.e. 96 bunches with a bunch spacing of 2.8 ns in a train. Therefore, the bunch spacings of the electron and laser beams for the positron production, which must agree with that of the main linac, are also 2.8 ns. The 2.8 ns bunch spacing is chosen in order to facilitate the arrangement of the laser optics for the positron source. The number of positrons (electrons) in a bunch for the main linac becomes 1.1×10^{10}, instead of 0.75×10^{10} in the standard GLC design.

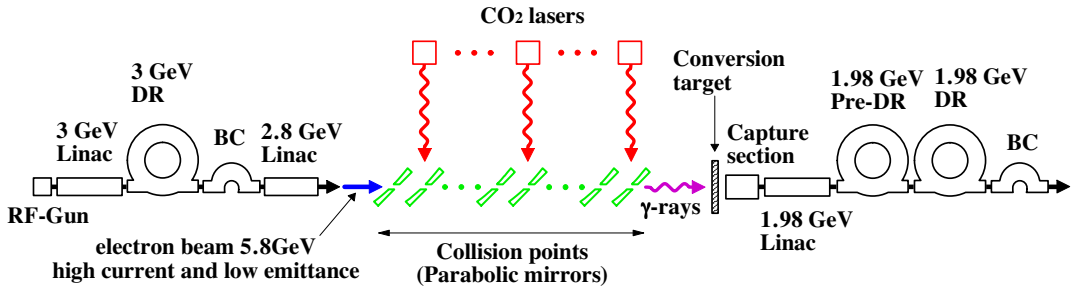

Figure 8: Configuration

A pair of off-axis parabolic mirrors located on the electron beam line is employed for each laser-electron collision point. The first mirror changes the direction of laser propagation, and focuses the laser beam as well, so that the laser beam and the electron beam run on the same axis in opposite directions. The focal length of the mirror is 90 mm and the rms spot size of the laser beam at the focal point is 17 μm. The laser beam collides head-on with the electron beam at the focal point of the laser beam. After the collision, the laser beam is extracted by the second mirror, as shown in Fig. 9. Each mirror has a hole at the center along the electron beam axis. The electron beam and the back-scattered γ-rays pass through these holes. The length of a mirror pair is approximately 200 mm. This compactness allows us to put many pairs in the electron beam line to have multiple collision points.

For multiple collisions of an electron beam at many collision points spread along the beam line, the electron beam is required to have a very low emittance, which is necessary to create a tightly focused beam over a long distance. A 3 GeV multi-bunch electron beam, which is delivered from a linac, is damped by the damping ring to achieve low

emittance: 1.25×10^{-6} rad-m in both the horizontal and vertical directions. The damping ring is operated in full horizontal-vertical coupling mode. Then, the electron beam is accelerated again by another linac up to 5.8 GeV. Since the emittance of the electron beam is small, a focus system with a large β value ($\beta^* = 3.6$ m) can be employed. The spot size of the electron beam at the waist is 20 μm in sigma, and the spot size remains 23 μm even at 2.1 m away from the waist. We put 20 pairs of the parabolic mirrors in one section, in which 20 collision points are available (see Fig. 9). A single laser provides laser bunches in those 20 collision points through all 20 parabolic mirror pairs. The laser beam firstly enters the pair located at the most downstream position of the electron beam, and travels to the upstream pair. Thus, the laser beam goes from one pair to the next pair, and finally reaches the 20-th pair, which is located at the most upstream position of the electron beam. The number of electrons in a bunch is 5×10^{10} and the laser bunch energy is 0.25 J. A train of the electron beam contains 96 bunches, while a train of the laser beam contains 115 bunches. These extra laser bunches are necessary to realize collisions at all of the 20 collision points. Then, when the distance and laser path length between adjacent collision points are properly arranged, it can be realized that all 96 bunches in the electron beam collide 20 times at the 20 collision points.

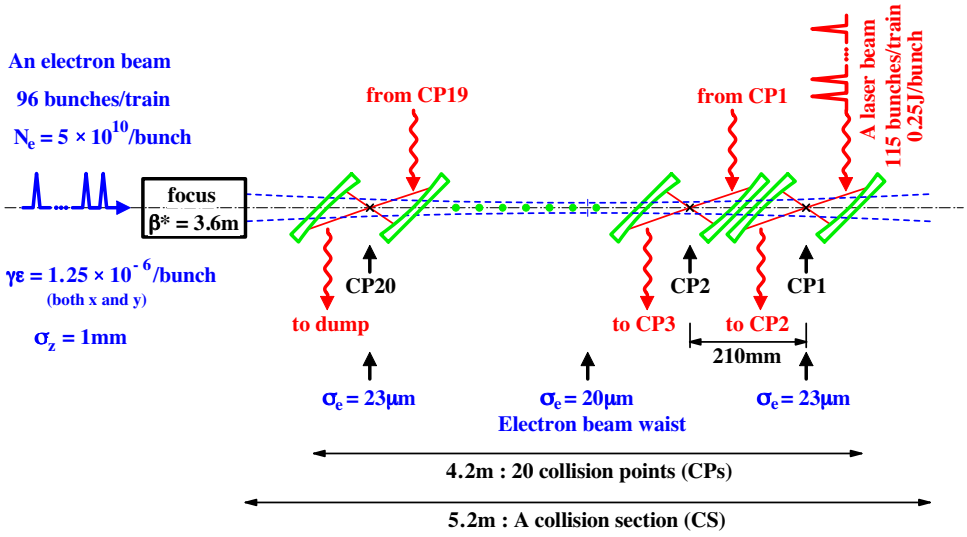

Figure 9: A collision section.

The number of γ-rays generated in the 20 collisions is not large enough to create the required number of positrons. Therefore, the electron beam is refocused so as to make another 20 collisions in the next section, to which another laser beam from another CO_2 laser is delivered. Such refocusing of the electron beam is repeated 9 times. Thus, the entire system has 200 collision points in 10 collision sections (Fig. 10).

The number of γ-rays generated in the 200 collisions is 8.3×10^{11}/bunch (see Fig. 11(a)). Out of them, 5.5×10^{11} γ-rays pass the collimators, which are located along the electron beam line to protect mirrors against radiation damage, and reach the conversion target. The electron-laser collision is simulated by using CAIN [187]. The thickness of the conversion target is 0.5 radiation length, and the target is made of tungsten. The number of positrons created from γ-rays is 6.9×10^{10} in each bunch (see Fig. 11(b)). The energy de-

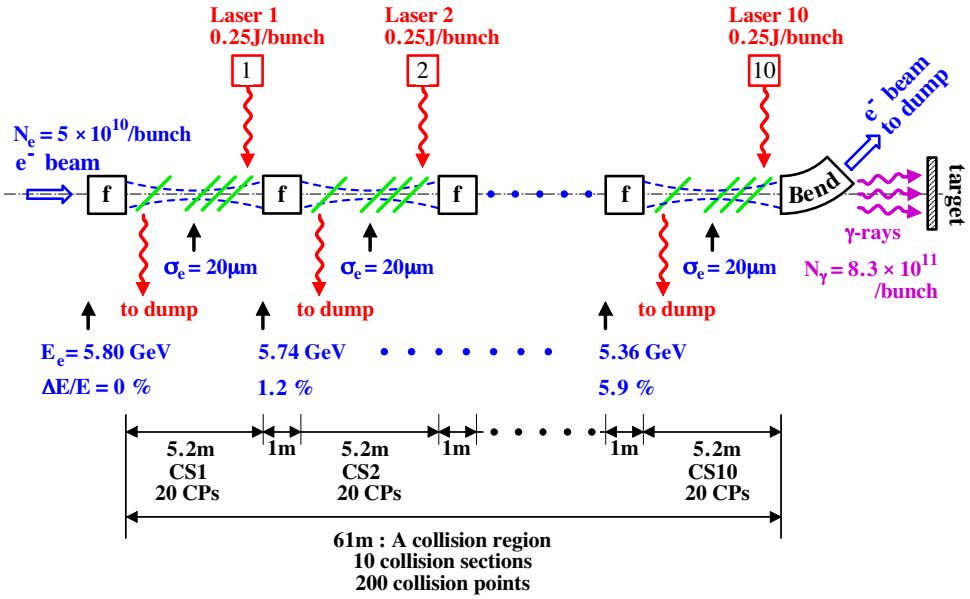

Figure 10: Entire collision region. There are 10 collision sections in total. Between adjacent collision sections, there are refocusing magnets to maintain an electron beam size small in every collision points. Many collimators (they are not written) are put in the electron beam line for mirror protection.

posit on the target by a train (96 bunches) of γ-ray beam is about 10 J, and thermal stress caused by this deposit is estimated to be within tolerable range. The continuous heat load on the target is rather small, 1.5 kW.

A positron capture section consisting of an L-band accelerating structure with a 6 Tesla solenoid magnet is equipped just after the conversion target. The linac, the pre-damping ring, and the damping ring all having an energy of 1.98 GeV follow the capture section (see Fig. 8), which can capture 18 % of pair-created positrons at the relatively high energy side of the spectrum. As a result, 1.2×10^{10} positrons/bunch are captured, and the achieved magnitude of the polarization is 54 %.

A rough estimation shows that the total power consumption, including every compornents shown in Fig. 8, of the positron source to be applroximately 22 MW.

At KEK, it has been pursued thta the development of advanced technologies for polarized γ-ray generation using the 1.28 GeV electron beam of KEK-ATF and a Nd-YAG laser beam [188]. It is remarked that recently the polarization of short pulse γ-rays has been successfully measured [189], and we plan to take a further steps of to produce polarized positrons and to measure of their polarization.

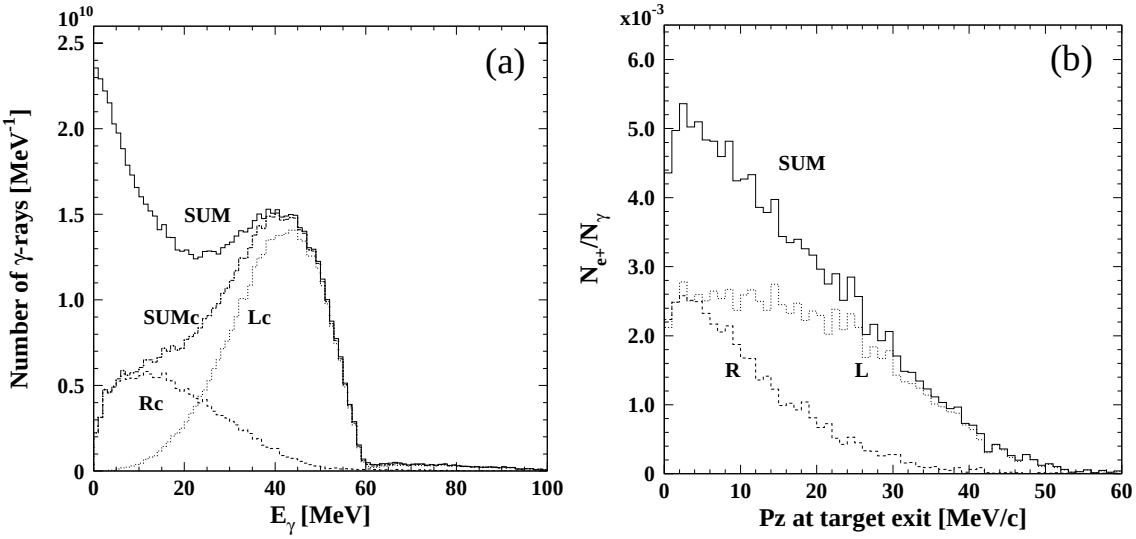

Figure 11: (a) Energy distribution of the whole γ-rays generated by a simulation of 200 collisions (SUM). Also, the γ-rays which pass all collimators and reach the target are indicated separately for the left-handed ones (Lc), the right-hand ones (Rc), and the total (SUMc). Here we assume that the initial laser beams have 100% right-handed polarization. (b) The energy distributions of the positrons at the target exit. The vertical axis is the number of positrons per MeV/c normalized by the total number of γ-rays on the target. Three lines show all positrons (SUM), positrons which have left-hand (L) and right-hand (R) helicity, respectively.

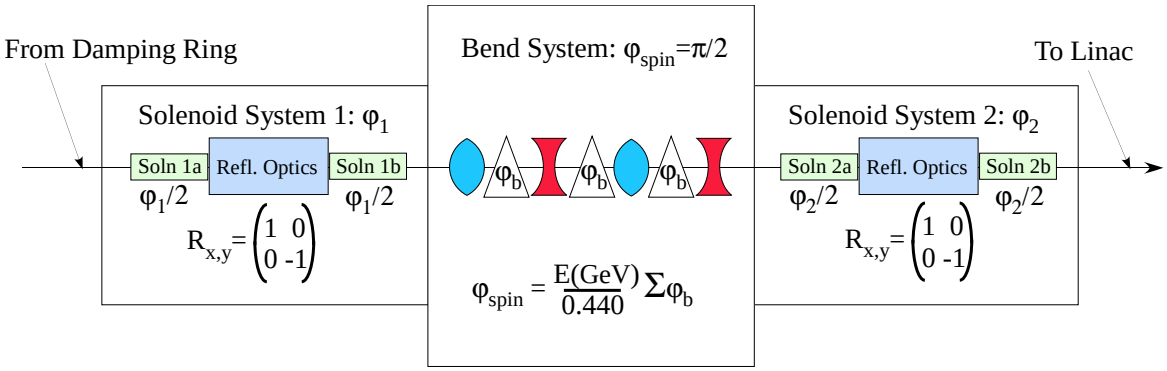

Figure 12: Spin rotation system to rotate vertical spin coming from the damping ring to an arbitrary spin orientation. See text for explanation.

4.4 Transverse Polarisation

If properly designed, the spin rotation system after the damping ring will allow the spins of the beams to be set to any arbitrary orientation. The system described in [refPE] accomplishes the desired spin manipulation while minimizing emittance dilution of the flat beams. Figure 1 illustrates the basic features of the system which consists of two solenoidal rotation systems with a bend rotation system in between. Starting with an initial vertical spin vector coming out of the damping ring, the final spin vector at the exit of the full system is [190]

$$\vec{S} = \overleftrightarrow{\Omega}_{tot} \cdot \begin{pmatrix} 0 \\ \pm 1 \\ 0 \end{pmatrix} = \begin{pmatrix} \mp \sin\phi_1 \cos\phi_2 \\ \pm \cos\phi_1 \cos\phi_2 \\ \pm \sin\phi_2 \end{pmatrix}, \tag{5}$$

where ϕ_1 and ϕ_2 are the spin rotations due to the first and second solenoidal rotation systems. From eq.5, it is seen that any arbitrary orientation of the spin vector is possible through the suitable choice of ϕ_1 and ϕ_2.

Each solenoid system is made up of an initial solenoid followed by an optical transport section which gives a unity transformation in the horizontal plane and a -1 transformation in the vertical plane, an optical reflection. The optical section is followed by a second solenoid. Each solenoid is set to provide a spin rotation of $\frac{1}{2}$ the total required for the particular solenoidal system, ϕ_i. The optical reflection transport is required to avoid transverse betatron coupling of the beam by canceling the rotation due to the solenoids.

The bend section has a constant spin rotation contribution of $\pi/2$ in the horizontal-longitudinal plane. The spin is rotated about the longitudinal axis in the solenoids.

Chapter 5

Polarisation Measurement at the ILC

5.1 General remarks

Still to be done: remark concerning Moeller polarimetry

The primary polarimeter measurement at the ILC will be performed by a Compton polarimeter. An accuracy of $(\Delta P_{e^-}/P_{e^-}) = 0.25\%$ should be achievable [191]. The polarimeters can be located upstream or downstream of the Interaction Point (IP) and it is desirable to implement polarimeters at both locations. The downstream polarimeter probably requires a crossing angle at the IP; polarimetry is one of many issues being considered for deciding on the IR crossing angles.

Compton polarimetry is chosen as the primary polarimetry technique for several reasons:

- The physics of the scattering process is well understood QED, with radiative corrections less than 0.1% [192];
- Detector backgrounds are easy to measure and correct for by using laser off pulses;
- Polarimetry data can be taken parasitic to physics data;
- The Compton scattering rate is high and small statistical errors can be achieved in a short amount of time (sub-1% precision in one minute is feasible);
- The laser helicity can be selected on a pulse-by-pulse basis;
- The laser polarization is readily determined with 0.1% accuracy.

5.2 Compton scattering kinematics

We define E_0 and ω_0 to be the incident energies of the electron and photon, and E and ω to be the scattered energies of the electron and photon. The dimensionless x, y and r scattering parameters are defined by:

$$x = \frac{4E_0\omega_0}{m^2}\cos^2(\theta_0/2) \simeq \frac{4E_0\omega_0}{m^2} \quad (1)$$

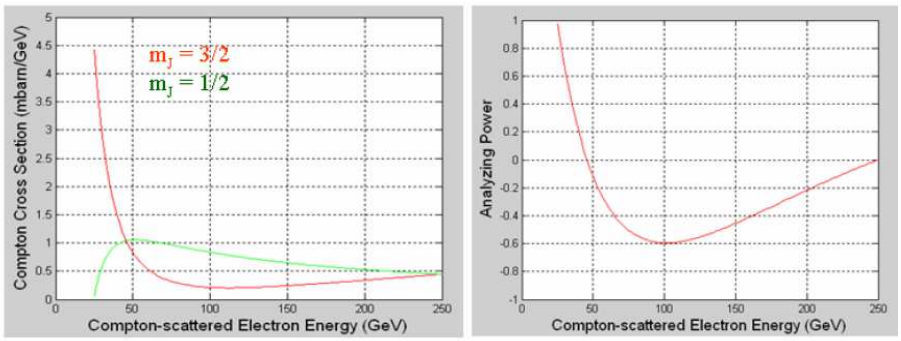

Figure 1: Compton cross section for scattering of 532 nm photons with a 250-GeV electron beam. The J_z=3/2 (J_z=1/2) cross section for electron and photon spins aligned (anti-aligned) is shown in dotted red (solid green).

$$y = 1 - \frac{E}{E_0} = \frac{\omega}{E_0} \tag{2}$$

$$r = \frac{y}{x(1-y)} \tag{3}$$

where m is the mass of the electron and θ_0 is the crossing angle between the electron beam and the laser beam. For polarimeters with small crossing angles at the Compton IP, $\cos^2(\theta_0/2) \simeq 1$.

The spin-dependent differential Compton cross section is given by:

$$\left(\frac{d\sigma}{dy}\right)_{Compton} = \left(\frac{d\sigma}{dx}\right)_{unpol} [1 + P\lambda A_z(x,y)] \tag{4}$$

$$\left(\frac{d\sigma}{dx}\right)_{unpol} = \frac{0.499\text{barn}}{x}\left[\frac{1}{1-y} + 1 - y - 4r(1-r)\right] \tag{5}$$

$$A_z(x,y) = rx(1-2r)(2-y) \tag{6}$$

where P is the longitudinal polarization of the electron and λ is the circular polarization of the laser photon. The Compton asymmetry analyzing power, $A_z(x,y)$, is maximal at the kinematic endpoint, corresponding to 180° backscattering in the center-of-mass frame, with

$$E_{\min} = E_0 \frac{1}{1+x} \tag{7}$$

For a 250 GeV electron beam colliding with a 532-nm laser, the Compton-scattered electrons have their kinematic endpoint at $E_{\min} = 25.1$ GeV with an analyzing power $A_z = 98\%$. Figure 1 shows the resulting J_z=3/2 and J_z =1/2 Compton cross sections and analyzing power.

5.3 Upstream Compton Polarimeter

The Compton Polarimeter upstream of the collider IP requires the Compton IP be just upstream of the energy collimation region so that off energy Compton electrons are not

lost in the Interaction Region. An additional requirement is that the beam trajectory at the Compton IP be parallel to the trajectory at the collider IP. A polarimeter satisfying these requirements was included in the TESLA design and we provide a brief description here [198].

The Compton IP is located 630 meters upstream of the collider IP, see Fig. 2. The

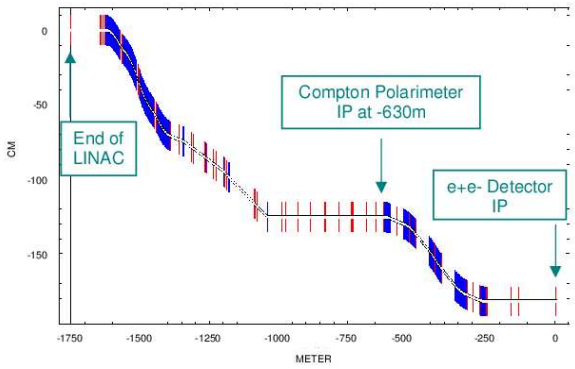

Figure 2: Upstream Compton Polarimeter in the TESLA design.

Compton laser is pulsed with a pattern that matches the pulse and bunch structure of the ILC. In this way it is possible to achieve high luminosity, typically six orders of magnitude higher than with continuous lasers of comparable average power.

Compton electron detection in the multi-event (integrating) mode is the principle detection method. Event rates and statistical errors have been calculated for different beam energies and laser parameters [198]. Table 5.1 gives typical polarimeter parameters for $\sqrt{s} = 500$ GeV. The performance is similar for other energy regimes. For much higher or lower beam energies, it will be advantageous to change the wavelength of the laser, to retain maximum coverage of the electron detector hodoscope.

5.4 Downstream Compton Polarimeter

The design criteria for an extraction line polarimeter seem to prevent a downstream polarimeter if there is no crossing angle at the IP. The 20-mrad crossing angle design considered for NLC, however, permitted a downstream polarimeter and we give a brief description for it here with beam parameters appropriate for the ILC design.

The Compton IP is located approximately 60 meters downstream from the collider IP (see Figure 3). [199] The Compton IP is at a secondary focus in the middle of a chicane with 20 mm dispersion, but with no net bend angle with respect to the e^+e^- collision IP. Beam losses in the extraction line are acceptable, both for machine protection and for ILC Detector backgrounds.

The Compton laser has a low repetition rate of 5-10 Hz, but has high power to give good signal-to-background ratio in the more difficult downstream environment with disrupted primary electrons and beamsstrahlung photons present. The Compton laser pulses collide with a small fraction of the 14 kHz electron bunch rate, but the timing of the Compton laser pulses can be varied so as to systematically sample all electron bunches in the train and determine any variation of the beam polarization along the train.

	e^+/e^- *beam*	**Upstream Laser beam**	**Downstream Laser beam**
energy	250 GeV	2.3 eV	2.3 eV
charge or energy/bunch	$2 \cdot 10^{10}$	$35\ \mu J$	100 mJ
bunches/sec	14100	14100	5
bunch length σ_t	1.3 ps	10 ps	1 ns
average current(power)	$45\ \mu A$	0.5 W	0.5 W
$\sigma_x \cdot \sigma_y\ (\mu m)$	$10 \cdot 1$ upstream $30 \cdot 60$ downstream	$50 \cdot 50$	$100 \cdot 100$
		Upstream Polarimeter	**Downstream Polarimeter**
beam crossing angle		10 mrad	11.5 mrad
luminosity		$1.5 \cdot 10^{32} cm^{-2} s^{-1}$	$5 \cdot 10^{30} cm^{-2} s^{-1}$
event rate at 25-GeV Endpoint		300,000/GeV/sec	10,000/GeV/sec
$\Delta P/P$ stat. error		$< 1\%$ / sec	$< 1\%$ / min
$\Delta P/P$ syst. error		$\leq 0.5\%$	$\leq 0.5\%$

Table 5.1: Compton Polarimeter Parameters at 250 GeV

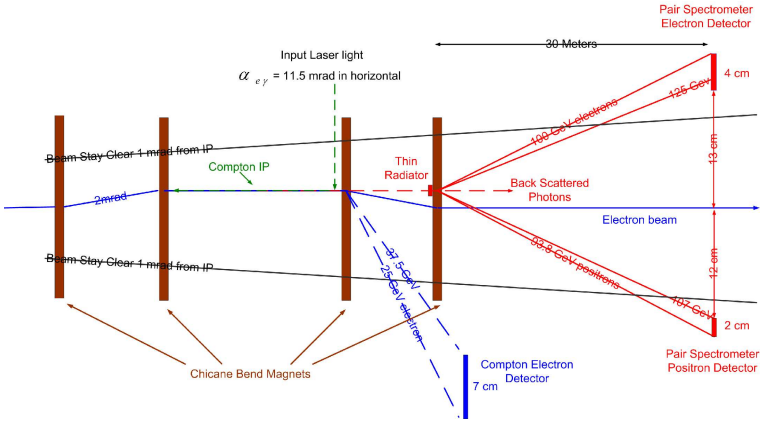

Figure 3: Compton Polarimeter System in the Extraction Line.

The primary Compton detector is envisioned to be a segmented electron detector operating in the multi-electron (integrating) mode, sampling the electron flux at energies near the Compton kinematic edge at 25.1 GeV (for 250 GeV primary electron energy and 532 nm laser photons). The Compton electron detector must discern between the Compton edge electrons and low energy disrupted primary electrons, and it must be located outside a 1-mrad stayclear cone from the IP that contains the intense flux of beamsstrahlung photons. Figure 4 shows the y-distribution of 25.1-GeV Compton-scattered electrons at the detector located ≈ 21 meters downstream of the Compton IP. The Compton-edge electrons peak at ≈ 18 cm, well separated from the tails of the disrupted electron beam. For polarimeter operation at electron beam energies other than 250 GeV, the chicane dipoles should retain the same B-field. This changes the dispersion at the Compton IP, but since the Compton edge endpoint energy does not change quickly with incident electron beam energy, the location of Compton-edge electrons at the Compton detector plane will only

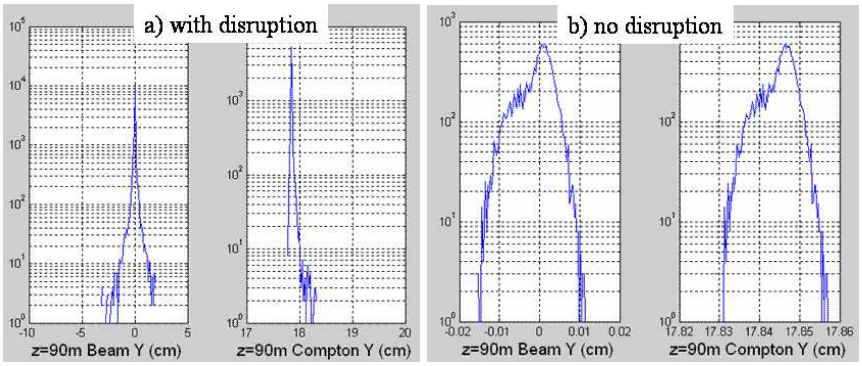

Figure 4: Vertical distributions of disrupted beam and Compton-edge electrons at the Compton detector plane a) with e^+e^- collisions and b) without collisions.

shift slightly. The parameters for the downstream Compton polarimeter are summarized in Table 5.1.

5.5 Luminosity-weighted Polarization

The luminosity-weighted beam polarization will differ from the measured polarization due to disruption and radiation in the beam-beam collision process. There are also effects from polarization spread and spin transport.

The spin motion of a deflected electron or positron beam in a transverse magnetic field follows from the familiar Thomas-Larmor expression

$$\theta^{spin} \;=\; \gamma\,\frac{g-2}{2}\,\theta^{orbit} \;=\; \frac{E_0}{0.44065\;GeV}\,\theta^{orbit} \tag{8}$$

where θ^{orbit} and θ^{spin} are the orbit deflection and spin precession angles, E_0 is the beam energy, $\gamma = E_0/m$, and $(g-2)/2$ is the famous g-factor anomaly of the magnetic moment of the electron.

We define the difference between the luminosity-weighted beam polarization and the polarimeter measurement to be $dP = P_z^{lum-wt} - P_z^{CIP}$. To achieve $dP < 0.1\%$, we require the beam direction at the Compton IP be aligned with the collision axis at the e^+e^- IP to within $50\mu rad$. We consider estimates of several contributions to dP, assuming full longitudinal spin alignment at the polarimeter IP. Having both an upstream and a downstream polarimeter will assist in achieving this and estimating the associated systematic error. [195]

We consider contributions to dP for the downstream polarimeter first, using estimates in the NLC design study. [195] Orbit misalignments between the polarimeter IP and the collision IP are expected to be below 50 μrad, which would give $dP = -0.04\%$. Imperfect compensation for steering effects due to the angle between the beam trajectory and the Detector solenoid is expected to give an additional trajectory alignment uncertainty of 30 μrad, and gives a contribution $dP = -0.01\%$. The effect of Sokolov-Ternov spin flips are expected to contribute $dP = +0.3\%$ ($dP = -0.1\%$) for downstream polarimeter measurements with (without) collisions. The angular divergence of the incoming beam is expected to contribute $dP = -0.03\%$, while the angular divergence of the outgoing

beam is expected to contribute $dP = +0.1\%$ ($dP = -0.25\%$) for downstream polarimeter measurements with (without) collisions. Lastly, effects from chromatic aberrations which were important at SLC are expected to be negligible. Adding all these contributions together, we expect a total difference $dP = +0.32\%$ ($dP = -0.43\%$) for downstream polarimeter measurements with (without) collisions.

A similar compilation of these effects for an upstream polarimeter leads to $dP = -0.42\%$. [195] The systematic errors associated with dP should be substantially smaller than the size of dP, and having independent information from 3 polarimeter measurements (upstream, downstream with and without collisions) will be important in minimizing this.

5.6 Future Design Work

The Beam Delivery Systems for each of 2 IRs at the ILC will be updated in the coming year. The same is true for the Extraction Lines from the collider IPs to the beam dumps. Design choices for the crossing angles of the IRs and Linacs will impact polarimeter designs, as will other design choices such as the optics and locations for the upstream energy collimation. Polarimeter design studies need to be an integral part of the beam optics design studies.

We want to find optics solutions where the beam trajectories are parallel at the upstream and downstream polarimeter Compton IPs and the collider IP. For the upstream polarimeter we need adequate energy collimation downstream of the Compton IP to mitigate against backgrounds from off-energy Compton-scattered electrons. For the downstream polarimeter, we need to evaluate its feasibility and expected performance for different IR crossing angle geometries. Extraction line optics for a downstream polarimeter should also accommodate an energy spectrometer.

The Compton laser system designs will be re-evaluated for optimizing the pulse energy, pulse length and pulse repetition rate, while achieving a simple and robust laser system. This will include revisiting design criteria for the measurement time needed to achieve 0.1% statistical precision and the time scale for monitoring dependence of polarization along the 1-ms train. We also want to evaluate a recent proposal to implement a Fabry-Perot cavity for the laser beam around the Compton IP [193]. A commercial laser with ≈ 10 nJ/pulse and 3-5 MHz pulse frequency could be used together with a high finesse cavity to reach in excess of ≈ 1 J/pulse inside the cavity. In order to amplify laser beam power with a Fabry-Perot cavity one must keep such a cavity at resonance, i.e. match the cavity length and laser beam frequency very precisely. The cavity gain factor is shown in Figure 5. A fast feedback system would be required to ensure these conditions. Such a device is used at the CEBAF accelerator [194] and at HERA.

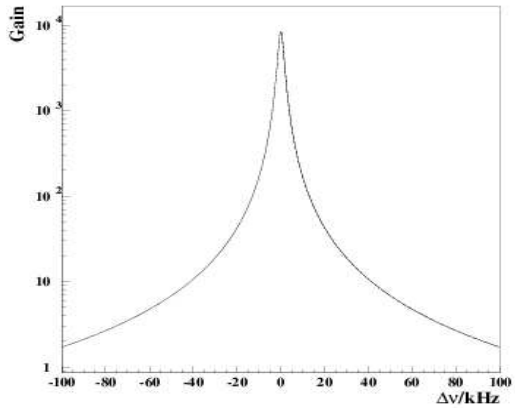

Figure 5: Gain of a 2 m long cavity as a function of the difference between the laser and cavity resonance frequencies. Values of the cavity mirror reflection and transmission are those of the HERA cavity [193].

5.7 Polarisation Measurements with Annihilation Data

Polarisation measurements with polarimeters are limited to a total precision around 0.25%. In addition polarimeters measure either the polarisation of the incoming beam that has not been depolarised by the beam-beam interaction or the one of the outgoing beam which has been depolarised three to four time as much as the interacting particles. On the other hand there are several processes at a linear collider whose polarisation structure is known and which might be used to measure the polarisation directly from data. The large luminosity of the linear collider offers the possibility to reach a precision much better then the polarimeters.

One example is the $\sin^2\theta_{\text{eff}}$ measurement with the Blondel scheme at GigaZ (see sec. 3.7) where the relevant observables can be extracted directly from the data without the use of polarimeters. One has, however, to take into account that all methods using annihilation data involve some physics assumptions that have to be considered in the framework of the model in which the data are analysed. The data driven methods also cannot replace completely the polarimeters. The data methods need a large luminosity to get to a precise result while polarimeters are completely systematics limited and statistics is no problem. In any case polarimeters are thus needed for a fast machine tuning. In addition there are some assumptions in the data-methods that have to be verified or corrected with the polarimeters. In all cases the data methods need the assumption that the absolute values of the polarisations of the left and right handed states are the same. If electron and positron polarisation is available the effective polarisations, explained in sec. 2.2 and the formulae to obtain the polarisation involve linear and quadratic terms of the polarisations. For these reasons any correlations between the two beam polarisations need to be known from beam-beam simulations and polarimeters.

5.7.1 Measurements with Electron Polarisation only

If only electron polarisation is available not only the Lorenz structure of the used process is needed but the exact helicity structure needs to be known. The only process fulfilling this requirement is the V-A structure of the W-fermion couplings. This coupling can be utilised in two processes at a linear collider, single W production and W-pair production. As can be seen from figure 6 both processes have a cross section of several pb so that a few million events are expected.

W-pair production proceeds through the Feynman diagrams shown in figure 7. In general the process is a complicated mixture of the neutrino t-channel exchange, only determined by the W-fermion couplings, and the γ and Z s-channel exchange that involve also anomalous gauge couplings. However, as shown in figure 8, the forward pole is completely determined by the neutrino exchange and insensitive to the anomalous couplings. For this reason it is possible to extract the polarisation and the triple gauge couplings [200] simultaneously from the W-pair data sample. The expected precision is $\Delta\mathcal{P}_{e^-}/\mathcal{P}_{e^-} = 0.1\%$ for a luminosity of $500\,\text{fb}^{-1}$ at $\sqrt{s} = 340\,\text{GeV}$. The correlation with the anomalous gauge couplings is negligible and the only assumption involved is that no right-handed W-fermion couplings appear. Experimental details of the analysis can be found in [201].

If electron and positron polarisation is available, both can be measured simultaneously from the W-pair sample. With equal luminosity at all four helicity combinations and

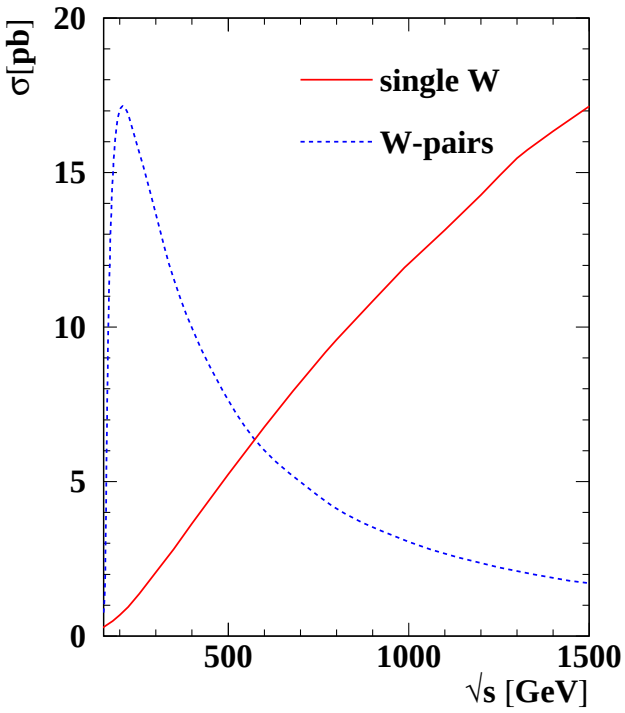

Figure 6: Cross section for single W and W-pair production at a LC

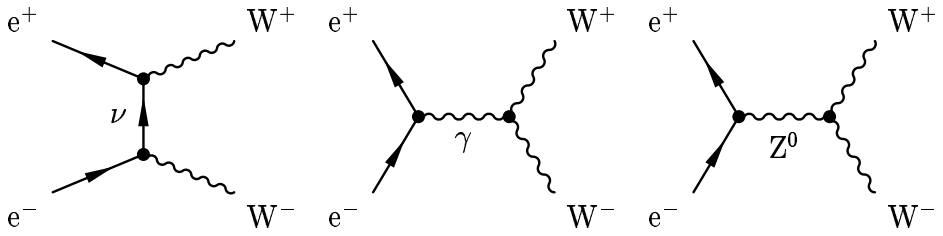

Figure 7: Feynman graphs for the production of W-pairs in e^+e^--annihilation.

$\mathcal{P}_{e^-} = 0.8$, $\mathcal{P}_{e^+} = 0.6$ one gets $\Delta\mathcal{P}_{e^-}/\mathcal{P}_{e^-} \approx 0.1\%$ and $\Delta\mathcal{P}_{e^+}/\mathcal{P}_{e^+} \approx 0.2\%$ and negligible correlations between the polarisations and between the polarisation and the couplings. If only 10% of the luminosity is spent on the equal helicities the polarisation errors increase by roughly a factor two with -50% correlation.

Single W production is dominated by the Feynman diagram shown in figure 9. Since this process involves the V-A coupling of the W to fermions a W^- can only be produced from a left-handed electron and a W^+ from a right-handed positron. Measuring the W-charge the polarisation can thus be measured for electrons and positrons separately. The outgoing electron usually disappears in the beampipe so that the W charge has to be reconstructed from the W decay products. This means that only leptonic W-decays can be used for the analysis. No detailed simulation study exists yet. The experimental signature is a single lepton in the detector which can be measured with high efficiency and small background. Because of the usually small W energy also the interference with W-pair production should be very small. Assuming $\sqrt{s} = 500\,\mathrm{GeV}$, $\mathcal{L} = 1\mathrm{ab}^{-1}$ and 100% efficiency for $W^- \to e^-, \mu^-$ an error of $\Delta\mathcal{P}_{e^-}/\mathcal{P}_{e^-} \sim 0.15\%$ is expected.

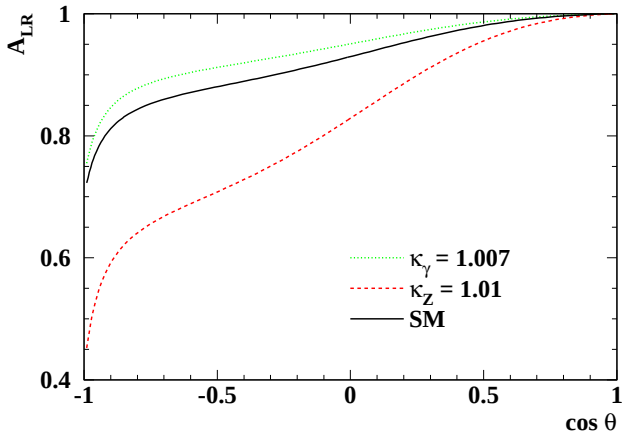

Figure 8: Left-right asymmetry of W-pair production as a function of the polar angle in the Standard Model and with anomalous triple gauge couplings.

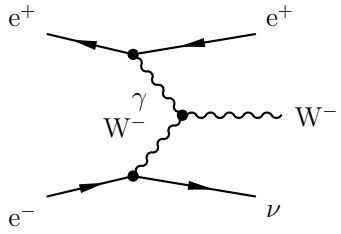

Figure 9: Dominating Feynman graph for single W production in $\mathrm{e^+e^-}$-annihilation.

5.7.2 The Blondel scheme

If a process $\mathrm{e^+e^-} \to \mathrm{f\,f}$ is mediated by pure s-channel vector-particle exchange the cross section for the different polarisation states with electron and positron polarisation available can be written as

$$\sigma \;=\; \sigma_u \left[1 - \mathcal{P}_{e^+}\mathcal{P}_{e^-} + \mathrm{A_{LR}}(\mathcal{P}_{e^+} - \mathcal{P}_{e^-})\right], \tag{9}$$

where $\mathcal{P}_{e^+}$ and $\mathcal{P}_{e^-}$ are the longitudinal polarisations of the positrons and electrons measured in the direction of the particle's velocity. σ_u denotes the unpolarised cross section and $\mathrm{A_{LR}}$ the left-right asymmetry. If the signs of the two polarisations can be switched independently four cross sections can be measured for four unknowns. From these cross sections the polarisations can be obtained, if $\mathrm{A_{LR}} \neq 0$:

$$\mathcal{P}_{e^\pm} \;=\; \sqrt{\frac{(\sigma_{+-} + \sigma_{-+} - \sigma_{++} - \sigma_{--})(\mp\sigma_{+-} \pm \sigma_{-+} - \sigma_{++} + \sigma_{--})}{(\sigma_{+-} + \sigma_{-+} + \sigma_{++} + \sigma_{--})(\mp\sigma_{+-} \pm \sigma_{-+} + \sigma_{++} - \sigma_{--})}}$$

where in σ_{ij} i denotes the sign of the positron- and j the sign of the electron-polarisation. As a drawback of this method some luminosity needs to be spent with the same helicities for both beams which is not very interesting for most physics processes.

To measure the polarisation with this scheme two processes have been considered,

- $\mathrm{e^+e^-} \to \mathrm{f\,f}$ with $\sqrt{s'} \approx \sqrt{s}$;

- radiative return events ($\mathrm{e^+e^-} \to \mathrm{Z}\gamma \to \mathrm{f\,f}\gamma$).

The cross section and left right asymmetry for the two processes at $\sqrt{s} = 350$ and $500\,\mathrm{GeV}$ is given in table 5.2. Both cross sections scale approximately with $1/s$. The high energy

$\sqrt{s}$	σ_{RR}	$\mathrm{A_{LR}}(RR)$	σ_{HE}	$\mathrm{A_{LR}}(HE)$
340 GeV	17 pb	0.19	5 pb	0.50
500 GeV	7 pb	0.19	2 pb	0.50

Table 5.2: Cross section and asymmetry for high energy and radiative return $\mathrm{f\,f}$ events.

events can be measured with high efficiency and almost no background. However the analysis relies on the assumption of s-channel vector-exchange, so for analyses like the search for R-parity violating sneutrinos the results cannot be used.

On the contrary radiative return events contain on-shell Z-decays which are well understood from LEP1 and SLD. In about 90% of the events the high-energy photon is lost in the beampipe. These events can be reconstructed kinematically and most backgrounds can be rejected. However, at TESLA energies the cross section for the fusion process $\mathrm{e^+e^-} \to \mathrm{Ze^+e^-}$ is of the same order as the signal. In those events one electron has almost the beam energy and stays at low angle while the other is extremely soft and also often lost in the beampipe resulting in a $\sim 30\%$ background of Zee events in the radiative return sample. The only way Zee events can be rejected is to require a photon above 7° where photons and electrons can be separated by the tracking detectors. Applying some additional event selection cuts on the hadronic mass and the balance of the event about 9% of the radiative return events are accepted with only a small Zee background. However in these events the slow electron is seen in the detector, so that they can easily be rejected by vetoing on an isolated electron.

Assuming $\mathcal{P}_{e^-} = 80\%$, $\mathcal{P}_{e^+} = 60\%$, an integrated luminosity of $500\,\mathrm{fb}^{-1}$ at $\sqrt{s} = 340\,\mathrm{GeV}$ and 50% or 10% of the luminosity spent with both beam polarisations with the same sign table 5.3 shows the obtainable errors on the two polarisations and their correlation. Due to the scaling of the cross sections the errors are about a factor $\sqrt{2}$ larger at $500\,\mathrm{GeV}$. It should be noted that the relative errors scale approximately with the product of the polarisations.

	$\mathcal{L}_{\pm\pm}/\mathcal{L} = 0.5$			$\mathcal{L}_{\pm\pm}/\mathcal{L} = 0.1$		
	HE	rr	WW	HE	rr	WW
$\Delta\mathcal{P}_{e^-}/\mathcal{P}_{e^-}$ [%]	0.10	0.51	0.07	0.21	1.11	0.11
$\Delta\mathcal{P}_{e^+}/\mathcal{P}_{e^+}$ [%]	0.12	0.53	0.11	0.15	1.13	0.21
corr	−0.49	−0.91	0	−0.56	−0.93	−0.52

Table 5.3: Relative polarisation error using the Blondel scheme for $\sqrt{s} = 340\,\mathrm{GeV}$, $\mathcal{L} = 500\,\mathrm{fb}^{-1}$, $\mathcal{P}_{\mathrm{e}^-} = 0.8$, $\mathcal{P}_{\mathrm{e}^+} = 0.6$ (HE = High energy events, rr = radiative return, WW = W-pair production).

Radiative corrections to the form of equation (9) have been checked with the KK MonteCarlo [202]. For the high energy events and for the radiative return events with a seen

photon they are negligible. For the radiative return events where the photon is lost in the beampipe, which are not used in this analysis, the corrections are on the percent level.

Because of the high losses in the selection of the radiative return events the errors on the single polarisations seem rather large. However the large negative correlation reduces the error substantially for the effective polarisations needed in the analysis. Table 5.4 compares the errors on the effective polarisations for the setups shown in table 5.3 and for polarimeter measurements assuming 0 or 50% correlation between the two polarimeters.

The effective polarisations considered are:

- $\mathcal{P}_{\text{eff}} = \frac{\mathcal{P}_{e^-}+\mathcal{P}_{e^+}}{1+\mathcal{P}_{e^-}\mathcal{P}_{e^+}}$, relevant for $\mathrm{A_{LR}}$ with s-channel vector exchange;
- $\mathcal{P}_{e^-}\mathcal{P}_{e^+}$, relevant for the cross section suppression/enhancement with s-channel vector exchange;
- $\mathcal{P}_{e^-} + \mathcal{P}_{e^+} - \mathcal{P}_{e^-}\mathcal{P}_{e^+}$, relevant for the cross section suppression/enhancement for t-channel W-pair production.

Due to the high anti-correlation even the results from the radiative return analysis with one tenth of the luminosity at the low cross sections are competitive to polarimetry with an optimistic 0.5% error.

	value	Rel. error [%]							
		$\mathcal{L}_{\pm\pm}/\mathcal{L} = 0.5$			$\mathcal{L}_{\pm\pm}/\mathcal{L} = 0.1$			Polarimeter	
		HE	rr	WW	HE	rr	WW	$\rho=0$	$\rho=0.5$
$(\mathcal{P}_{e^-}+\mathcal{P}_{e^+})/(1+\mathcal{P}_{e^-}\mathcal{P}_{e^+})$	0.95	0.02	0.08	0.02	0.05	0.17	0.02	0.13	0.16
$\mathcal{P}_{e^-}\mathcal{P}_{e^+}$	0.48	0.11	0.22	0.13	0.18	0.42	0.18	0.71	0.87
$\mathcal{P}_{e^-}+\mathcal{P}_{e^+}-\mathcal{P}_{e^-}\mathcal{P}_{e^+}$	0.92	0.03	0.12	0.03	0.06	0.25	0.03	0.19	0.21

Table 5.4: Relative error on the effective polarisations for the discussed setups and $\sqrt{s} = 340\,\text{GeV}$, $\mathcal{L} = 500\,\text{fb}^{-1}$, $\mathcal{P}_{\text{e}^-} = 0.8$, $\mathcal{P}_{\text{e}^+} = 0.6$. For the polarimeter a total error of 0.5% has been assumed. (HE = High energy events, rr = radiative return, WW = W-pair production).

5.7.3 Experimental Aspects

Although the methods presented here measure in the luminosity weighted polarisation directly from the annihilation data some experimental assumptions are involved. In all cases it is assumed that the absolute values of the polarisation of the left- and right-handed state are the same and possible corrections have to be obtained from polarimeters. If the polarisation is written as $\mathcal{P} = \pm\langle|\mathcal{P}|\rangle + \delta\mathcal{P}$ The shift in the measured polarisation using Ws in the case of electron polarisation only is given by $\Delta\mathcal{P}/\mathcal{P} = \delta\mathcal{P}$

Using the Blondel scheme with electron and positron polarisation the corresponding errors are

$$\begin{aligned} \Delta\mathcal{P}_{e^-} &= 1.0\delta\mathcal{P}_{e^-} + 0.6\delta\mathcal{P}_{e^+} \\ \Delta\mathcal{P}_{e^+} &= -0.5\delta\mathcal{P}_{e^-} - 0.7\delta\mathcal{P}_{e^+} \end{aligned}$$

for the high energy events and

$$\begin{aligned}\Delta\mathcal{P}_{e^-} &= \quad 2.4\delta\mathcal{P}_{e^-} + 2.1\delta\mathcal{P}_{e^+} \\ \Delta\mathcal{P}_{e^+} &= -1.7\delta\mathcal{P}_{e^-} - 1.7\delta\mathcal{P}_{e^+}\end{aligned}$$

for the radiative return sample.

The corresponding corrections have to be obtained from polarimeters. This is possible in a Compton polarimeter where the laser polarisation can be flipped easily. To assure that the electron-laser luminosity does not depend on the laser polarisation, or to correct for such effects, one should have a multichannel polarimeter with a large lever arm in the analysing power.

If electron and positron polarisation is available, in the formulae for the effective polarisations and for the Blondel scheme products of the two polarisations appear so that one has to understand the correlations between the electron and positron polarisation. In principle there can be a correlation due to the depolarisation in the bunch. Studies with CAIN [203], however, indicate that these correlations are small. Another source of correlation can come from time dependencies or spatial correlations due to the beam delivery system. If half of the luminosity is taken with a polarisation 5% higher and the other half 5% lower than average the polarisations obtained with the Blondel scheme are off by around 0.25% affecting the effective polarisation by the same amount. Measuring the polarisation with polarimeters would only result in a 0.16% error in the effective polarisation.

Time correlations have to be tracked with polarimeters. Spacial correlations due to the beam delivery system have to be obtained from simulations and should be minimised already in the design.

Chapter 6

Summary and Outlook

Maybe remark concerning rough cost estimates and polarised e+ already for the baseline design and conventional e+ source

The clean and fundamental nature of e^+e^- collisions at the linear collider is ideally suited for the search for new physics in direct as well as indirect searches and for determining precisely the underlying structure of the model. Polarised beams are a very powerful tool to reach these goals.

The physics examples have shown that using both beams simultaneously polarised are a very efficient tool to be prepared for the 'Unexpected' in new physics searches. It has been shown that both beams polarised may be decisive to determine the properties and quantum numbers of the new particles and to test the model assumptions, e.g. in Supersymmetry. Furthermore, it offers a larger number of observables which are important to reveal the structure of the underlying model and to determine the new parameters in model independent analyses. Even marginal signals of new physics may be accessible only if the signal has been maximised with the help of both beams polarised. Both beams polarised lead also to better statistics and reduce the dominant sytematical error in indirect searches which give access to physics scales which may be far beyond the direct kinematical reach of any present and future experiments. Concerning the high precision tests of the Standard Model at GigaZ both beams polarised are needed. Due to the extremely high statistics the polarisation also has to be known with highest precision which can not be provided with polarimetry methods. In order to reach the requested precision in the left-right-asymmetry measurement the Blondel Scheme for the polarisation measurement has to be used.

Moreover, having both beams polarised enables the possibility to use even transversely polarised beams at a e^+e^- LC. With transversely polarised beams, it is possible to observe gravitons in indirect searches and distinguish between different models, i.e. far below the energy threshold where the spin 2 were direct accessible. Furthermore this option provides new efficient observables for the detection of possible CP violation and enables to test specific TGC which are not accessible with polarised electrons only. An overview about the given examples here in the report and the qualitative as well as quantitative effects of employing both beams polarised compared with using only polarised electrons are listed in Tables 3.16 and 3.17.

An overview has been given about the possible technical realisations for polarised beams at the ILC. The SLC established that reliable electron beams with a polarization at high energy approaching 80% can be provided over periods of years. The standard source for polarised electrons is a DC gun with a strained photocathode and today a polarisation degree of even more than 80% is expected.

Concerning polarised positrons at the ILC mainly two methods are discussed:
a) Circularly polarised photons from a helical undulator generate longitudinally polarised positrons in a target via $e^{\pm}$ pair production;
b) Circularly polarised photons are obtained by backscattering of a laser light off an electron beam; they also generate longitudinally polarised positrons in a target.

The feasibility of undulator–based polarised positron sources will be checked in the E-166 experiment which is being prepared at SLAC and will run in 2005. Superconducting as well as permanent magnet prototypes of helical undulators with 10 or 20 periods length for the ILC beam structure are already under construction at AsteC, Daresbury Laboratory. The concept of the laser-based positron source will be tested in an experiment being conducted at KEK.

For the precise physics analyses at the ILC it will also be important to measure the polarisation very accurately. The primary polarimeter measurement at the ILC will be performed by a Compton polarimeter. An accuracy of $(\Delta P_{e^-}/P_{e^-}) = 0.25\%$ should be achievable. The polarimeters can be located upstream or downstream of the Interaction Point (IP) and it might be desirable to implement polarimeters at both locations. The downstream polarimeter requires a crossing angle at the IP; therefore polarimetry is one of main issues being considered for deciding on the IR crossing angles.

Since polarimeters measure either the polarisation of the incoming beam that has not been depolarised by the beam-beam interaction or the one of the outgoing beam which has been depolarised as much as the interacting particles it is also important to measure the polarisation directly from the data via processes with precisely known polarisation structure, e.g. WW production or applying the Blondel Scheme at the GigaZ option. Polarised positrons are needed to get the desired precision applying the Blondel Scheme. However, all the methods using annihilation data involve some physics assumptions that have to be considered in the framework of the model in which the data are analysed. The data driven methods therefore cannot replace completely the polarimeters but provide an independent complementary measurement. The data methods need a large luminosity to get to a precise result while polarimeters are completely systematics limited and statistics is no problem. Since the ILC provides a very large luminosity the data methods offers the possibility to reach a precision even better than the polarimeters.

In summary it has been shown in the report that simultaneously polarised e^- and e^+ beams are a very efficient tool for direct as well as indirect searches for new physics, preparing the ILC even perfectly for the 'Unexpected'. Polarised positrons are absolutely needed for specific physics questions and enrich the physics potential considerably. The possible technical realisations for generating the polarised particles as well as measuring precisely the actual polarisation are both well on track so that one could even schedule to have both beams polarised already for the upgraded ILC baseline design.

Acknowledgements

Bibliography

[1] S. Heinemeyer, S. Kraml, W. Porod and G. Weiglein, JHEP **0309** (2003) 075 [arXiv:hep-ph/0306181]; G. Weiglein, Nature **429** (2004) 613.

[2] J. H. Kuhn, LC-TH-2001-004

[3] J. A. Aguilar-Saavedra and T. Riemann, arXiv:hep-ph/0102197.

[4] E. W. N. Glover *et al.*, arXiv:hep-ph/0410110; J. A. Aguilar-Saavedra, arXiv:hep-ph/0409342.

[5] L. Chikovani and T. Djobava, arXiv:hep-ex/0205016.

[6] S. Rindani, hep-ph/0304046.

[7] B. Grzadkowski, Z. Hioki, Nucl. Phys. **B 585**, 3 (2000), arXiv:hep-ph/0004223.

[8] M. Beneke *et al.*, arXiv:hep-ph/0003033.

[9] B. C. Allanach *et al.*, in *Proc. of the APS/DPF/DPB Summer Study on the Future of Particle Physics (Snowmass 2001)* ed. N. Graf, Eur. Phys. J. C **25** (2002) 113 [eConf **C010630** (2001) P125] [arXiv:hep-ph/0202233].

[10] C. Blochinger, H. Fraas, G. Moortgat-Pick and W. Porod, Eur. Phys. J. C **24** (2002) 297 [arXiv:hep-ph/0201282].

[11] DESY Reports 92-123 A+B, 93-123 C, 96-123 D, 99-123F, P.M. Zerwas *ed.*.

[12] K. Desch, ECFA/DESY LC–workshop, Obernai, October 1999.

[13] D.J. Summers, Phys. Lett. D 274, 1992, 209

[14] A. Gurtu, talk given at ICHEP 2000, Osaka, July 2000, to appear in the proceedings.

[15] S. Heinemeyer, W. Hollik and G. Weiglein, Eur. Phys. J. C **9** (1999) 343 [arXiv:hep-ph/9812472].

[16] B. Kniehl, ECFA/DESY LC–workshop, Hamburg, September 2000.

[17] D. Atwood and A. Soni, Phys. Rev. D **45** (1992) 2405; M. Davier, L. Duflot, F. Le Diberder, A. Rouge, Phys. Lett. B306 (1993) 411; M. Diehl, O. Nachtmann, Z. Phys. C62 (1994) 397; K. Hagiwara, S. Ishihara, J. Karnoshita, B.A. Kniehl, Eur. Phys. J. C14 (2000) 457.

[18] Ch. Baltay, ECFA/DESY LC–workshop, Obernai, October 1999.

[19] K. Abe *et al.* [SLD Collaboration], Phys. Rev. Lett. **84** (2000) 5945 [arXiv:hep-ex/0004026].

[20] S.B. Gunst, L.A. Page, Phys. Rev. **92** (1953) 970.

[21] R. Hawkings and K. Monig, Eur. Phys. J. directC **1** (1999) 8 [arXiv:hep-ex/9910022].

[22] G. Alexander and E. Reinherz-Aronis,*The Gain to Polarimetry and A(LR) Measurements from a Polarised Positron Beam in TESLA*, LC-PHSM-2003-032.

[23] S. Heinemeyer, T. Mannel and G. Weiglein, arXiv:hep-ph/9909538; S. Heinemeyer and G. Weiglein, arXiv:hep-ph/0012364.

[24] J. Erler, S. Heinemeyer, W. Hollik, G. Weiglein and P. M. Zerwas, Phys. Lett. B **486** (2000) 125 [arXiv:hep-ph/0005024].

[25] R. Hawkings and K. Mönig, Eur. Phys. J. directC **1** (1999) 8 [arXiv:hep-ex/9910022].

[26] K. Mönig, private communication.

[27] [The LEP Higgs Working Group], Phys. Lett. B **565** (2003) 61 [arXiv:hep-ex/0306033].

[28] P. Wells, talk presented at HEP2003 Europhysics Conference, Aachen, July 2003.

[29] S. Heinemeyer, W. Hollik and G. Weiglein, Eur. Phys. J. C **9** (1999) 343 [arXiv:hep-ph/9812472];
G. Degrassi, S. Heinemeyer, W. Hollik, P. Slavich and G. Weiglein, Eur. Phys. J. C **28** (2003) 133 [arXiv:hep-ph/0212020].

[30] S. Heinemeyer and G. Weiglein, JHEP **0210** (2002) 072 [arXiv:hep-ph/0209305].

[31] S. Heinemeyer, W. Hollik and G. Weiglein, Comput. Phys. Commun. **124** (2000) 76 [arXiv:hep-ph/9812320];
T. Hahn, S. Heinemeyer, W. Hollik and G. Weiglein, in preparation;
The code is obtainable at `www.feynhiggs.de`.

[32] T. Omori, "A polarized positron beam for linear colliders," KEK-PREPRINT-98-237 *Presented at the 1st ACFA Workshop on Physics Detector at the Linear Collider, Beijing, China, 26-28 Nov 1998*.

[33] S. Riemann, LC-TH-2001-007.

[34] R. Casalbuoni, S. De Curtis, D. Dominici, R. Gatto and S. Riemann, LC-TH-2000-006, arXiv:hep-ph/0001215.

[35] T. Hahn, S. Heinemeyer and G. Weiglein, Nucl. Phys. B **652** (2003) 229 [arXiv:hep-ph/0211204]; Nucl. Phys. Proc. Suppl. **116** (2003) 336 [arXiv:hep-ph/0211384].

[36] S. Y. Choi, A. Djouadi, M. Guchait, J. Kalinowski, H. S. Song and P. M. Zerwas, Eur. Phys. J. C **14** (2000) 535 [arXiv:hep-ph/0002033].

[37] F. Franke and H. Fraas, Standard Model," Int. J. Mod. Phys. A **12** (1997) 479 [arXiv:hep-ph/9512366] and references therein.

[38] F. Franke, H. Fraas and A. Bartl, Phys. Lett. B **336** (1994) 415 [arXiv:hep-ph/9408217].

[39] F. Franke and H. Fraas, Z. Phys. C **72** (1996) 309 [arXiv:hep-ph/9511275].

[40] U. Ellwanger and C. Hugonie, Eur. Phys. J. C **5** (1998) 723 [arXiv:hep-ph/9712300].

[41] S. Hesselbach, F. Franke and H. Fraas, Eur. Phys. J. C **23** (2002) 149 [arXiv:hep-ph/0107080] and references therein.

[42] F. Franke and S. Hesselbach, Phys. Lett. B **526** (2002) 370 [arXiv:hep-ph/0111285].

[43] S. Hesselbach and F. Franke, arXiv:hep-ph/0210363.

[44] G. Moortgat-Pick, S. Hesselbach, F. Franke and H. Fraas, arXiv:hep-ph/9909549.

[45] S. Hesselbach, F. Franke and H. Fraas, arXiv:hep-ph/0003272.

[46] N. Ghodbane and H. U. Martyn, arXiv:hep-ph/0201233.

[47] B. C. Allanach *et al.*, Eur. Phys. J. C **25** (2002) 113 [eConf **C010630** (2001) P125] [arXiv:hep-ph/0202233].

[48] B. de Carlos and J. R. Espinosa, Phys. Lett. B **407** (1997) 12 [arXiv:hep-ph/9705315].

[49] S. Y. Choi, J. Kalinowski, G. Moortgat-Pick and P. M. Zerwas, Eur. Phys. J. C **22** (2001) 563 [Addendum-ibid. C **23** (2002) 769] [arXiv:hep-ph/0108117].

[50] M. Heyssler, R. Ruckl and H. Spiesberger, arXiv:hep-ph/9908319 and private communication with H. Spiesberger.

[51] H. E. Haber and G. L. Kane, Phys. Rept. **117** (1985) 75.

[52] J. A. Aguilar-Saavedra *et al.* [ECFA/DESY LC Physics Working Group Collaboration], TESLA Technical Design Report, Part III, eds. R.-D. Heuer, D. Miller, F. Richard and P. Zerwas, [arXiv:hep-ph/0106315]; F. Richard, J. R. Schneider, D. Trines and A. Wagner, arXiv:hep-ph/0106314.

[53] Y. Kizukuri and N. Oshimo, Phys. Lett. B **249** (1990) 449.

[54] S. Y. Choi, H. S. Song and W. Y. Song, Phys. Rev. D **61** (2000) 075004 [arXiv:hep-ph/9907474].

[55] A. Bartl, H. Fraas, O. Kittel and W. Majerotto, arXiv:hep-ph/0308143; A. Bartl, H. Fraas, O. Kittel and W. Majerotto, Phys. Rev. D **69** (2004) 035007 [arXiv:hep-ph/0308141]. .

[56] A. Bartl, H. Fraas, O. Kittel and W. Majerotto, Eur. Phys. J. C **36** (2004) 233 [arXiv:hep-ph/0402016].

[57] Phys. Lett. B **598** (2004) 76 [arXiv:hep-ph/0406309].

[58] O. Kittel, A. Bartl, H. Fraas and W. Majerotto, arXiv:hep-ph/0410054.

[59] A. Bartl, T. Kernreiter and O. Kittel, Phys. Lett. B **578** (2004) 341 [arXiv:hep-ph/0309340].

[60] S. Y. Choi, M. Drees, B. Gaissmaier and J. Song, Phys. Rev. D **69** (2004) 035008 [arXiv:hep-ph/0310284].

[61] A. Bartl, H. Fraas, S. Hesselbach, K. Hohenwarter-Sodek and G. Moortgat-Pick, JHEP **0408** (2004) 038 [arXiv:hep-ph/0406190].

[62] L. J. Hall and J. Polchinski, Phys. Lett. B **152** (1985) 335.

[63] I. S. Altarev *et al.*, Phys. Lett. B **276** (1992) 242; I. S. Altarev et al., Phys. Atom. Nucl.**59** (1996) 1152 and Yad. Fiz. **59 N 7**; E. D. Commins, S. B. Ross, D. DeMille, B. C. Regan, Phys. Rev. **A 50** (1994) 2960.

[64] G. Moortgat-Pick, H. Fraas, A. Bartl and W. Majerotto, Eur. Phys. J. C **9** (1999) 521 [Erratum-ibid. C **9** (1999) 549] [arXiv:hep-ph/9903220].

[65] G. Moortgat-Pick, in *Proc. of the APS/DPF/DPB Summer Study on the Future of Particle Physics (Snowmass 2001)* ed. N. Graf, eConf **C010630**, E3008 (2001) [arXiv:hep-ph/0202082]; G. Moortgat-Pick, A. Bartl, H. Fraas and W. Majerotto, Eur. Phys. J. C **18** (2000) 379.

[66] A. Bartl, H. Fraas, S. Hesselbach, K. Hohenwarter-Sodek and G. Moortgat-Pick, in preperation.

[67] S. Y. Choi, H. S. Song and W. Y. Song, Phys. Rev. D **61** (2000) 075004 [arXiv:hep-ph/9907474].

[68] Y. Kizukuri and N. Oshimo, Phys. Lett. B **249** (1990) 449.

[69] G. Moortgat-Pick, H. Fraas, A. Bartl and W. Majerotto, Eur. Phys. J. C **9**, 521 (1999) [Erratum-ibid. C **9**, 549 (1999)] [arXiv:hep-ph/9903220].

[70] A. Bartl, H. Fraas, O. Kittel and W. Majerotto, arXiv:hep-ph/0308141.

[71] E. Boos, H. U. Martyn, G. Moortgat-Pick, M. Sachwitz, A. Sherstnev and P. M. Zerwas, Eur. Phys. J. C **30** (2003) 395 [arXiv:hep-ph/0303110];

[72] A. Bartl et al., Eur. Phys. J. direct C **2** (2000) 6.

[73] A. Bartl et al., s**(1/2) = 0.5-TeV to 2-TeV," Z. Phys. C **76** (1997) 549; H. Eberl, A. Bartl and W. Majerotto, Nucl. Phys. B **472** (1996) 481; H. Eberl, S. Kraml and W. Majerotto, JHEP **9905** (1999) 016; S. Kraml, arXiv:hep-ph/9903257.

[74] M. Berggren et al., arXiv:hep-ph/9911345.

[75] T. Abe, S. Chen, B. Dobos, T. Dorland, J. Goodson, J. Gray, A. Han, A. Martinez, U. Nauenberg, J. Proulx, *Positron Polarization and Supersymmetry Measurements*, private discussion.

[76] G. W. Wilson, LC-PHSM-2001-010.

[77] L. Vacavant and I. Hinchliffe, arXiv:hep-ex/0005033.

[78] E. Eichten, K. Lane and M. E. Peskin, Phys. Rev. Lett. **50** (1983) 811;
R. Rückl, Phys. Lett. B **129** (1983) 363.

[79] A. A. Babich, P. Osland, A. A. Pankov and N. Paver, Phys. Lett. B **518** (2001) 128 [hep-ph/0107159].

[80] A. A. Babich, P. Osland, A. A. Pankov and N. Paver, LC Note LC-TH-2001-021 (2001), hep-ph/0101150.

[81] A. A. Babich, P. Osland, A. A. Pankov and N. Paver, Phys. Lett. B **481** (2000) 263 [hep-ph/0003253].

[82] K. Flottmann, DESY-95-064;

[83] K. Fujii and T. Omori, KEK-PREPRINT-95-127.

[84] B. Schrempp, F. Schrempp, N. Wermes and D. Zeppenfeld, Nucl. Phys. B **296** (1988) 1.

[85] W.T. Eadie, D. Drijard, F.E. James, M. Roos, B. Sadoulet, *Statistical methods in experimental physics* (American Elsevier, 1971).

[86] F. Cuypers and P. Gambino, Phys. Lett. B **388** (1996) 211 [hep-ph/9606391];
F. Cuypers, hep-ph/9611336.

[87] C. J. S. Damerell and D. J. Jackson, eConf **C960625** (1996) DET078.

[88] A. A. Pankov and N. Paver, [hep-ph/0209058], to appear in Eur. Phys. J. C.

[89] N. Arkani-Hamed, S. Dimopoulos and G. R. Dvali, Phys. Lett. B **429** (1998) 263 [hep-ph/9803315].

[90] For a review see, *e.g.*, J. Hewett and M. Spiropulu, Ann. Rev. Nucl. Part. Sci. **52** (2002) 397 [hep-ph/0205106].

[91] J. L. Hewett, Phys. Rev. Lett. **82** (1999) 4765 [hep-ph/9811356].

[92] P. Osland, A. A. Pankov and N. Paver, [hep-ph/0304123], to be published in Phys. Rev. D.

[93] T. G. Rizzo, Phys. Rev. D **59** (1999) 113004 [hep-ph/9811440].

[94] B. Ananthanarayan and S. D. Rindani, Phys. Rev. D **70** (2004) 036005 [arXiv:hep-ph/0309260].

[95] G. V. Dass and G. G. Ross, Phys. Lett. B **57** (1975) 173; G. V. Dass and G. G. Ross, Nucl. Phys. B **118** (1977) 284.

[96] K. Hagiwara, R. D. Peccei, D. Zeppenfeld and K. Hikasa, Nucl. Phys. B **282** (1987) 253.

[97] M. Diehl, O. Nachtmann and F. Nagel, Eur. Phys. J. C **27** (2003) 375 [arXiv:hep-ph/0209229].

[98] ALEPH Collaboration, Eur. Phys. J. C **21** (2001) 423 [arXiv:hep-ex/0104034];
DELPHI Collaboration, Phys. Lett. B **459** (1999) 382;
L3 Collaboration, Phys. Lett. B **467** (1999) 171 [arXiv:hep-ex/9910008];
L3 Collaboration, Phys. Lett. B **487** (2000) 229 [arXiv:hep-ex/0007005];

[99] G. Abbiendi *et al.* [OPAL Collaboration, Eur. Phys. J. C **19** (2001) 1 [arXiv:hep-ex/0009022];
OPAL Collaboration, Eur. Phys. J. C **19** (2001) 229 [arXiv:hep-ex/0009021].

[100] M. Pohl and H. J. Schreiber, DESY-99-030

[101] R. . (. Brinkmann, G. . (. Materlik, J. . (. Rossbach and A. . (. Wagner, DESY-97-048

[102] F. Franco-Sollova, LC-PHSM-2004-011.

[103] M. Diehl, O. Nachtmann and F. Nagel, arXiv:hep-ph/0306247.

[104] M. Diehl and O. Nachtmann, Z. Phys. C **62** (1994) 397.

[105] M. Diehl and O. Nachtmann, Eur. Phys. J. C **1** (1998) 177 [arXiv:hep-ph/9702208].

[106] W. Menges, LC-PHSM-2001-022.

[107] W. Bernreuther, U. Löw, J. P. Ma and O. Nachtmann, Z. Phys. C **43** (1989) 117; J. G. Körner, J. P. Ma, R. Münch, O. Nachtmann and R. Schöpf, Z. Phys. C **49** (1991) 447.

[108] W. Bernreuther, G. W. Botz, D. Bruß, P. Haberl and O. Nachtmann, Z. Phys. C **68** (1995) 73 [arXiv:hep-ph/9412268]; P. Haberl, arXiv:hep-ph/9611430.

[109] D. Buskulic *et al.* [ALEPH Collaboration], Phys. Lett. B **384** (1996) 365.

[110] O. Nachtmann and C. Schwanenberger, Eur. Phys. J. C **9** (1999) 565 [arXiv:hep-ph/9901343]; O. Nachtmann and C. Schwanenberger, Eur. Phys. J. C **13** (2000) 315 [arXiv:hep-ph/9909527].

[111] D. Topaj, "Suche nach CP-Verletzung in hadronischen Z-Zerfällen", Diploma thesis (1997), University of Heidelberg (unpublished); T. Pauly, "Suche nach CP-Verletzung in den 4-Jet-Zerfällen des Z^0", Diploma thesis (1999), University of Heidelberg (unpublished).

[112] F. Richard, J. R. Schneider, D. Trines and A. Wagner, "TESLA Technical Design Report Part I: Executive Summary," arXiv:hep-ph/0106314;

[113] O. Nachtmann and C. Schwanenberger, Eur. Phys. J. C **32** (2004) 253 [arXiv:hep-ph/0308198].

[114] W. Bernreuther, A. Brandenburg, P. Haberl and O. Nachtmann, Phys. Lett. B **387** (1996) 155 [arXiv:hep-ph/9606379]; W. Bernreuther and O. Nachtmann, Eur. Phys. J. C **9** (1999) 319 [arXiv:hep-ph/9812259].

[115] U. Baur, I. Hinchliffe and D. Zeppenfeld, Int. J. Mod. Phys. A **2** (1987) 1285; U. Baur, M. Spira and P. M. Zerwas, Phys. Rev. D **42** (1990) 815.

[116] T. Han and J. L. Hewett, Phys. Rev. D **60** (1999) 074015 [arXiv:hep-ph/9811237].

[117] B. Ananthanarayan, S. D. Rindani, R. K. Singh and A. Bartl, Phys. Lett. B **593** (2004) 95 [arXiv:hep-ph/0404106].

[118] B. Ananthanarayan and S. D. Rindani, arXiv:hep-ph/0410084.

[119] H. Czyz, K. Kolodziej and M. Zralek, Z. Phys. C **43** (1989) 97.

[120] D. Choudhury and S. D. Rindani, Phys. Lett. B **335** (1994) 198 [arXiv:hep-ph/9405242].

[121] S. D. Rindani and J. P. Singh, Phys. Lett. B **419** (1998) 357 [arXiv:hep-ph/9703380].

[122] S. D. Rindani, Pramana **45** (1995) S263 [arXiv:hep-ph/9411398].

[123] J. L. Hewett and T. G. Rizzo, Phys. Rept. **183**, 193 (1989).

[124] A. Leike, Phys. Rept. **317**, 143 (1999) [arXiv:hep-ph/9805494]; M. Cvetic and S. Godfrey, arXiv:hep-ph/9504216.

[125] W. Buchmuller, R. Ruckl and D. Wyler, Phys. Lett. B **191** (1987) 442 [Erratum-ibid. B **448** (1999) 320]. J. L. Hewett and T. G. Rizzo, Phys. Rev. D **58**, 055005 (1998) [arXiv:hep-ph/9708419], Phys. Rev. D **56**, 5709 (1997) [arXiv:hep-ph/9703337] and Phys. Rev. D **36**, 3367 (1987).

[126] J. Kalinowski, R. Ruckl, H. Spiesberger and P. M. Zerwas, Phys. Lett. B **414**, 297 (1997) [arXiv:hep-ph/9708272]; J. Kalinowski, R. Ruckl, H. Spiesberger and P. M. Zerwas, Phys. Lett. B **406**, 314 (1997) [arXiv:hep-ph/9703436]; T. G. Rizzo, Phys. Rev. D **59**, 113004 (1999) [arXiv:hep-ph/9811440].

[127] F. Cuypers and S. Davidson, Eur. Phys. J. C **2** (1998) 503 [arXiv:hep-ph/9609487].

[128] J. L. Hewett, Phys. Rev. Lett. **82** (1999) 4765 [arXiv:hep-ph/9811356]. G. F. Giudice, R. Rattazzi and J. D. Wells, Nucl. Phys. B **544**, 3 (1999) [arXiv:hep-ph/9811291]; T. Han, J. D. Lykken and R. J. Zhang, Phys. Rev. D **59**, 105006 (1999) [arXiv:hep-ph/9811350]; T. G. Rizzo, Phys. Rev. D **59**, 115010 (1999) [arXiv:hep-ph/9901209].

[129] For an overview of RS phenomenology, see H. Davoudiasl, J. L. Hewett and T. G. Rizzo, Phys. Rev. D **63**, 075004 (2001) [arXiv:hep-ph/0006041]; Phys. Lett. B **473**, 43 (2000) [arXiv:hep-ph/9911262]; Phys. Rev. Lett. **84**, 2080 (2000) [arXiv:hep-ph/9909255]; J. L. Hewett, F. J. Petriello and T. G. Rizzo, JHEP **0209**, 030 (2002) [arXiv:hep-ph/0203091].

[130] N. Arkani-Hamed, S. Dimopoulos and G. R. Dvali, Phys. Lett. B **429**, 263 (1998) [arXiv:hep-ph/9803315]; I. Antoniadis, N. Arkani-Hamed, S. Dimopoulos and G. R. Dvali, Phys. Lett. B **436**, 257 (1998) [arXiv:hep-ph/9804398]; N. Arkani-Hamed, S. Dimopoulos and G. R. Dvali, Phys. Rev. D **59**, 086004 (1999) [arXiv:hep-ph/9807344].

[131] L. Randall and R. Sundrum, Phys. Rev. Lett. **83** (1999) 3370 [arXiv:hep-ph/9905221].

[132] See, for example, I. Antoniadis, Phys. Lett. B **246**, 377 (1990); T. G. Rizzo and J. D. Wells, Phys. Rev. D **61**, 016007 (2000) [arXiv:hep-ph/9906234]; M. Masip and A. Pomarol, Phys. Rev. D **60**, 096005 (1999) [arXiv:hep-ph/9902467]; T. G. Rizzo, Phys. Rev. D **64**, 015003 (2001) [arXiv:hep-ph/0101278].

[133] S. Cullen, M. Perelstein and M. E. Peskin, Phys. Rev. D **62** (2000) 055012 [arXiv:hep-ph/0001166].

[134] G. Pasztor and M. Perelstein, in *Proc. of the APS/DPF/DPB Summer Study on the Future of Particle Physics (Snowmass 2001)* ed. N. Graf, eConf **C010630** (2001) P315 [arXiv:hep-ph/0111471].

[135] R. Budny, Phys. Rev. D **14** (1976) 2969; H. A. Olsen, P. Osland and I. Overbo, Phys. Lett. B **97** (1980) 286; K. i. Hikasa, Phys. Rev. D **33** (1986) 3203; C. P. Burgess and J. A. Robinson, Int. J. Mod. Phys. A **6** (1991) 2707; A. Djouadi, F. M. Renard and C. Verzegnassi, Phys. Lett. B **241** (1990) 260; F. M. Renard, Z. Phys. C **45** (1989) 75; J. L. Hewett and T. G. Rizzo, Z. Phys. C **36** (1987) 209; for a recent discussion of this option at the LC, see K. Desch, talk given at the *International Workshop on the Linear Collider, LCWS2002*, Jeju Island, Korea, Aug. 2002.

[136] J. Fleischer, K. Kolodziej and F. Jegerlehner, Phys. Rev. D **49** (1994) 2174.

[137] G. Moortgat-Pick, private communication.

[138] T. G. Rizzo, JHEP **0210** (2002) 013 [arXiv:hep-ph/0208027].

[139] E. Eichten, K. D. Lane and M. E. Peskin, Phys. Rev. Lett. **50** (1983) 811.

[140] For a review of the current and anticipated future collider reaches for extra dimensions, see J. Hewett and M. Spiropulu, Ann. Rev. Nucl. Part. Sci. **52** (2002) 397 [arXiv:hep-ph/0205106].

[141] A. Datta, E. Gabrielli and B. Mele, Phys. Lett. B **552** (2003) 237 [arXiv:hep-ph/0210318].

[142] More details can be found in T. G. Rizzo, JHEP **0302** (2003) 008 [arXiv:hep-ph/0211374].

[143] H. A. Olsen, P. Osland and I. Øverbø, Phys. Lett. B **97** (1980) 286.

[144] G. Corcella *et al.*, interfering gluons (including supersymmetric processes)," JHEP **0101** (2001) 010 [hep-ph/0011363]; G. Corcella *et al.*, hep-ph/0210213.

[145] H. Baer, F. E. Paige, S. D. Protopopescu and X. Tata, hep-ph/0001086.

[146] T. Sjöstrand, P. Edén, C. Friberg, L. Lönnblad, G. Miu, S. Mrenna and E. Norrbin, Comput. Phys. Commun. **135** (2001) 238 [hep-ph/0010017]; T. Sjöstrand, L. Lönnblad and S. Mrenna, hep-ph/0108264.

[147] P. Richardson, JHEP **0111**, 029 (2001) [hep-ph/0110108].

[148] R. Kuhn, F. Krauss, B. Ivanyi and G. Soff, Comput. Phys. Commun. **134**, 223 (2001) [hep-ph/0004270]. SHERPA is available from: `http://www.physik.tu-dresden.de/~krauss/hep/`.

[149] M. Bertini, L. Lönnblad and T. Sjöstrand, Comput. Phys. Commun. **134**, 365 (2001) [hep-ph/0006152].

[150] S. Gieseke, hep-ph/0210294.

[151] M. Kobel *et al.*, hep-ph/0007180.

[152] M. W. Grunewald *et al.*, hep-ph/0005309.

[153] S. Dittmaier and M. Roth, Nucl. Phys. B **642**, 307 (2002) [hep-ph/0206070].

[154] G. Montagna, M. Moretti, O. Nicrosini and F. Piccinini, Eur. Phys. J. C **2**, 483 (1998) [hep-ph/9705333];
F. Gangemi *et al.*, Eur. Phys. J. C **9**, 31 (1999) [hep-ph/9811437] and Nucl. Phys. B **559**, 3 (1999) [hep-ph/9905271];
F. Gangemi, hep-ph/0002142.

[155] K. Kołodziej, Eur. Phys. J. C **23**, 471 (2002) [hep-ph/0110063] and Comput. Phys. Commun. **151**, 339 (2003) [hep-ph/0210199];
A. Biernacik and K. Kołodziej, Nucl. Phys. Proc. Suppl. **116** (2003) 33 [hep-ph/0210405].

[156] E. Accomando, A. Ballestrero and M. Pizzio, Nucl. Phys. B **547** (1999) 81 [hep-ph/9807515];
E. Accomando, A. Ballestrero and M. Pizzio, hep-ph/9709277.

[157] F. Krauss, R. Kuhn, and G. Soff, JHEP **02**, 044 (2002) [hep-ph/0109036].

[158] A. Pukhov *et al.*, hep-ph/9908288. COMPHEP is available from: `http://theory.sinp.msu.ru/comphep/`.

[159] MINAMI-TATEYA group, T. Ishikawa *et al.*, KEK-92-19. GRACE is available from: `http://minami-home.kek.jp/`.

[160] A. Kanaki and C. G. Papadopoulos, Comput. Phys. Commun. **132**, 306 (2000) [hep-ph/0002082].

[161] C. G. Papadopoulos, Comput. Phys. Commun. **137**, 247 (2001) [hep-ph/0007335].

[162] F. Maltoni and T. Stelzer, JHEP **02**, 027 (2003) [hep-ph/0208156];
T. Stelzer and W. F. Long, Comput. Phys. Commun. **81**, 357 (1994) [hep-ph/9401258].
MADGRAPH/MADEVENT is available from: `http://madgraph.physics.uiuc.edu/`.

[163] H. Murayama, I. Watanabe and K. Hagiwara, KEK-91-11.

[164] T. Ohl, hep-ph/0011287;
W. Kilian, LC-TOOL-2001-039 *In '2nd ECFA/DESY Study 1998-2001', 1924-1980*. `WHIZARD` is available from:
`http://www-ttp.physik.uni-karlsruhe.de/Progdata/whizard/`. For `O'MEGA`, see:
`http://heplix.ikp.physik.tu-darmstadt.de/~ohl/omega/`.

[165] F. Caravaglios and M. Moretti, Phys. Lett. **B358**, 332 (1995) [hep-ph/9507237].

[166] M. Moretti, T. Ohl, and J. Reuter, hep-ph/0102195.

[167] E. Boos *et al.*, hep-ph/0109068.

[168] N. Ghodbane, hep-ph/9909499;
S. Katsanevas and P. Morawitz, Comput. Phys. Commun. **112**, 227 (1998) [hep-ph/9711417]. `SUSYGEN` is available from:
`http://lyoinfo.in2p3.fr/susygen/susygen3.html`.

[169] 1 T. Omori, contribution to the 1st ILC Workshop, Nov.13-15, 2004, KEK, Tsukuba, http://lcdev.kek.jp/ILCWS/Talks/13wg3-6-WG3-06PositronDiscussionOmori.pdf.

[170] S. Hiramatsu, contribution to the 11th KEK-SLAC ISG Meeting Dec.16-19, 2003, KEK, Tsukuba, http://lcdev.kek.jp/ISG/ISG11/Source/10miconFEL.pdf.

[171] D.P. Barber, G. Ripken, *Handbook of Accelerator Physics and Engineering*, Eds. A.W. Chao, M. Tigner, World Scientific, 2nd edition (2002).

[172] ICFA, *Parameters for the Linear Collider*, webpage: www.interactions.org/linearcollider/documents/index.htm.

[173] D.P. Barber and W. Decking, *Polarization Preservation in the NLC and TESLA Damping Rings*, Hamburg, August 2002; ILC-TRC, *International Linear Collider Technical Review Committee Second Report 2003*, SLAC-R-606, webpage: http://www.slac.stanford.edu/xorg/ilc-trc/2002/2002/report/03rephome.htm;
R.W. Assmann, F. Zimmermann, CERN SL-2001-064.

[174] H. Olsen, L.C. Maximom, *Photon and Electron Polarization in High-Energy Bremsstrahlung and Pair Production with Screening*, Phys. Rev. **114**, (1959) 877.

[175] V. Balakin, A. Mikhailichenko, *The Conversion system for obtaining high polarized electrons and positrons*, INP 79-85, 1979.

[176] K. Yokoya and P. Chen. SLAC-PUB-4692, 1988.

[177] Kathleen A. Thompson, SLAC-PUB-8716, 2001.

[178] K. Floettmann, *Positron source options for linear colliders*, contribution to EPAC, Lucerne, July, 2004.

[179] T.A. Vsevolozhskaya, A.A. Mikailichenko, E.A. Perevedentsev, G.I. Silvestrov, A.D. Chernyakin, SLAC-TRANS-0225, (Oct. 1986); proceedings of the *XIII International Conf. on High Energy Accelerators*, Novosibirsk, USSR, August 1986.

[180] A. Mikhailichenko, *Short-Period SC Undulator*, Cornell.

[181] K. Floettmann, *Investigations toward the development of polarized and unpolarized high intensity positron sources for linear colliders*, PhD Thesis, Hamburg (1993)

[182] A. Mikhailichenko, Proceedings of *Workshop on Superconducting Undulators and Wigglers*, Grenoble, June (2003), webpage: www.esrf.fr/Accelerators/files/Conferences/mikhailichenko.pdf.

[183] G. Alexander *et al.*, E-166 collaboration, SLAC-TN-04-018, LC-DET-2003-044.

[184] U.S. Linear Collider Steering Group, Accelerator Sub-committee, Linear Collider Option Task Forces, *U.S. Linear Collider Technology Options Study*, March 2004.

[185] T. Omori, T. Aoki, K. Dobashi, T. Hirose, Y. Kurihara, T. Okugi, I. Sakai, A. Tsunemi, J. Urakawa, M. Washio, K. Yokoya, Nucl. Instrum. Meth. A **500** (2003) 232 [Erratum-ibid. A **503** (2003) 658].

[186] K. Abe et al., KEK Report 2003-7.

[187] K. Yokoya, CAIN, http://www-acc-theory.kek.jp/members/cain/default.html

[188] I. Sakai, T. Aoki, K. Dobashi, M. Fukuda, A. Higurashi, T. Hirose, T. Iimura, Y. Kurihara, T. Okugi, T. Omori, J. Urakawa, M. Washio, and K. Yokoya Phys. Rev. ST Accel. Beams **6**, 091001 (2003).

[189] M. Fukuda, T. Aoki, K. Dobashi, T. Hirose, T. Iimura, Y. Kurihara, T. Okugi, T. Omori, I. Sakai, J. Urakawa, and M. Washio, Phys. Rev. Lett. **91**, 164801 (2003).

[190] P. Emma, *A Spin Totator System for the NLC*, NLC Note 7, December, 1994.

[191] P. C. Rowson and M. Woods, arXiv:hep-ex/0012055, SLAC-PUB-8745.

[192] M. L. Swartz, Phys. Rev. D **58** (1998) 014010 [arXiv:hep-ph/9711447].

[193] V. Brisson, R. Chiche, M. Jaquet-Lemire, S. Kurbasov, L. Losev, C. Pascaud, A. Reboux, V. Soskov, Z. Zhang, F. Zomer, *A Fabry-Perot cavity for a precise measurement of the longitudinal polarisation in a future linear collider*, Paris, August 2004.

[194] N. Falletto *et al.*, Nucl. Instrum. Meth. A **459** (2001) 412.

[195] M. Woods and K. C. Moffeit, SLAC-PUB-10669,SLAC IPBI TN-2004-3, 2004, *Presented at International Conference on Linear Colliders (LCWS 04), Paris, France, 19-24 Apr 2004*

[196] I. Will, P. Nickles and W. Sandner, *A Laser System for the TESLA Photo-Injector*, internal design study, Max-Born-Institut, Berlin, 1994.

[197] M. Woods, *The Scanning Compton Polarimeter for the SLD Experiment*, SLAC-PUB-7319, 1996, arXiv:hep-ex/9611005; 12th Int. Symposium on High-Energy Spin Physics (Spin96), NIKHEF, Amsterdam, Proceeding eds. C.W. de Jager et al., World Scientific, 1997, p. 843.

[198] V. Gharibyan, N. Meyners and P. Schuler, LC-DET-2001-047; see http://www.desy.de/~lcnotes.

[199] M. Woods, K. C. Moffeit, T. O. Raubenheimer, A. Seryi, C. Sramek and A. Florimonte, SLAC-PUB-10353, 2004, arXiv:physics/0403037.

[200] M. S. Bilenky, J. L. Kneur, F. M. Renard and D. Schildknecht, Nucl. Phys. B **409** (1993) 22.

[201] K. Mönig, *The use of Positron Polarisation for precision Measurements*, LC-PHSM-2000-59.

[202] S. Jadach, B. F. L. Ward and Z. Was, Comput. Phys. Commun. **130** (2000) 260 [arXiv:hep-ph/9912214].

[203] P. Chen, T. Ohgaki, A. Spitkovsky, T. Takahashi and K. Yokoya, Nucl. Instrum. Meth. A **397** (1997) 458 [arXiv:physics/9704012].